A tomographic imaging system for pneumatic conveyors using optical fibres.

RAHIM, R. Abdul.

A TOMOGRAPHIC IMAGING SYSTEM FOR PNEUMATIC CONVEYORS USING OPTICAL FIBRES

by

R. ABDUL RAHIM (AMIEE)
BEng(Hons)(UK)

A thesis submitted to
Sheffield Hallam University
for the degree of Doctor of Philosophy
in the School of Engineering Information Technology

FEBRUARY 1996

Dedication

This work is dedicated to my family and my wife Hafidzah for being very patient, understanding and for organising everything in an excellent manner for the whole family especially looking after our beloved children, Khairulhafiy Muhammad and Raudhatusyahirah during those difficult years.

Acknowledgements

I would like to record my sincere thanks to my main supervisor, Professor Bob Green, for his intelligent supervision, helpful suggestions and constructive criticisms of my work. I am extremely grateful for his outstanding support and encouragement throughout the course of this research.

I would like also to express my sincere thanks to my co-supervisors, Dr. Tony Pridmore and Dr. Fraser Dickin for their help and advice. Also thanks to Stuart Birchall for helping me to use EE Design, Brett Naylor for the power supply design and all the technicians, especially Don Rimmer, Ken Duty, Adrian and Imad for their part in helping me during my research.

For my colleagues in Room 2302 School of Engineering Information Technology, Jan, Fuad, Neil, Marshall, Joe, Roy and Paul thank you for your valuable discussions and suggestions.

The financial assistance from the Malaysian Government and Universiti Teknologi Malaysia is highly appreciated and without which this research could not have been possible.

ABSTRACT

This thesis presents an investigation into the application of optical fibre sensors to a tomographic imaging system.

Several sensing mechanisms for measurement using non-intrusive techniques are discussed and there relevance to pneumatic conveying discussed. Optical systems are shown to be worthy of investigation. The optical sensor is modelled to predict the expected sensor output voltage profiles arising from different, artificially produced flow regimes. These artificial flow regimes are created by placing a shaped obstruction inside a gravity drop conveyor in the path of the flowing solids. It is shown that for two arrays, each consisting of sixteen transducers, approximately 30% of the measurement volume is sampled.

An image reconstruction method for optical tomography is described, based on the back projection between view lines algorithm.

The design of the optical tomography system is described, with emphasis on preparation of the ends of the optical fibre, beam collimation and design of the transmitter and receiver circuits.

The optical sensors are evaluated singly and as a tomographic array. Results relating to concentration measurement are presented for solids flow using sand with a mean of 300 micron and plastic beads of 2 mm nominal diameter. Measurements were made with a single optical sensor using the gravity flow rig. The results demonstrate the suitability of the optical sensor for concentration measurement for lightly loaded flows (up to approximately 2% solids by volume in the test). The test is extended to all thirty-two sensors using a range of solids mass flow rates from 40 to 320 gm/s with both dry sand and plastic beads over a range of artificially created flow regimes. The results obtained by comparing the measured and predicted flowrates show good general agreement. The statistical parameters for the error of the sand flow measurement have been calculated as having a mean of 6.76% and standard deviation of 3.94% and for plastic beads is 5.43% and standard deviation of 0.21%. The results also demonstrates that the system is reasonably independent of flow regime and so the optical fibre system is suitable as a concentration meter.

Back projection is used to generate tomographic images as an alternative representation of the data on concentration measurement. This provides a visual representation of optical density (concentration) information which is not obvious from the concentration measurements.

Results from experiments on particles with different sizes are presented. The results are analysed using frequency spectrum techniques and shown to be dependent upon the particle size for approximately spherical particles with diameters between 600 μm and 5 mm.

Suggestions for further work on optical fibre sensors and optical fibre tomographic measurements are made.

Contents

CHAPTER 1

Introduction

1.1 An Overview of Process Tomography

Tomography comes from the Greek words tomo (slice) and graph (picture). As defined in one encyclopaedia (Helicon 1991) , it is the obtaining of plane section images, which show a slice through an object. In this project, the objective is to use arrays of optical fibres as the primary sensors to make tomographic measurements in pneumatic conveyors transporting dry powders. The measured data will be processed to generate, on-line, an image which displays the concentration and velocity profile over a cross-section of the conveyor.

Process tomography evolved in the late 1980's (Beck 1986) to meet a widespread need for the direct analysis of the internal characteristic of process plants in order to improve the design and operation of equipment. The measuring instruments for such applications must use robust non-invasive sensors which, if required, can operate in aggressive and fast moving fluids and multiphase mixtures. Process tomography involves using tomographic imaging methods to manipulate data from remote sensors in order to obtain precise quantitative data from inaccessible locations (Dickin *et al* 1991a). The need for tomography in process engineering is analogous to the medical need for body scanners, which has been met by the development of computer-aided tomography (Dickin *et al* 1991a).

Process tomography is a developing measurement technology. It is gaining attention from industry because of some recent successes and the increased work into various

fundamental aspects of the technology. This is demonstrated by the first international workshop on Process Tomography held in 1992 (ECAPT92 1992) and in three subsequent years which reported new sensing techniques, new algorithms and began to address the fundamental challenges such as spatial resolution, speed of acquisition, quality of information and other factors that are essential to make the technology acceptable to industrial practice.

The specific characteristic of tomographic measurement is its proven ability to interrogate the dynamic state of a process condition within a unit operation such as a mixing vessel or conveyor without interfering with the process itself (Dickin 1992). This is achieved using non-invasive sensors along a cross-sectional boundary of the process equipment. The tomographic measurement data is manipulated using algorithms for image reconstruction, profile analysis and computation of numerical quantities such as flow rates, concentration, size and phase distribution.

From the knowledge of material distribution and movement, improved internal models involving kinetic and dynamic parameters can be derived and used as an aid to optimise process design. This is in sharp contrast to present day design methodology which usually assumes time and spaced averaged parameters such as well mixed reactors, completely fluidised beds, fully dispersed emulsions and so on.

Currently, models based on for example, a computational fluid dynamics approach, are used to simulate the internal phenomenon of a particular process (Dickin 1992). Tomographic techniques can contribute further by validating these models, which eventually may lead to better dynamic models when the two technologies are combined (Illyas and Williams 1993).

For instance process tomography will improve the operation and design of processes handling multi-component mixtures by enabling boundaries between different components in a process to be imaged in real-time using non-intrusive sensors. Information about the flow regime, vector velocity, component size distributions and concentrations in process vessels and pipelines may be determined from the images (Bidin 1993).

The basic tomographic system consists of an array of sensors around the pipe or vessel to be imaged (Dickin *et al* 1991b). The sensors output signals dependent on the position of the component boundaries within their sensing zones. The sensor signals are transferred to a computer which is used to reconstruct a tomographic image of the cross section being observed by the sensors.

Tomographic imaging techniques are widely used for medical diagnosis (Nordin 1995). Many techniques, such as X-ray computerised tomography (Banholzer *et al* 1987) and Positron Emission Tomography (Bemrose *et al* 1988) have been successfully developed for medical applications. But these radiation-based source methods require expensive radiation detecting sensors. Their use is also undesirable on the grounds of safety. Nuclear Magnetic Resonance (Mckee 1995) has also been very successful, but the high cost of magnets and associated circuits limits the present areas of application. Ultrasound and electrical sensing methods are alternative and safer techniques (Hoyle and Xu 1995).

The need for process imaging is analogous to that of medical imaging. In the process industry, information describing material distribution and validating internal modes of the process are necessary for the optimum design and operation of process equipment.

Hence, there is need for the process engineer to be able to visualise the inside of the mixing vessel or reactor, thus relevant measurement techniques are necessary. However, complex experimental approaches are not economically viable for many process design and operation needs. For these latter cases, the process tomography approach using simple non-invasive sensors has much to offer.

1.2 Use of tomography in powder and particulate processes

Pneumatic and hydraulic conveying is currently used to transport solids over distances ranging from a few metres to several kilometres, and may often offer a less expensive method of transport than conventional road or rail. Further, the use of a pipeline designated for the conveying of a specific substance, such as a pharmaceutical products, will negate the possibility of any extraneous contamination.

In pneumatic conveying, particles are moved by drag forces from the air flow. The parameters which affect the conveying process include the flow velocity, distribution of gas/solid fraction, the pressure gradient and physical size distribution of the material. These may all contribute to the different flow characteristics or regimes in the conveying pipeline, and thus effect the efficiency of energy consumption (Beck 1986) or cause blockage and damage to pipes.

In horizontal pneumatic conveying, the flow regimes generated depend primarily upon the conveying gas velocity. In dense phase transport, where the conveying gas velocity is relatively low, the distribution of solid particles tend to become less uniform and form a moving bed on the base of the pipeline. At a critical deposition velocity, particles will deposit on the surface of these beds, an effect known as saltation (Rhodes 1990).

Hence, knowledge of these regimes, in particular when an internal image is made available, will help to monitor effects during transport.

On the other hand, in vertical pneumatic transport, at low gas velocities and high solids loading, that is dense phase conveying, the particles move in 'clouds' through the pipe in a flow regime very similar in formation to slug flow in gas/liquid transport. At high gas velocities and low solids loading, that is light phase conveying, the flow has a more uniform distribution, At lower gas velocity, a transition from homogeneous or uniform flow to annular flow is observed. This transition may be a useful parameter for plant control if it can be monitored; tomography would have the ability to provide near real time information about these regimes (Bidin 1993).

Another type of conveyor is the gravity drop feeder. It is a form of conveyor where gravity produces the movement of the particles. It is used in the work presented in this thesis. In order to simulate some operational aspects of a normal pneumatic conveyor artificially induced concentration profiles (section 3.4.2) are used.

Many measurement techniques have been applied to pneumatically transported powder and particulates (Henry and Beck 1977, Yan *el al* 1992). Tomography will provide an increase in the quantity and quality of information available when compared to earlier techniques.

The information that can be derived from the tomography sensors will enable velocity and concentration to be determined over a wide range of flow regimes by providing better averaging in time and space through multi-projections of the same cross-section.

1.4 Aims and objectives of the thesis

The aim of the thesis is to investigate the feasibility of using optical fibres for concentration measurement and tomographic imaging.

The specific objectives of this thesis are :

1. To become familiar with the concepts of process tomography, associated sensor technology and optical fibres.

2. Investigate design parameters associated with using optical fibres as optical sensors. Produce a model of an optical fibre concentration measurement system.

3. Design and test an optical fibre sensor which will detect dry flowing powders.

4. Design and implement two arrays of optical fibre sensors around a measurement section.

5. Design and implement an electronic measurement system which will provide data from the optical sensors in a form suitable for processing to produce concentration profiles tomographic images and particle size determination.

6. Develop a reconstruction algorithm enabling data from the optical fibre measurement system to be processed and displayed to show concentration profiles and tomographic images.

7. Test the complete system on a gravity drop conveyor using a range of dry materials.

8. Consider the work presented in this thesis and make suggestions for further work.

1.4 Organisation of the thesis

Chapter one presents an introduction to process tomography.

Chapter two presents an overview of several sensing mechanisms for measurement using non-intrusive techniques.

Chapter three consists of two parts. The first part describes modelling to predict the optical sensor output voltage profiles arising from different, artificially produced flow regimes. The second part describes an image reconstruction method for optical tomography.

Chapter four discusses the complete optical fibre tomographic measurement system, including preparation of the optical fibre and design of the transmitters and receivers.

Chapter five presents results of concentration measurement.

Chapter six presents results of concentration profiles and tomographic images.

Chapter seven presents results of particle size measurements.

Lastly chapter eight discusses the conclusions to be drawn from this work and makes suggestions for future work.

CHAPTER 2

Review of Tomography Sensors and Applications

2.1 Introduction

This chapter provides an overview of measurement systems for process tomography applications. The structure of a typical capacitance tomography system is shown in figure 2.1.

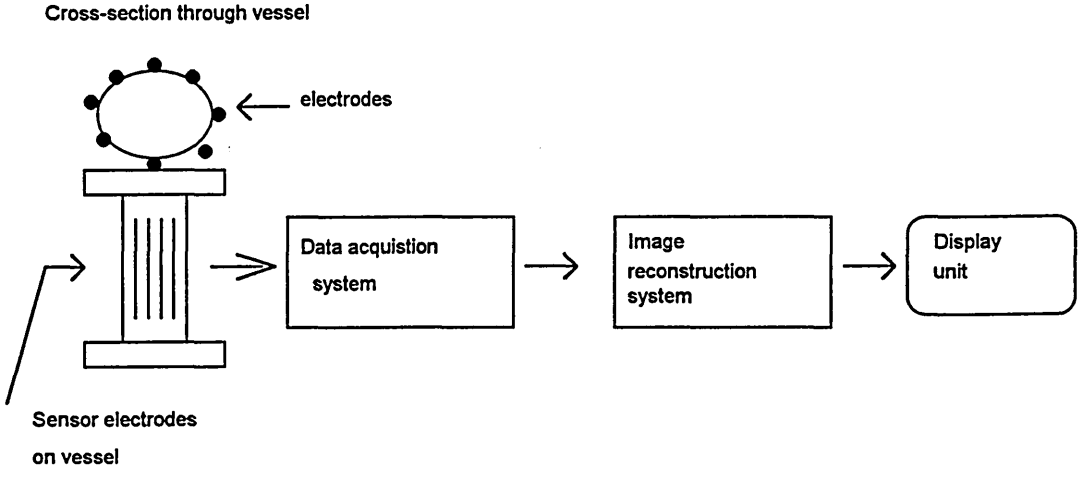

Figure 2.1 Process tomography system using capacitance electrodes.

2.2 Tomography sensors

There are three basic components in a typical process tomography system :

a. The sensors

b. The data acquisition system

c The image reconstruction system and display.

Sensor technology is the most essential and critical part of any measurement system (Dickin *et al* 1991a). The sensors in a tomography system are usually placed in a circular array around the circumference of the process vessel. This is to provide multiple projections of the object or event being measured. The main advantage derived from such a configuration is multi-component spatial distributions can be obtained through image reconstruction techniques.

There are many reports on work relating to imaging of liquid-liquid and gas-liquid flows (Dickin *et al* 1991). Two possible reasons for this are the interest of oil production companies in using capacitance techniques for oil production pipeline monitoring (Huang 1988) and the direct applications of medical electrical impedance tomography (Barber and Brown 1984) to mixing, hydraulic transport and separation processes in the process industry.

There are few reports of work to visualise the flow of pneumatically conveyed solids from physical measurements. However, experimental work done using liquid media does not necessarily exclude the use of the basic principles for gas/solids flow. For example, Plaskowski *et al* (1991) developed an imaging system for two component air/solids flow intended for the food industry using capacitance transducers.

The following subsection provides a short review of several process tomography systems currently being investigated.

2.2.1 Positron Emission Tomography (PET)

Positron emission tomography is based upon the distribution of activity of positron emitters. The fundamental measurement is the coincidence detection of two almost non-

parallel photons, which are emitted as a result of the annihilation of a positron with an electron. A function of position and time in relation to the emitters is obtained from external coincidence measurements. Imaging systems involve either circular geometry, with rings of sensors around the flow to be imaged, or position sensitive detectors, such as gamma cameras or multiwire proportion chambers. (Parker *et al.* 1992)

Applications in medicine include studies of blood flow and oxygen distributions. The technique was pioneered after being used by high energy physicists in particle physics experiments, and is now being applied to areas such as the study of the mechanism involved in mixing processes (Bemrose *et al.* 1988). The advantage and characteristic of this method of imaging is that it pinpoints the positions of individual particles in the medium, and not bulk masses as in X-ray tomography. The disadvantages of the system relate to safety problems which arise from the use of the radioactive isotopes required to produce the positron emissions and the fact that the isotopes have to be injected into the flow. The cost and size of the detectors are also a limitation. This limits its present applications to laboratory studies or processes where injection and mixing are easy to arrange.

2.2.2 X-rays

X-ray transmission computed tomography is one of the main imaging techniques used in diagnostic medicine (Nordin 1995). It was through its success at solving medical imaging problems that it was chosen to be applied in other areas such as engineering.

Two kinds of X-ray imaging are X-ray transmission radiography and X-ray transmission tomography (Simon, 1975) For X-ray transmission radiography, the image is static. It is

the shadow of the object formed by transmitted X-ray impinging on a detector such as a photographic film. This is not a desirable method where flow imaging is concerned, as it provides no method of providing a continuous image of the flow.

In X-ray transmission tomography, the concern is with the provision of images of a section or thin slices through an object at different depths. This is achieved by the carefully calculated and controlled relative motion of the X-ray source and the detector during the exposure. This technique has become known as computerised tomography, (i.e. CT scan). The equipment needed for this is large and bulky, and a high element of danger is involved due to the presence of ionising radiation (Simon 1975). This restricts its application for flow imaging in an industrial environment. Also, it is unlikely to be of use in light phase pneumatic conveying because of the low level of absorption or scattering produced by the dispersed flowing solids.

2.2.3 Nuclear Magnetic Resonance (NMR)

Nuclear magnetic resonance imaging is also used in medicine (Pykett, 1982). Many atomic nuclei exhibit the property 'spin', and as a consequence possess a magnetic moment aligned along the axis of the spin. The spin is quantified, and is characterised by the quantum number I, which may be either an integer or half integer. The nuclei most commonly used in NMR are those with $I = 1/2$, e.g. hydrogen (Cady 1990).

When a nucleus with spin is placed in a magnetic field, it will attempt to line up with the applied magnetic field. With a quantum number $I = 1/2$, the nucleus can take up one of two stable states - namely parallel to the field, or in the opposite direction. These

correspond to high and low energy states, but there will be a bias to the lower energy state, as given by Boltzmann's equation:

$$N_{down} / N_{up} = \text{exp. } (hf / kT)$$

where N_{down}, N_{up} are the number of nuclei exhibiting spin up and spin down respectively, k is Boltzmanns constant, h is Planck's constant and T is the absolute temperature.

In this aligned state, the sample will achieve a net magnetisation, which is the quantity observed in NMR, and is proportional to the applied field - so a higher applied field gives a greater sensitivity. The magnetic field is applied by an RF magnetic field pulse generator, and the received signals are weak, free induction signals emanating from the subject. The actual image obtained is of proton density within the subject. This is an expensive way of imaging due to the cost of the magnets and at present is only suitable for laboratory investigations but not viable for imaging flows in large process vessels or pneumatic conveyors.

2.2.4 Ultrasound

A major use for ultrasound imaging is in diagnostic medicine. Its distinguishing feature is its ability to provide accurate cross-sectional views of soft tissue (Crecraft 1983). Ultrasound waves are acoustic waves of the order of 18 kHz to 10 MHz in frequency. Imaging using ultrasound waves has been reviewed by Wells, 1977.

The equipment needed for ultrasound measurement include an ultrasonic generator, transducers to transmit and receive ultrasonic waves and a computerised image processing system. A technique known as Doppler ultrasound is used to image a moving interface (Kremkau 1990). An interface is the boundary region between two different

objects, or types of tissue. The ultrasound signal is strongly reflected wherever there is an interface between one tissue and another - allowing a degree of localisation and discrimination which is not possible with X-ray images. When the ultrasonic waves strike the moving interface, the frequency of the reflected waves is altered in proportion to the velocity of the moving interface. This technique can be used to visualise flow in blood vessels throughout the body (Jaffe 1984).

Ultrasound is now being applied to flow imaging in pipes, and research is being undertaken to develop a tomographic system for flow imaging in liquid borne mixtures with ultrasound. Research is now in progress at Leeds University (Li and Hoyle 1995) to explore the use of multiple active receiving sensors and multiple segmented receivers in ultrasonic process tomography. However, ultrasound has several specific problems which may limit its application to pneumatic conveyors where transport velocities are generally high for medium to light solids loading. The speed of sound in gas limits the data acquisition rate and particle impact on the flow pipe and sensors may produce very high levels of noise at the transducer. The ultrasonic transmitters often can be driven with voltages of hundreds of volts (Xu *et al* 1988) which makes an intrinsically safe system hard to develop.

2.2.5 Electrical Impedance Tomography (EIT)

Electrical impedance sensors have been used with success in process tomography (Abdullah *et al* 1993). Based on earlier work done by Barber and Brown (1984), Abdullah (1993) developed a system that can generate a sequence of images depicting the distribution of components or concentration profiles of components across a given plane within a reactor or pipeline as a function of time. Electrodes are placed into a

vessel wall in order to make measurements of the distribution of electrical resistance within an object plane. Measurements are performed by injecting an ac current via one pair of adjacent electrodes and measuring the voltages at all other pairs of adjacent electrodes. The procedure is repeated for all possible pairs of electrodes and is referred to as the 4-electrode adjacent pair measurement protocol (Dickin *et al* 1991b). The reconstruction of images from these data uses a series of procedures performed iteratively to determine the distribution of regions of different resistivities representing for instance, component concentrations within a cross section of the pipe or vessel.

This technique is being applied to industrial measurement where the process uses a conducting fluid to carry immiscible fluids and solids which possess different bulk conductivities. It cannot be used for pneumatic conveying which contain large electrically non-conducting solids.

2.2.6 Electrical Capacitance Tomography (ECT)

Electrical capacitance tomography (ECT) systems are suitable for imaging industrial multi-component processes involving non-conducting fluids (Xie 1993). An ECT system basically consists of three sub-systems, the primary capacitance sensor with multiple electrodes, the capacitance data acquisition electronics and the computer system for image reconstruction and process data interpretation.

Capacitance tomography involves taking a set of dielectric permittivity measurements from electrodes situated around the circumference of an imaging plane, and using the measurements to generate an image of the material lying within the imaged area. The process of generating an image from a measurement set is called image reconstruction,

and is a solution of the inverse problem; where the forward problem would involve a computation of the set of capacitance values from a known material distribution. In this case the resulting image is of the permittivity distribution of a cross-section, and from this the material profile can be deduced (Chen *et al* 1992)

However, accurate quantitative information from such a system is quite hard to obtain, due to the following five problems associated with the capacitance techniques (Isaksen and Nordtvedt 1992):

1. In X-ray tomography, a simple expression exists relating the measured quantity (the intensity of the transmitted photons) and the parameter whose distribution is sought. In capacitance tomography, however, there is no simple linear relation between the measured capacitance and the dielectric distribution.

2. In computerised tomography (CT), the use of a narrow, collimated X-ray beam ensures that the region of sensitivity for a given measurement is well defined; in a capacitance system, the electric field between the source and detector electrodes determines the sensitivity region, which does not posses a sharp boundary.

3. For capacitance tomography, unlike the CT, the sensitivity for the measured parameters is not constant within the region of interest.

4. In X-ray CT, the measurements have negligible sensitivity for changes in the attenuation coefficient outside the region of measurement; in capacitance tomography, there may be regions of negative sensitivity

5. The number of independent readings is small (<100) in present capacitance systems; this is because the electrode size cannot be decreased without limit, due to fringe field effects.

Capacitance systems are suitable for medium to high solid loading in process conveyors (Isaksen and Nordtvedt 1992). However, as the solids loading decreases the systems fail to produce meaningful images because of the relatively low signal to noise ratio of the capacitance to voltage transducer and non-uniform sensing fields (Xie, 1993). The existing ECT systems are unsuitable for light phase pneumatic conveying systems.

2.2.7 Optical Sensors (Visible and Infra-red)

This method has been developed by Dugdale *et al* (1991) based on an earlier theoretical investigation by Saeed *et al* (1988).

Optical systems can be used where the conveying fluid is transparent to the incident optical radiation. The received signals are modulated by the relative attenuation factors of the components in the flow.

Optical tomography involves projecting a beam of light through some medium from one boundary point and detecting the level of light received at another boundary point, this single beam is termed a view. Several beams of light are used in parallel to produce one projection. This procedure provides information from which a profile of the flow can be gained. In practice several projections are required to minimise aliasing that occurs when two particles intercept the same view. This process is described by Saeed, 1988, where two component flows are investigated.

Changes in a physical property (e.g. the optical density) of a volume of the mixture, are measured by arrays of transducers placed in a plane perpendicular to the direction of the flow. Information obtained in this way allows an image of the cross-section of the flow pipe to be reconstructed by a computer for display on a VDU.

An optical system can be designed using a pair of optical transducers (Dugdale *et al* 1993). The transducer pair consists of an infra-red emitting diode (LED) and a sensing photodiode (Dugdale *et al* 1993). Pulses of infra-red light are generated by the emitter and optically configured to form a collimated beam through the fluid in the pipe. The voltage generated by the sensor is related to the amount of attenuation in the path of the beam, caused by the flow regime. The analogue signals from an array of multiplexed sensors, covering a cross-section of a pipe, are converted into digital form and passed into an image reconstruction system. Data acquired in this way can form the basis for a number of reconstruction algorithms enabling an image of the cross-section of the flow regime to be created.

Such an optical system has a high data capture rate. Its major problem is due to the physical size of the transmitter and receiver which limits the obtainable resolution. Smaller optical devices will improve the resolution and enable optical systems to be applied to pneumatic conveying systems. These smaller devices can be based on optical fibres.

2.3 Tomographic Imaging System Using Optical Fibres

Optical fibres provide an opportunity to design sensors with a very wide bandwidth (Ghassemlooy 1992), enabling measurements of high speed flowing particles. To generate high resolution tomographic images, a large number of optical fibres are needed

(Snyder and Hesselink 1989) and this infers that high speed data acquisition must be used.

The proposed system will use multiple arrays of optical fibres as both light transmitters and receivers. Light will ideally be generated as collimated beams. Collimation increases beam intensity and ensures that a particular sensors only detects light from its corresponding emitter. It also enables the use of reconstruction algorithms developed for medical x-ray tomography (Dugdale *et al* 1993). Collimation also results in the detected optical intensity being dependent on the length of attenuating component traversed by the beam, and relatively independent of the distance of the attenuating component from the source (Dugdale *et al* 1993).

The fibre optic based measurement system is described in the chapter four.

CHAPTER 3

Modelling and the reconstruction algorithm

3.1 Introduction

This chapter consists of two parts. The first part describes modelling to predict the sensor output voltage profiles arising from different artificially produced flow regimes. The method used to produce the flow regimes is described.

The second part describes the back projection used for tomographic image reconstruction in chapter seven..

3.2 Arrangement of transducers

A single transducer pair, termed a 'view', provides very limited information about the solids flow since it only interrogates a small regime of the cross-section. A tomographic image requires many views to be used and these may be arranged into several parallel groups; where each parallel group is termed a projection. These projection measurements provide significantly more information about the flow in the measurement cross-section than the single fibre.

Various sensors have been developed for flow imaging and these have various forms of projection associated with them (figure 3.1)(Plaskowski *et al* 1995). Figure 3.1a shows the parallel projection frequently used with radiation methods, such as X-rays, gamma rays, and light. A technique in which a single photon-energy measuring detector and a multi-channel analyser is used with a number of radiation sources each having a different energy is shown figure 3.1b (Omotosho *et al* 1989). Figure 3.1c shows an ultrasonic

echo method where the same sensor can be used for transmission and reception, the ultrasonic echo gives information on the presence and on the distance of the flow component in the object space, in contrast to the other forms of projection described which only indicate that an object is present along the interrogated beam without reference to its position. Figure 3.1d shows the electrostatic field sensing zones which are encountered when using capacitance sensing plates distributed around the surface of the pipe.

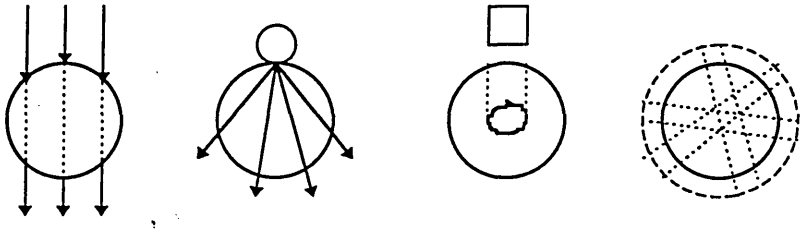

(a) Parallel projection **(b) Fan beam projection** **(c) Ultrasonic echo projection** **(d) Electrostatic field projection**

Figure 3.1 Various forms of projection

3.2 Optical transducer arrangement

Two ways of arranging views of optical transducers are with the transducers aligned at intervals along a cross-section or diametrically around the pipe (figure 3.2).

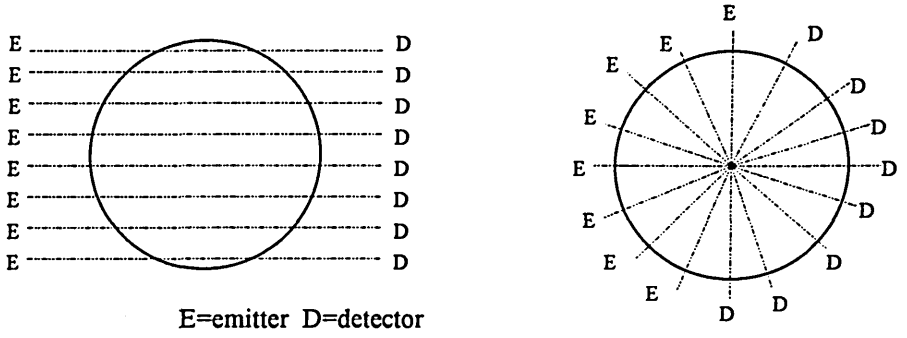

Figure 3.2 Different arrangements of optical views

The diametric arrangement provides an uneven resolution across the pipe, high at the centre and low at the sides. Also, since only one beam will intercept a small object, placed between the emitter and the centre of the pipe, there is no way of positioning the obstacle along the radius, so this arrangement is rejected. However, if the obstruction is detected by two orthogonal beams, the intersection of the beams corresponds to the position of the obstacles.

With the parallel arrangement of beams, several projections can be placed around a pipe (figure 3.3). This arrangement provides intercepting views, enabling particles to be positioned in space. Two projections still restrict the total information required for a complete reconstruction and give rise to aliasing. In aliasing the position of some particles is ambiguous (Dugdale, et. al 1992). However, two projections are sufficient to investigate the feasibility of using the optical fibre system for concentration measurement and concentration profile measurement.

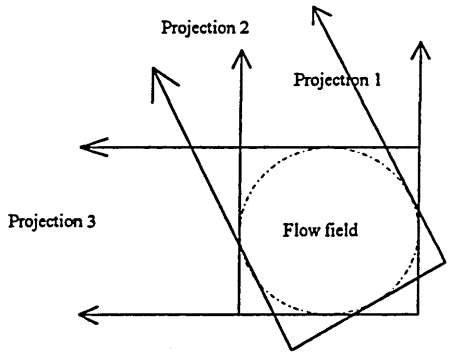

Figure 3.3 Example of a three projection tomographic system

3.3 Volume of measurement section interrogated by the optical fibre sensor

This section investigates the volume of the measurement volume actually interrogated. The fibres are mounted into slots machined into the measurement section in an invasive

but non-intrusive (i.e. the flow pattern is not affected by their presence) manner. In order to investigate the feasibility of the proposed system two arrays of sixteen transducers each are placed along orthogonal projections (Figure 3.4). This choice of sixteen per projection is a compromise between high resolution (more sensors) and the limited financial budget available for the project.

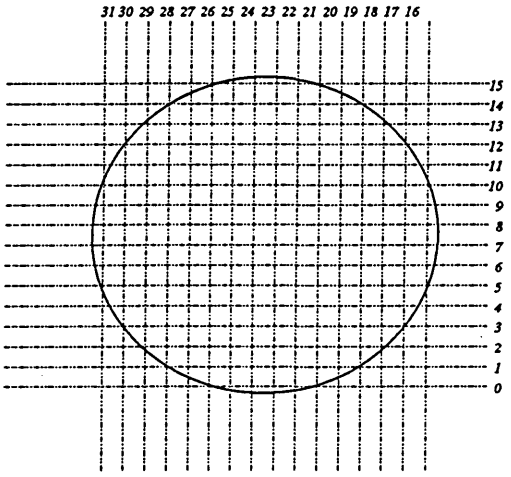

Figure 3.4 Arrangement of two orthogonal 16 transducer projections

Figure 3.5 shows the beam width and spacing inside the pipe for one array.

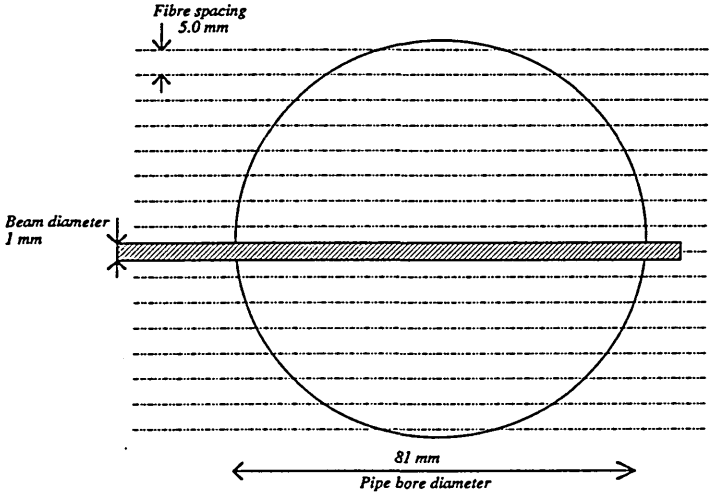

Figure 3.5 Dimensions of 16 transducer projection

The pipe in which the sensors are mounted has a nominal bore of 81 mm with a sensor spacing of 5 mm. This spacing means, with an optical fibre diameter of 1 mm, that approximately one fifth of the cross-section is directly interrogated, the remaining four fifths not being in a direct path between a source and its receiver, though there may be some output due to the beam spreading out from the transmitter fibre due to its optical aperture and light scattering by the particles. The effects of diffraction and scattering (section 5.1.4) are ignored, because the primary effect is attenuation of optical energy by particles intercepting the beam. Thus each fibre is taking only a sample measurement of the particles flowing in the pipe. However, it is assumed that each fibre produces readings which represent a realistic sample of the solids passing through the space at each side of the fibre.

Although the transmitted beam diameter expands to a maximum of 4 mm, the width of the detected beam is only 1 mm, the diameter of the optical fibre. Then the total volume of the measurement section, V_T being interrogated is

$$V_T = \pi \frac{d^2 l}{4}$$
$$= 5.15 \times 10^3 \text{ mm}^3$$

where d=81 mm, l=1 mm is the width of the fibre.

The volume being monitored by each projection of sixteen views, V_{16} is

$$V_{16} = \pi \frac{l^2}{4} \left(\sum_0^{15} \text{path length}\right)$$
$$= 796 \text{ mm}^3$$

This means that, neglecting the effect of crossing beams, each projection provides a statistical sample consisting of 15.4% of the flow in the sensing volume. With two projections approximately 30% of the volume is sampled. To increase this resolution either the sensors could be spaced at 2.5 mm without the expanded beams over-lapping the detectors or the transmitters could be interspersed by receivers. This would enable a 32 x 32 arrangement to be attained, and the volume sampled to be 60% (section 8.3).

In light phase conveying, on average, only single particles will intercept the beam at a given instant. Then with a uniform particle distribution for a given sensing volume the number of particles intercepted by a beam will be a linear function of concentration,

$$V_i \propto \text{concentration (C)} \tag{3.1}$$

where the voltage, V_i, is the output of the ith transmitter receiver pair. The voltage will also depend on the path length of the beam inside the conveyor for a given concentration,

$$V_i \propto \text{path length of i th beam } (P_i) \tag{3.2}$$

Therefore,

$$V_i \propto C\, P_i \tag{3.3}$$

However, within a gravity conveyor the concentration at any cross-section below the feeder is linearly related to the mass feedrate $\dot{m}$ assuming a uniform concentration profile. Thus the voltage detected by the i th sensor, V_i, is given by

$$V_i = kP_i\dot{m} \tag{3.4}$$

where k is a constant of proportionality. Each sensor voltage is an estimate of the local solids concentration, which is time averaged by computer processing after data acquisition (section 4.5). The sum of all voltages is an estimate of the total concentration. The sum of the sensor voltages is obtained by summations of equation 3.4 over all the sensors.

Therefore

$$V_{Total} = \sum_{i=0}^{31} V_i = k \dot{m} \sum_{i=0}^{31} P_i \qquad (3.5)$$

3.4 Volume sensing by multiple fibre

3.4.1 Artificial flow regime production

The pipe on the flow rig has been fitted with a shaped cut-off blade in the path of the oncoming sand flow (figure 3.6). This blade is positioned approximately 15 cm below the screw feeder (figure 3.7), to artificially create a range of separated flow regimes (chapter 6).

The regimes created and tested are:

1. Full flow

   This is generated by not putting any obstacle in the pipe so that a full, continuous flow is obtained (figure 3.6a).

2. Three quarter flow

This is created by the baffle blocking a quarter of the pipe diameter and leaving the other three quarters clear for sand flow (figure 3.6b)

3. Half flow

This is created by the baffle blocking half the pipe diameter and leaving the other half clear for sand flow (figure 3.6c).

4. Quarter flow

This is created by the baffle blocking three quarters of the pipe diameter and leaving the other quarter clear for sand flow (figure 3.6d)

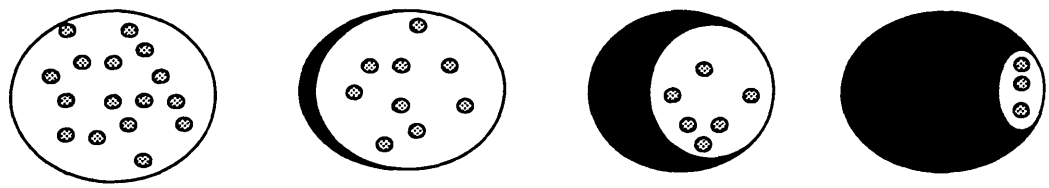

a. Full flow **b. Three-quarter flow** **c. Half flow** **d. Quarter flow**

Figure 3.6 Diagram of baffle configurations for generating flow regimes

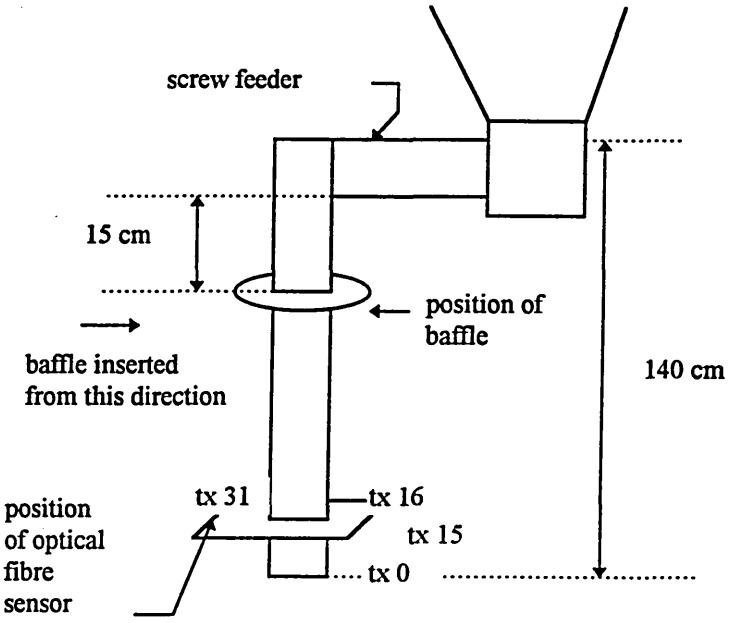

Figure 3.7a Flow rig

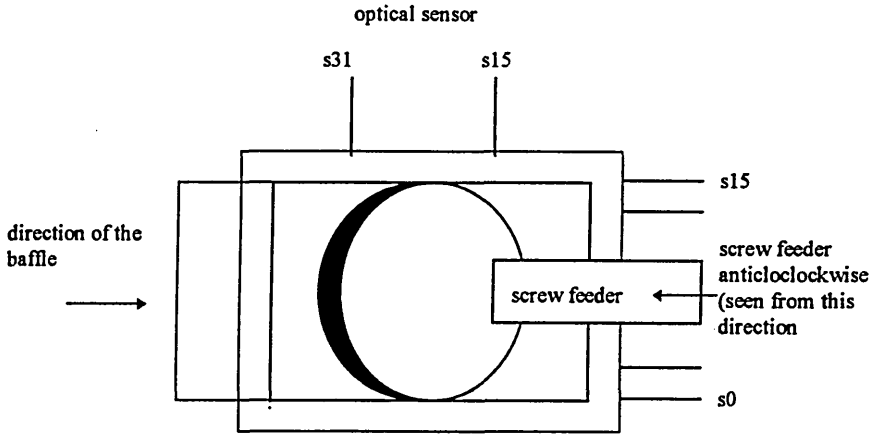

Figure 3.7b Plan view of the flow rig

Assuming that the solids drop vertically downwards from the baffle, i.e. the flow pattern is the same as the baffle shape, the measurements to be expected from the sensor array may be predicted. The predicted values are compared with the measured values in section 5.2.1

3.4.2 Predicted response of optical fibre arrays to artificial flow regimes

3.4.2.1 Full flow

The volume of the measurement section interrogated by a single beam is a linear function of the beam's length in the pipe (Table 3.1). With a uniform distribution of particles within the conveyor, the individual sensor outputs will be proportional to their path lengths (equation 3.2).

Sensor number	Path length-mm
0, 15, 16, 31	26
1, 14, 17, 30	46
2, 13, 18, 29	57
3, 12, 19, 28	67
4, 11, 20, 27	73
5, 10, 21, 26	77
6, 9, 22, 25	80
7, 8, 23, 24	81

Table 3.1

Using table 3.1 the output voltages to be expected from the individual sensors may be calculated. The result is shown in figure 3.8 in the form of a voltage profile. The shape of this profile is independent of solids flow rate as the only assumption is for a uniform solids distribution. However, the graph can be scaled for any desired flow rate by multiplying each reading by a suitable scaling factor. The scaling factor may be obtained using physical measurement in a flow rig to obtain voltages at a known flowrate and then

dividing the total path length into the sum of the measured voltages. Each optical fibre path length is multiplied by the scaling factor to obtain quantitative values for the profile.

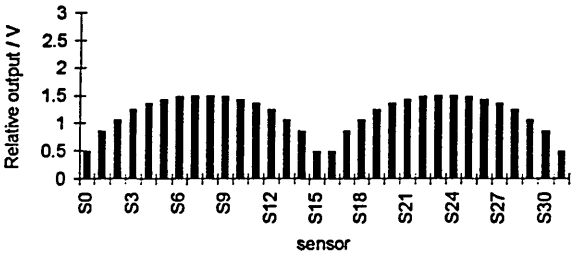

Figure 3.8 Predicted output voltage profile for full flow

3.4.2.2 Three quarter flow

The process outlined in section 3.4.2.1 may be applied to the other profiles. Figure 3.9.

Table 3.2 shows the path length of the optical fibre.

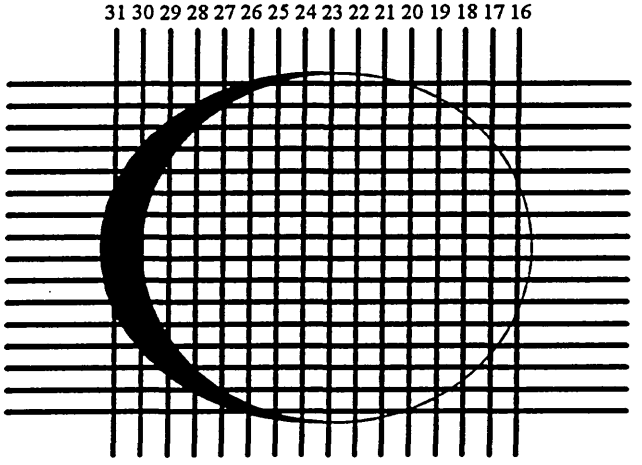

Figure 3.9 Position of the baffle

The individual fibre path lengths may be determined by scale drawing and measurement using figure 3.9. The values are listed in table 3.2.

Sensor number	Path length mm
0, 15, 16	26
1, 14	42
2, 13	53
3, 12	60
4, 11	66
5, 10	69
6, 9	72
7, 8	73
17	46
18	57
19	67
20	73
21	77
22	80
23	81
24	80
25	76
27	65
28	55
29	41
30, 31	0

Table 3.2

The path lengths shown in table 3.2 are converted to a voltage profile in a similar manner to section 3.4.2.1 and the resulting profile shown in figure 3.10.

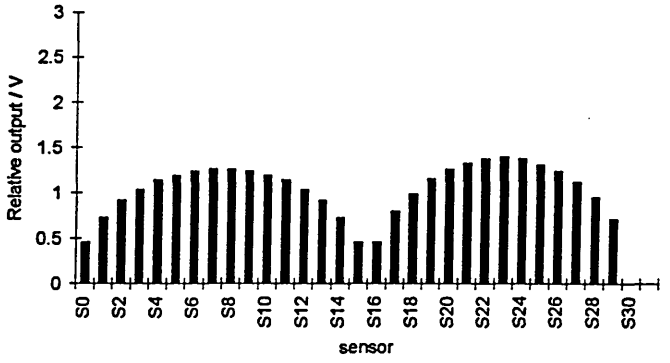

Figure 3.10 The predicted output for three quarter flow.

3.4.2.3 Half flow

The calculations shown in section 3.4.2.1 are repeated for half flow. Figure 3.11 shows the actual position of the baffle compare to the optical fibre.

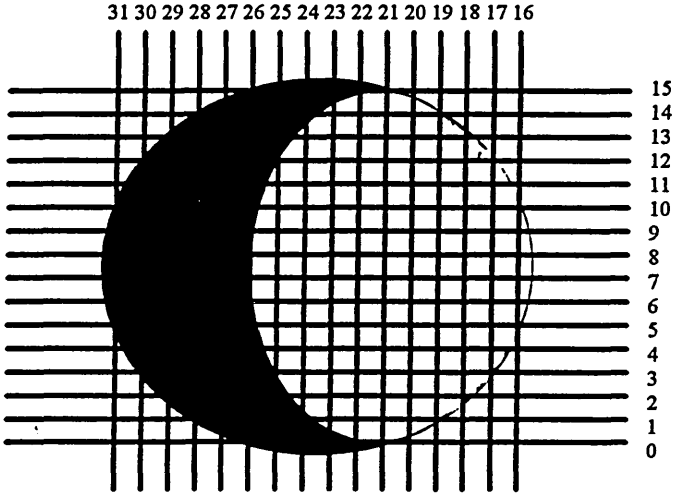

Figure 3.11 Position of the baffle for half flow

The path lengths have been determined by scale drawing and are shown in table 3.3

Sensor number	Path length mm
0, 15, 26, 27, 28, 29, 30, 31	0
1, 14	22
2, 13	33
3, 12	41
4, 11	45
5, 10	49
6, 9	51
7, 8	53
16	26
17	46
18	57
19	67
20	73
21	77
22	75
23	71
24	63
25	45

Table 3.3

These path lengths are converted to a voltage profile in a similar manner to section 3.4.2.1 and the profile is shown in figure 3.12.

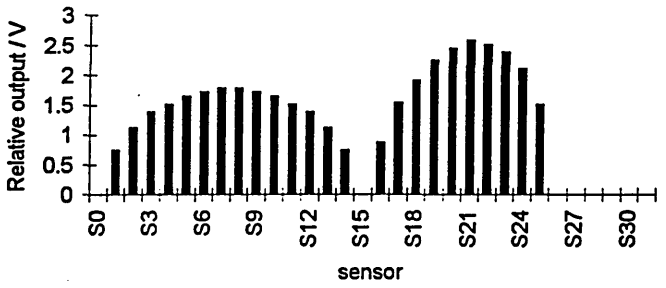

Figure 3.12 Predicted output voltage for half flow

3.4.2.4 Quarter open

The optical path lengths for quarter flow are now determined. Figure 3.13 shows the actual position of the baffle compare to the optical fibre.

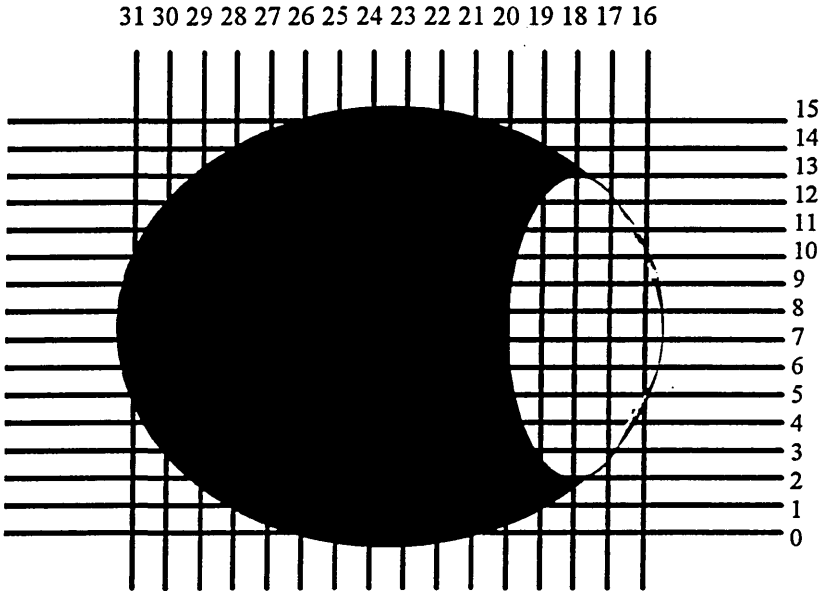

Figure 3.13 Position of the baffle

The individual path lengths are shown in table 3.4.

Sensor number	Path length mm
0, 1, 2, 13, 14, 15, 20, 21, 22, 23, 24, 25, 26, 27, 28, 29, 30, 31, 27, 28, 29, 30, 31	0
3, 12	11
4, 11	17
5, 10	19
6, 9	22
7, 8	23
16	26
17	46
18	57
19	47

Table 3.4

The flow profile has been determined using the path lengths of table 3.4 and are shown in figure 3.14.

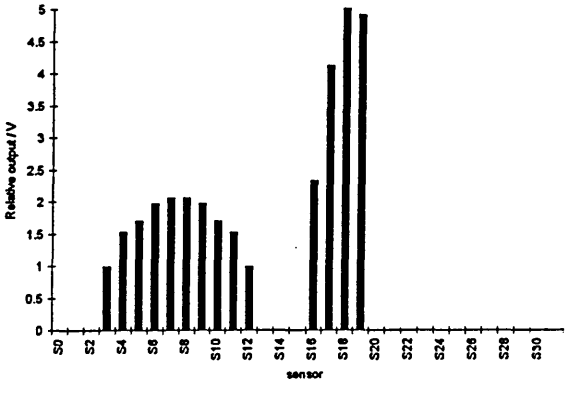

Figure 3.14 Predicted output voltage for quarter flow

The expected flow profiles have been determined for four artificial flow regimes using equation 3.2. These predicted profiles are tested in chapter 5.

3.5 Image reconstruction

3.5.1 Introduction

In this work visible light is used for scanning the two component flow to enable the beams to be set up visually. In optical transmission systems the radiation is attenuated when the optical beams traverse the system. The laws governing light are complex (Longhurst, 1957), but with approximations, they can be simplified. So, for the purpose of the reconstruction algorithm it is assumed that the beams of light travel in straight lines and are only attenuated (Nordin 1995). In the next sub-section the theory of the method used, which is based on the principle of optical attenuation, is described.

3.5.2 Mathematical preliminaries

In the following analysis the effects of reflection and refraction are neglected and only attenuation is considered. The linear attenuation coefficient μ, is used to describe the optical attenuation property of an isotropic medium. For optical radiation (Nordin 1995),

$$I = I_o \exp. (-\mu s) \qquad (3.6)$$

where, I_o = original intensity of source

I = measured intensity

μ = linear attenuation coefficient

s = thickness of object

Figure 3.15 shows the co-ordinate system used to describe the flow pipe. Points within the object are described by a fixed (x,y) co-ordinate frame.

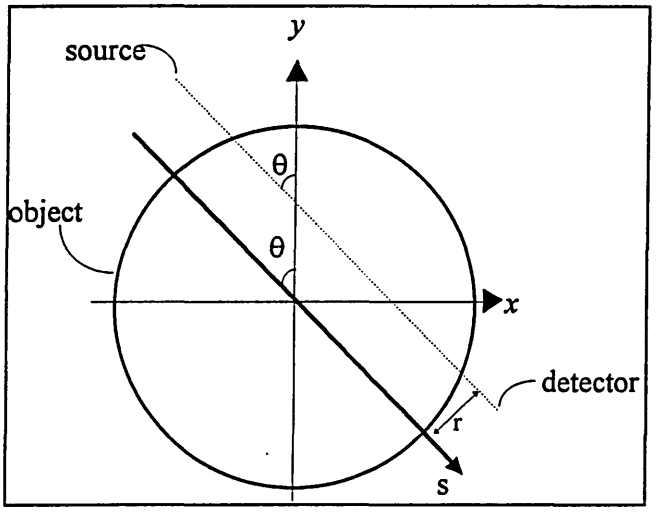

Figure 3.15 The co-ordinate system.

A straight line from the source to the detector, which the path of the radiation (visible light) follows, is termed the ray-path or view. Each ray is represented by a polar co-ordinate system (r,θ), where r is the distance from the origin and θ is the angle of the ray with respect to the y-axis. The s co-ordinate denotes distance along the ray.

The optical density function $f(x,y)$, denotes the contribution of each point on a given ray towards the final detected image. Given our co-ordinate system, the total attenuation along that ray is given by the line integral,

$$p(r,\theta) = \int_{r,\theta} f(x,y)\, ds \qquad (3.7)$$

where

$$f(x,y) = \mu s$$

i.e. $I = I_o \exp.(p(r,\theta))$ (3.8)

In a discretised system, such as that considered here, each ray path is divided into n segments, each of length D. Then

$$\int_{r,\theta} f(x, y)\, ds = \sum_{i=0}^{n} \frac{-\mu_i D}{n} = \frac{D}{n} \sum_{i=0}^{n} (-\mu_i) \quad (3.9)$$

Therefore, for a constant distance across a circular pipe and a constant light intensity the received light strength is a function of the average attenuation coefficient over the path length.

3.5.3 Image reconstruction for optical tomography

The physical limitations in real-time industrial applications infer it is not possible to obtain a large number of projections using optical tomography. Therefore the work presented in this thesis provides an approximate answer which contains the principal features of a more exact solution. The algorithm used in this thesis was developed by Nordin for an optical tomography application (Nordin 1995). The algorithm is based on a layergram (Gabor 1982) and is a simplification of the back projection algorithm.

Measurements of light intensity passing through an object at a certain cross-section make it possible to calculate the internal distribution of optical density. The reconstruction problem is stated as follows: estimate from a finite number of projections the density distribution in the section of the original object. The principle of measurement acquisition is shown in figure 3.16.

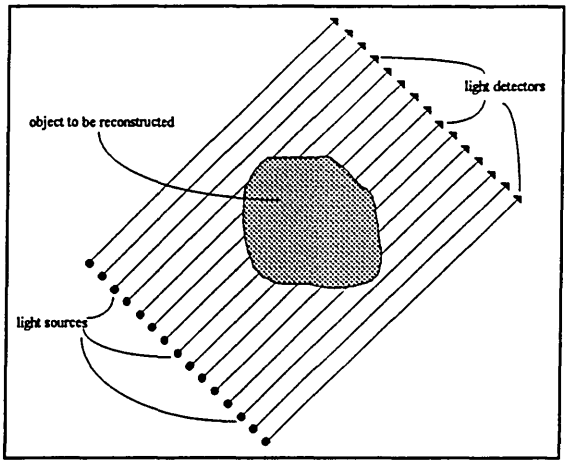

Figure 3.16 Acquisition of the projections

The ray intensity decreases with the density and the length of material passed through. The ray attenuation, called the ray sum, P_k, (equation (3.10)) is proportional to the natural logarithm of the ratio of the incident ray intensity to the passed ray intensity. P_k is the line integral along the ray path of the object density. To solve the integral equation that characterises the image reconstruction problem, the continuous function corresponding to the object density should be determined, however, the problem also can be stated in a discrete way, by dividing the cross section in to n small finite squares (*i.e.* pixels) as shown in Fig. 3.17.

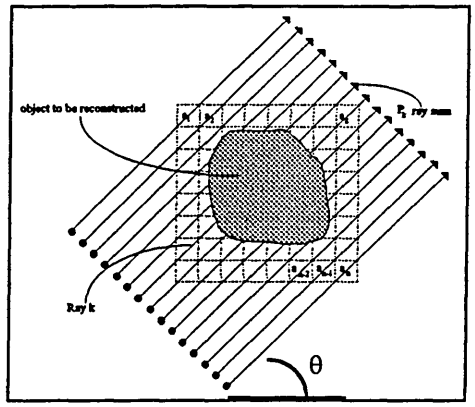

Fig. 3.17 The square pixels model for optical tomography image reconstruction showing projection inclined a θ° to the horizontal

Thus

$$P_k = \sum_{i=1}^{n} a_i w_{ik} \qquad (3.10)$$

$i = 1, 2, ..., n$ for each ray,

where P_k is the ray sum of the kth ray (*i. e.* ray attenuation), a_i is the value of the ith pixel, and w_{ik} is a geometric factor corresponding to the effect of the kth ray on the ith pixel; it is zero if the ray does not pass through the pixel. The image reconstruction problem is to determine the pixel values $a_1, a_2, \ldots, a_n$ from the set of ray sums P_k. This work uses the back-projection method because it is straight forward and the optical data is limited to two projections (θ = 0°, θ = 90°).

3.5.4 The Back Projection Method

The technique used in this algorithm is referred to as back projection between view lines. The view line consists of pixels along the line between the transmitter and the receiver

position. The ray-sum values at the receivers are back projected to light intensity values in the area between the two overlapping lines as shown in figure 3.18.

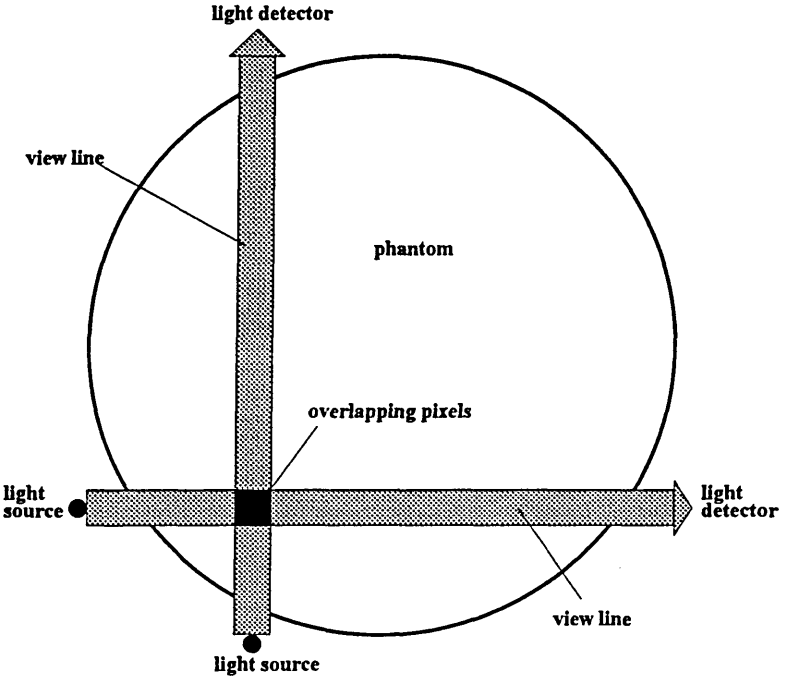

Figure 3.18 Overlapping pixels for two view lines

The density for each point in the reconstructed image is obtained by summing up the densities of all the rays which pass through that point. The magnitude of each ray-sum is applied to all points that make up the ray. The process may be described by the equation (Nordin 1995)

$$\hat{f}(x,y) = \Sigma_{j=1}^{m} P_j(x \cos\theta_j + y \sin\theta_j)\Delta\theta \qquad (3.11)$$

which is the general case for m projections ,where

θ_j = is the jth projection angle,

$\Delta\theta$ = is the angular distance between projections and the summation extends over all the m projections.

$\hat{f}(x,y)$ is only used to emphasise that the density values are not equivalent to the true densities f.

Therefore for a constant distance across a circular pipe and a constant initial light intensity, the final light intensity measured at the receivers is obtained by summing up all the pixel values of all the rays which pass through the sensing path as shown in figure 3.19. Hence, for the limited data provided by the two projections, the whole of the pipe cross section, which is represented by 16×16 squares, can be obtained by superimposing the sensitivity paths produced by each projection.

This reconstruction algorithm is designed to reconstruct images where two orthogonal projections are used (figure 3.19). There are 16 parallel beams for each projection. Each beam is regarded as having one source and one detector. The output signals from the detectors are pre-processed so that a zero value is obtained if the beam traverses an empty pipe and a maximum value (5V) is obtained if the beam traverses an opaque section (Nordin 1995) with a linear relationship between voltage and mass flowrate between these two values. Pixels outside the circle representing the pipe must contain air. This *a priori* knowledge enables all such pixels to be automatically assigned a zero value.

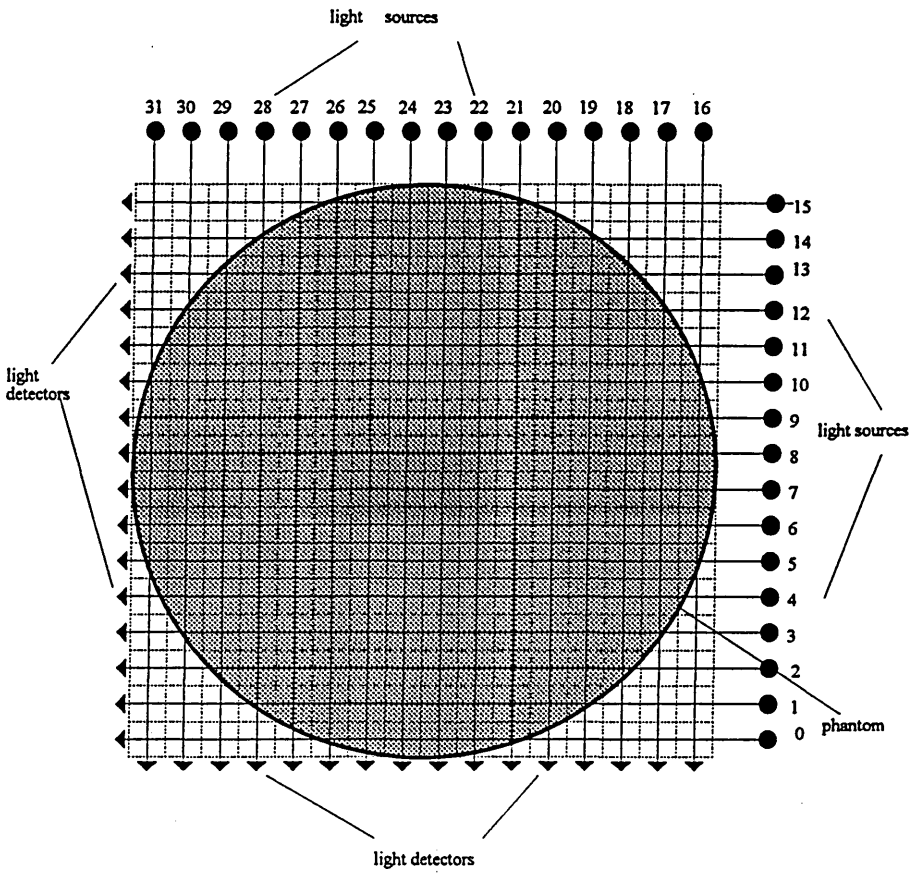

Figure 3.19 The square model used for the reconstructed image

When the 16 x 16 matrix values have been calculated the values are imported into Matlab to create a picture for each flow as shown in chapter 6.

The overall function of the reconstruction algorithm can be summarised by the following segment of pseudo-code and the flowchart shown in figure 3.20. Note that the temporary sum equals the number of air pixels in a view multiply by the optical density expected of air pixels.

The reconstructions are done off-time and typically take four minutes using a personal computer 486DX 33.

```
BEGIN

    Read input values for all views

    REPEAT

        Check if ray sum for this view represents air

        IF represent air THEN indicate all pixels for this view as air pixels

    UNTIL end of view (i.e. 32 views)

    REPEAT

        REPEAT

            Check if pixel_j in this view is air pixel

            IF air pixel THEN accumulate temporary ray sum

            ELSE increment counter for pixel not air

                store the position of j

        UNTIL (j > 16)

        Assign all pixels that are not air =

            (measured ray sum - temporary ray sum) / total pixels not air

    UNTIL end of projection (i.e. 2 projections)

END
```

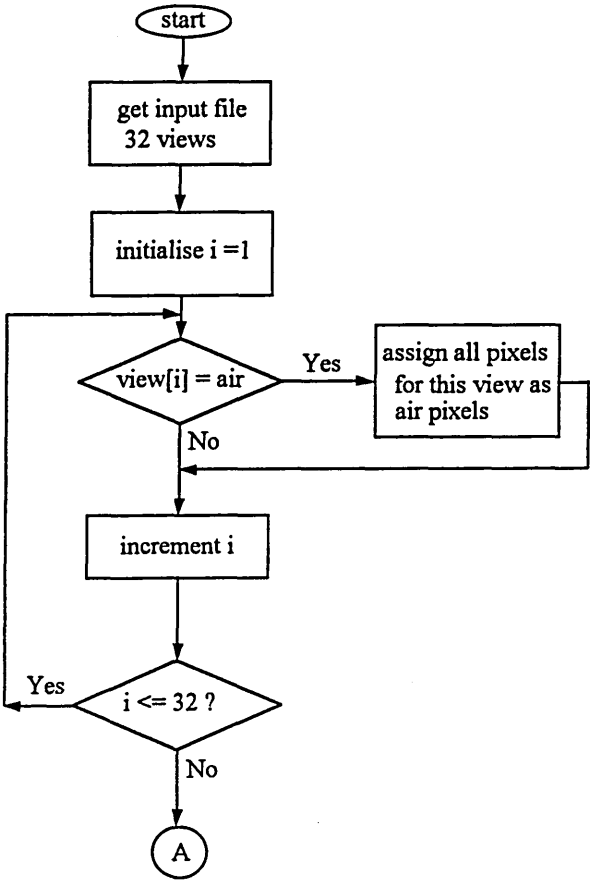

Figure 3.20a Flowchart to reconstruct the image for an optical system (continued on next page)

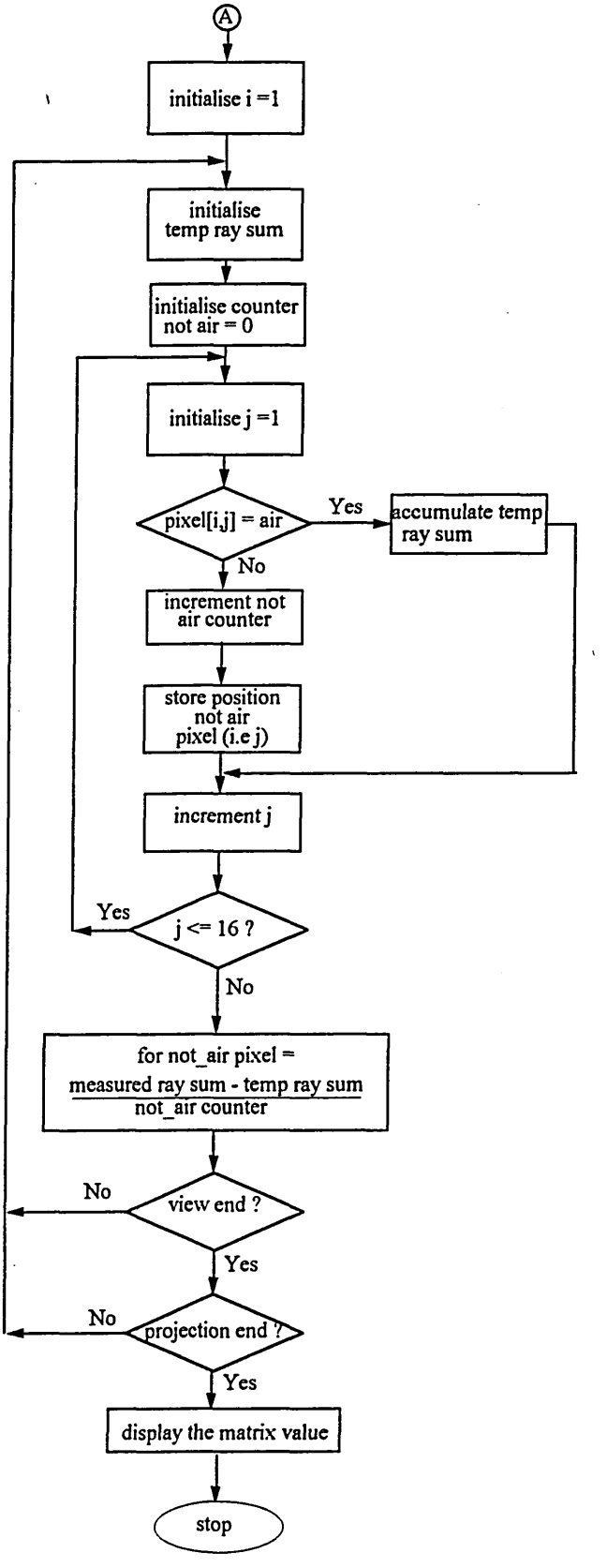

Figure 3.20b Flowchart to reconstruct the image for an optical system

CHAPTER 4

The measurement system

4.1 Introduction

This chapter describes the design of the individual components which combine to form an optical tomography system.

In order to select the optimum pair of transducers it is necessary to consider the requirements of the proposed system, which is to have transducers arranged around a flow pipe to simulate industrial conditions. Secondly one must consider the requirements of the optical imaging process, i.e. the radiant intensity of the transmitter, and for the receiver the luminous sensitivity (how much current to expect for a given illuminance), responsivity (how much current to expect for a specified amount of radiant power), noise threshold (smallest signal it is possible to detect), the leakage current and the speed of response. For a semiconductor receiver a small surface area helps these last three (Chaimowicz 1989). For a system with high resolution a large number of views is required.

4.2 Overview of optical components

4.2.1 Transmitter devices

A range of optical light emitters and sensors is shown in figure 4.1. The advantages and disadvantages of the different emitters is now discussed.

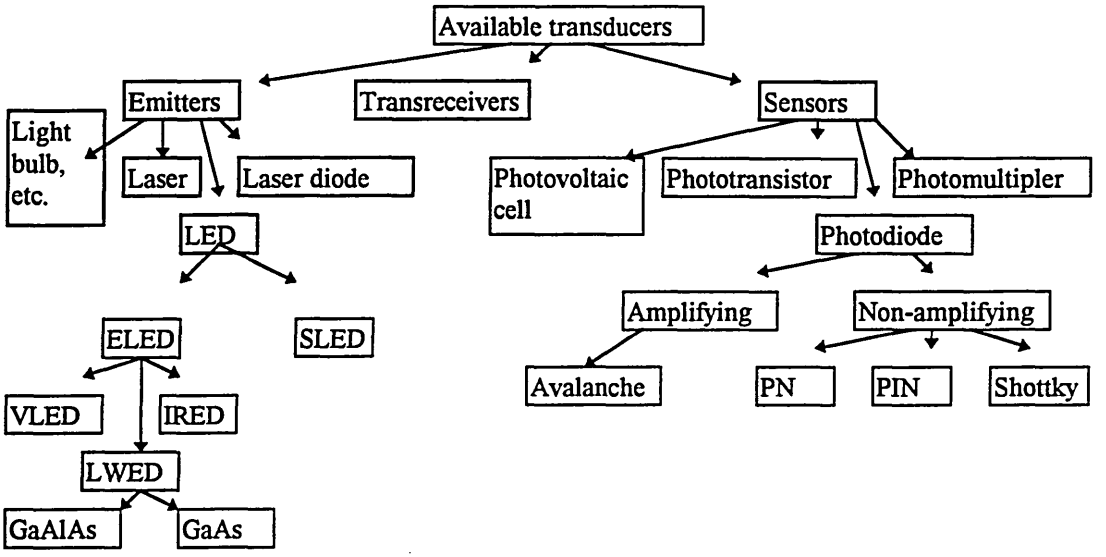

Figure 4.1 Family of optoelectronic products

Although more powerful and coherent than radiation from other sources, the Laser is unsuitable for a prototype construction, since the optical system (e.g. beam splitters) it would require is expensive to construct and complicated to control.

Laser diodes, contained in much smaller discrete packages, are better suited than Lasers, however at a price of approximately thirty pounds, excluding optics, they are an expensive choice for a prototype system. Further their physical size restricts the closeness with which adjacent transmitter/receiver pairs may be mounted. They also require careful handling being especially susceptible to static charge and electrical transients.

Light emitting diodes (LED) have been used successfully for process tomography (Dugdale et al, 1992). However the physical dimensions of the LED and its

associated optical system restrict the numbers of views which can be obtained over a section. This problem can be solved by using optical fibres.

An optical fibre may be used to convey light energy from an energy source to a remote place to provide illumination. An optical fibre bundle may be used as a light source to provide many light inputs to a pipe from a single lamp. The fibre providing illumination to the system may be spaced at just over 1 mm centres to provide a large number of views. The bundle may be illuminated monochromatically by laser or with wide bandwidth light from a filament lamp. A further advantage of optical fibres is that the electrical interfaces may be remote from the process, enabling an intrinsically safe system to be constructed.

4.2.2 The receiver

To take advantage of the facilities (section 4.2.1) provided by the optical fibres used as transmitters, optical fibres must also used as the primary receivers. These receiving fibres may be positioned adjacent to each other to provide a large number of views. The light received by each fibre can be transmitted to a site remote from the conveyor before being converted to an electrical signal.

A range of sensors is shown in figure 4.1. Light to electrical converters consist mainly of photovoltaic cells (light dependent resistors, LDRs), phototransistors, photodiodes and photomultipliers.

The ideal photoelectric semiconductor can be described in terms of energy levels with a lower band of electronic states (valence band) completely filled at absolutely zero, separated by an energy gap from a higher band of allowed states

(conduction band) which are completely empty at absolute zero. At ambient temperatures electrons can be thermally excited to the conduction band leaving free holes in the valence band. This is termed the intrinsic excitation of carriers and can also be produced by absorption of photons, thus producing photon excited carriers. The wavelength needed to induce this photo response depends on the energy gap between the bands. The photo response can be extended to longer wavelengths by doping with impurity atoms, giving rise to extrinsic conductivity (Jenkins 1987, Chaimowicz 1989).

The photovoltaic cell is essentially a junction formed between two sections of the same semiconductor, one N type, the other P type. At their interface there is recombination of electrons and holes leaving a region devoid of free carriers (depletion region). As described above, free charge carriers are generated when light enters the cell. When the electrons and holes reach the PN transition they are separated by the electrical field in the depletion region. This generates a photovoltage which supplies photocurrent. Thus the photovoltaic cell converts luminous into electrical energy. This puts the emphasis on large sensitive areas (square centimetres rather millimetres). However to attain a high resolution the project requires a sensor with a small surface area.

For low-light-level detection and measurement (and, incidentally, for nanosecond resolution) the photomultiplier is the best choice. This device allows a photon to eject an electron from a photosensitive alkali metal "photocathode". The photomultiplier then amplifies this small photocurrent by accelerating the electron onto successive surfaces (dynodes), from which additional electrons are easily

ejected. This use of "electron multiplication" yields extremely low noise amplification of the initial photocurrent signal. When compared with photodiodes, photomultiplier tubes have the advantage of high quantum efficiency while operating at high speed (2ns rise time, typically). Photomultipliers have several disadvantages such as, they are expensive, bulky and they require a stable source of high voltage, since the tube's gain rises exponentially with applied voltage. (Horowitz 1993).

Photo-transistors and photodiodes have advantages over photomultipliers since they are smaller, more durable, convenient to use and less expensive. The photo-transistor works as follows: the flow of photon generated carriers takes the place of the conventional base currents, and like it, is amplified by the transistor part of the device. This makes them more sensitive than the photodiode without an amplifier, i.e. high responsivity, but they suffer from poor linearity, are temperature sensitive and above all are intrinsically slow (Chaimowicz 1989).

There are two main types of photodiodes, non-amplifying and amplifying. The first case is essentially a PN junction as for the photovoltaic cell, with reverse bias applied, i.e. a negative voltage applied to the P side with respect to the N side. The potential barrier due to the interface is increased. This inhibits the flow of holes from the P to N region and of electrons from N to P region. As a result of thermally generated electron hole pairs there will be electrons in the P region and holes in the N region. These are called minority carriers and for them the potential barrier represents a drop in potential. Minority carriers in the depletion region will be swept across the junction producing a reverse current. In addition minority

carriers outside the depletion region may diffuse into the high field region and be swept across the junction. This current, that flows in the absence of light, is called the dark current. When light falls onto the surrounding of the PN junction free charge carriers are generated as for the photovoltaic cell. These photo carriers produced at or within a diffusion length of the PN junction will be swept away by the depletion field; electrons into the N type and holes into the P type, which leads to an increase in the reverse current. This photocurrent is proportional to the illumination, thus photodiodes are particularly suited to quantitative light measurements.

The avalanche photodiode is an amplifying photodiode. In the depletion layer of a PIN photodiode, the strong electric field sweeps away the photon-generated free carriers. If the field is very strong and the path of a free electron sufficiently long, the continually accelerating particle can gather sufficient momentum to knock out, like a projectile, another electron from an atom on its way. Should this happen, two electrons are produced for each original one, and, if conditions are favourable, the multiplication may continue, giving rise to geometrical growth of the number of free carriers, hence the name of the device. Practical gain figures range from 50 to 300 (Chaimowicz 1989).

There are several practical disadvantages in using the avalanche photo-diode. Firstly, a reverse bias V_R as much as 300 - 500 V is necessary to create a field intensity that will ensure avalanching. This is not always easily accommodated, especially in portable equipment. Secondly, the exact operating value of V_R is not only critical within 0.1 V, but also temperature dependent. These two constraints

call for accurate stabilisation of V_R, causing complication and expense. Thirdly, the gain is also temperature dependent so that gain compensation or stabilisation circuits are often required.

An improvement over the PN junction is the PIN photodiode. This has a sandwich like structure, with Positive, Intrinsic and Negative layers. The presence of an I layer increases the speed of the device, improves the device's linearity and reduces it's leakage current and noise. The third type of non-amplifying photodiode is the surface barrier or Schottky, where the positive silicon layer of the PN device is replaced by a thin layer of gold. This gives the device good blue/violet sensitivity and a high speed of response. But in the infra red the responsivity is reduced by the high surface reflectance of the gold.

From the above review a suitable arrangement for the prototype transducer pair is a halogen bulb, which is suitable for illuminating all the emitter fibres simultaneously and continuously, coupled via optical fibre receivers cables, which enable large number of views to be obtained from a single cross-section, with non-amplifying PIN photodiode sensors to provide the required sensitivity (figure 4.2). The proposed system is outlined in figure 4.3. The design of the illumination system and receiver system are described in more detail in the following sections.

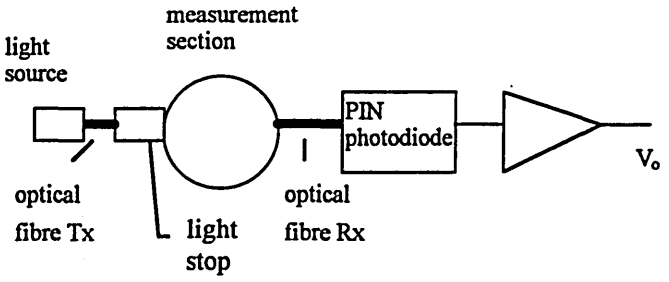

Figure 4.2 Photodiodes via optical fibres

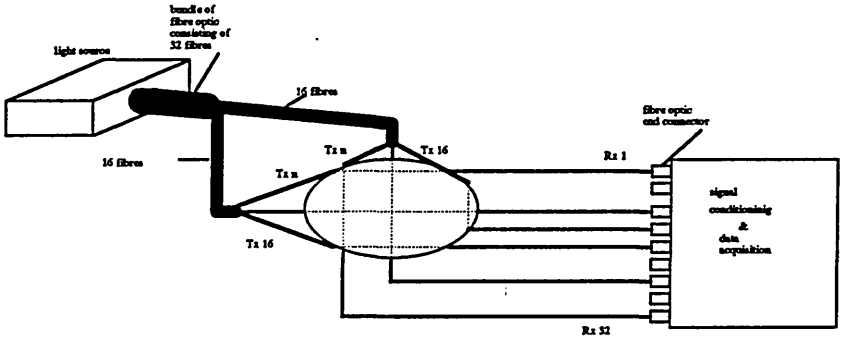

Figure 4.3 System block diagram

4.3 Design of the illumination system

The illumination system consists of a light source, thirty-two optical fibres arranged to form an optical bundle at one end and terminating at the measurement section in the collimators. The component parts are discussed in the following sub sections.

4.3.1 The light source

This section describes the choice of dichroic (constant colour coating) light source; 35W, 50W and 75W dichroic halogen bulbs with integral reflectors and

beam angles of 27°, excited from a stabilised DC voltage were investigated as the light source for the optical fibres, because they have a large beam area and a single bulb can be used to provide illumination for a large number of optical fibres when they are arranged in a bundle.

A single transmitter fibre is mounted 30 mm in front of the bulb being investigated with their optical axes aligned. The receiver fibre is mounted with its optical axis aligned with the output axis of the transmitter fibre (figure 4.4).

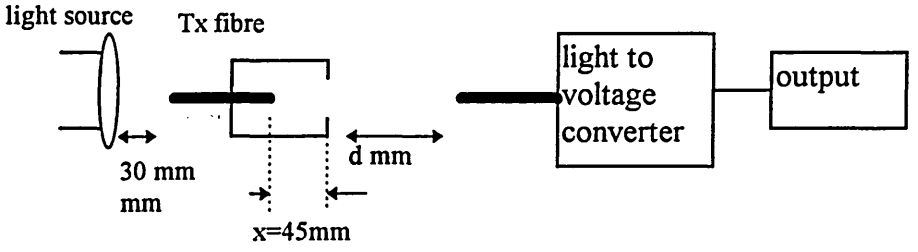

Figure 4.4. System alignment along the optical axis

The separation between the receiver and transmitter (d mm) fibre was varied from 5 mm up to 100 mm using the 35W bulb as the light source and the output from the light to voltage converter (section 4.4) noted. The test was repeated for the 50W and 75W bulbs. The results are summarised in figure 4.5.

Figure 4.5 shows little difference in output between the 75W and 50W bulbs at 81 mm separation, the diameter of the measurement section, but both are significantly better than the 35W bulb at this distance. The 50W dichroic halogen bulb has been chosen instead of the 75W due to its reduced heat dissipation to the optical fibre.

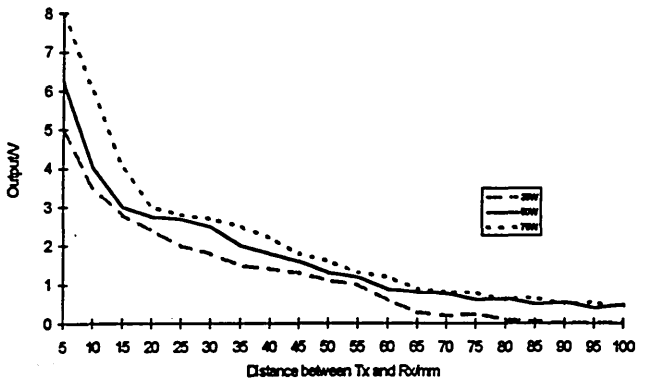

Figure 4.5 Different light source powers.

The light source must be excited from a stabilised DC voltage to prevent fluctuations in supply voltage modulating the light intensity as shown in figure 4.6. The top trace shows a 100 Hz 40 mV peak to peak superimposed on a d.c. level of 700 mV output from the receiver amplifier due to an unsmoothed supply voltage being fed to the bulb. The lower trace shows the significant reduction in noise level, to less than 2 mV peak to peak on the same d.c. level, when a smoothed supply is used

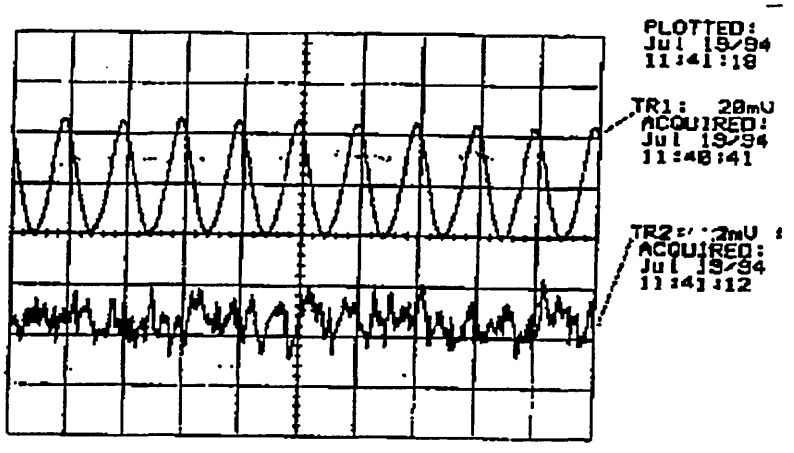

Figure 4.6 Receiver amplifier output (1) top trace unsmoothed supply (2) bottom trace smoothed supply for light bulb.

4.3.2 Preparation of the optical fibre

Multimode plastic fibre of 1 mm in diameter (overall diameter is 2.23 mm) has been used throughout this project to maximise the transmission of light into and out of the fibre. The optical fibre is made from polymethyl-methacrylate and enclosed with a polymer cladding and protective sheath. Both ends of the fibre require treatment.

An investigation has been made into different methods of terminating the optical fibre. Figure 4.7 shows the preparation of optical fibre for the transmitter. A short piece of sleeving is removed from one end of the fibre, as shown in figure 4.7 (1), by gently cutting around the circumference, or by using gauge wire strippers. Great care should be taken when cutting through the covering sheath, to prevent scoring the fibre inside.

Remove the end covering and cleanly cut the exposed fibre core to two millimetres long, as shown in figure 4.7 (2 and 3). Only a single, straight cut should be made to keep the end smooth, this being important for maximum light transfer. Cuts should be made with a sharp knife. If the fibre end is to remain flat, the ends of the fibres are cut and polished flat to minimise scattering effects.

A form of lens can be produced on the fibre in the following way. The cut fibre end is placed close to a naked flame for a few seconds until the end softens and forms a curved surface due to surface tension effects, as shown in figure 4.7 (4). Excessive heat will melt the fibre completely, and this should be avoided. This curvature develops a 'lens' in the fibre(figure 4.8), which is an improvement over

an unlensed fibre, because it provides improved light transfer as shown in table 4.1.

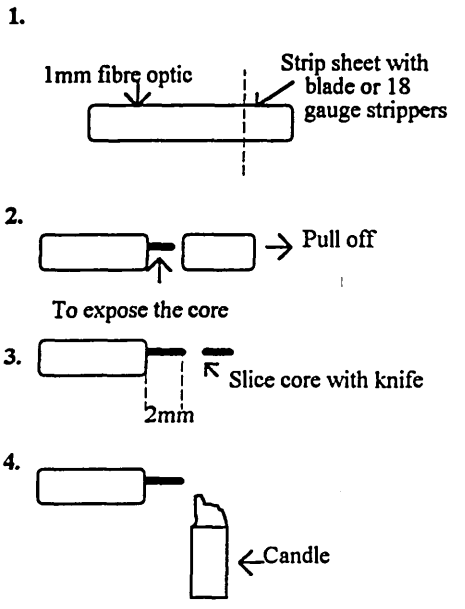

Figure 4.7 Preparation the optical fibre

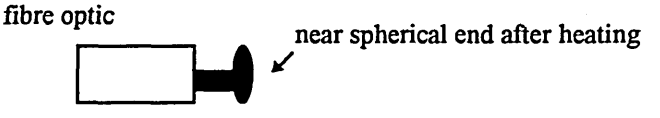

Figure 4.8 'Lens' produced by heating the fibre

Figure 4.9 shows the preparation of the optical fibre for the input to the transmitter. Steps 1 to 3 in figure 4.7 are followed, however, instead of using a flame, fine grades of emery paper followed by diamond paper are gently rubbed, squarely across the fibre end to polish the surface. The finish is ultimately dependent upon the fineness of the final abrasive paper used.

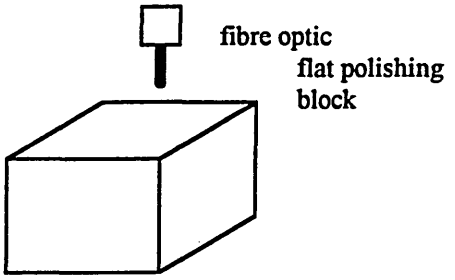

Figure 4.9 Polishing the fibre

An investigation was made into the optimum combination of termination between transmitter and receiver of the optical fibre. All the inputs to the transmitters and all the outputs from the receivers were flat, polished fibre for all the tests. Table 4.1 shows the result of the experiments.

Transmitter	Receiver	Separation between Transmitter and Receiver		
		40 mm	80 mm	120 mm
Melted	Melted	1.5V	0.3V	0.2V
Melted	Polished	1.8V	0.8V	0.4V
Polished	Polished	0.8V	0.1V	0.05V
Polished	Melted	1.15V	0.15V	0.07V

Table 4.1 Experiments results

The table shows that the second combination gives the better coupling and the greater output. For all the remaining work presented in this thesis the coupling between the light source and the transmitter fibre via a polished fibre interface, the transmitter couples into the conveyor via a 'lensed' surface and both ends of the receivers fibres are flat and polished.

After preparing all the transmitter fibres transmission tests were carried out to check the comparability of the individual fibres by positioning the polished end 30 mm from the halogen bulb and measuring the output from the lensed end using a proprietary fibre optic power meter. Results for all the transmitter fibres are shown in Appendix B.

The power transmitted by the fibres has a mean of 5.15 μW with a standard deviation of ±0.07 μW.

4.3.3 Beam collimation

The beam of light must diverge as little as possible to avoid overlap of the received signals and loss of the beam intensity. This can be achieved either by using optical lenses or, with some loss in the transmitted light intensity, by the use of an optical stop.

Optical lenses are either large in diameter compared with an optical fibre or expensive. For these reasons it was decided to use an optical stop. This method sets the light source (the optical fibre) in a metal block with a small hole in the middle which acts as the first light stop, which is positioned 45 mm (distance X in figure 4.10) (section 4.3.4) from the wall of the pipe. The hole in the pipe wall (point A in figure 4.10) acts as a second optical stop. The fibre optic is a push fit in the block as shown in figure 4.10. This has the effect, in conjunction with the stops, of cutting out some of the diverging light and providing physical support for the fibre. The resulting system is a compromise between beam intensity and beam spread.

As discussed in section 3.3, the distance between adjacent transmitter optical fibres is 5 mm. The maximum permitted diameter of the beam after travelling 81 mm (the pipe diameter) is 4 mm as shown in figure 4.11, which provides a minimum gap of 1 mm between the beams arriving at the receivers. The intensity of the transmitted beam is strong enough to be detected by the PIN photodiode light sensor over the range of 81 mm, the diameter of the metal pipe.

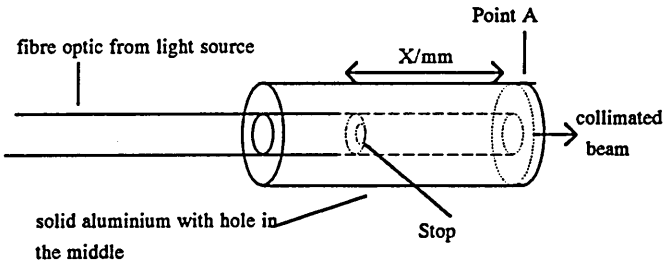

Figure 4.10 Collimated beam

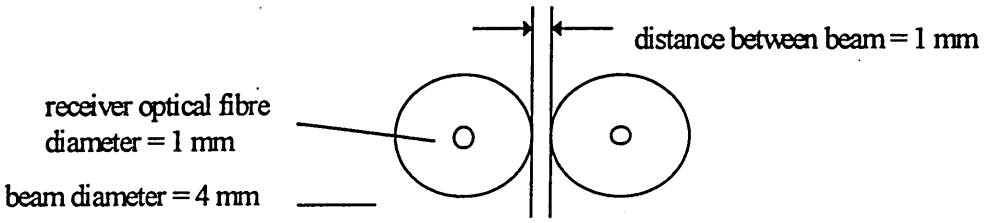

Figure 4.11 Beam diameter

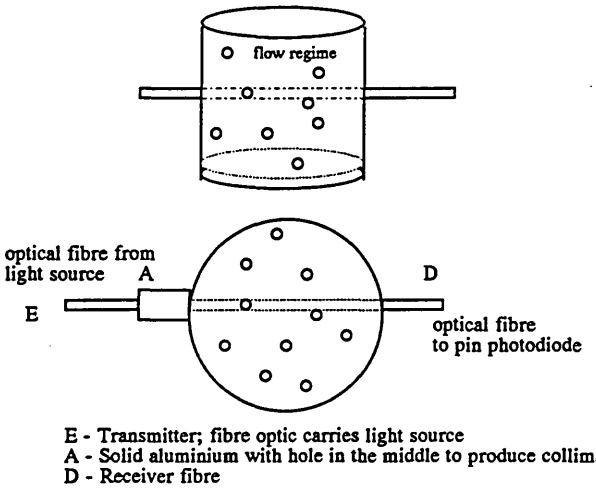

Figure 4.12 Plan view of transmitter/receiver pair

The fibres are also mounted into slots machined into a carrier mounted on the measurement section in an invasive but non-intrusive (i.e. the flow pattern is not affected by their presence) manner as shown in figure 4.12.

4.3.4 Tests on the beam collimation

In the experiment the transmitter and receiver are placed 81 mm apart, on an optical bench in a simulation of the measurement section. The relationship between the position of the first stop relative to the second stop is investigated.

Figure 4.13 shows the relationship between the beam diameter and the separation of the stops for a range of distances between the transmitter and receiver. The optimum stop separation is 45 mm for a received beam diameter of 4 mm at 81 mm from the second stop.

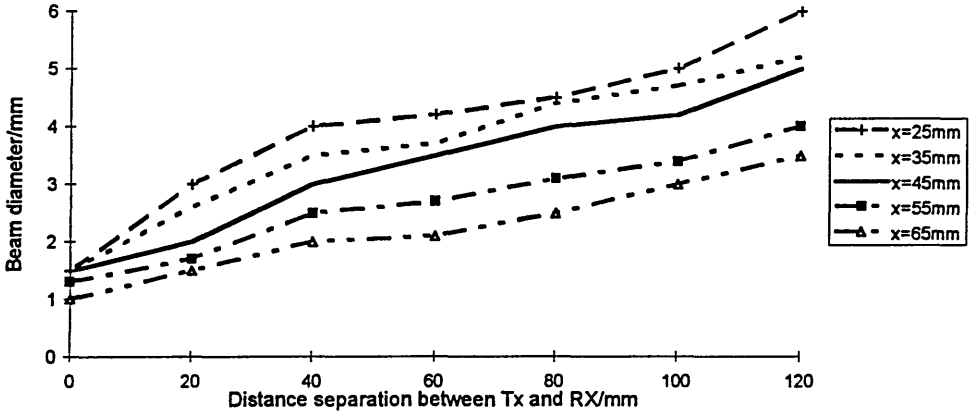

Figure 4.13 Effect of beam diameter

The results in figure 4.14 show that as the distance from point A is increased the intensity of the beam decreases. With a stop separation of 45 mm the output is 4.8V when the distance between transmitter and receiver is 81 mm (equivalent to diameter of the pipe). Figure 4.14 also shows that a reasonable degree of collimation exists, complete collimation would mean the output voltage remained constant.

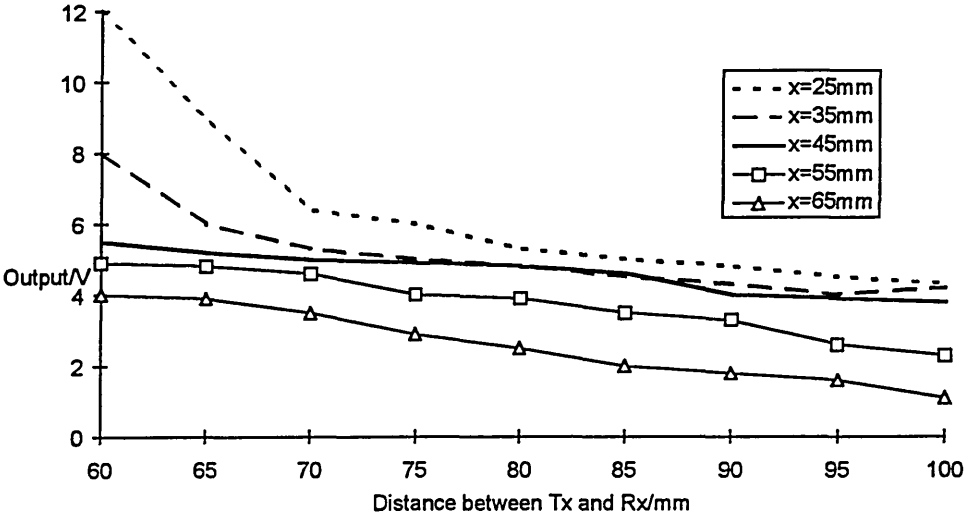

Figure 4.14 Output for various distance of optical fibre from point A

4.4 Design of the receiving system

The receiver consists of an optical fibre, polished at both ends, which couples the received light to a PIN photodiode for conversion to an electrical signal. The effects of diffraction caused by the particles are thought to be small in this system and are ignored in the present study (see section 8.3), because the primary effect being investigated is attenuation of optical energy by particles intercepting the beam. The PIN photodiode supplies a current which is dependent on the level of light received. This current is converted to a voltage, signal conditioned and transformed to digital format for feeding to a PC. The receiver circuit block diagram is shown in figure 4.15. The individual components are described in the following sections.

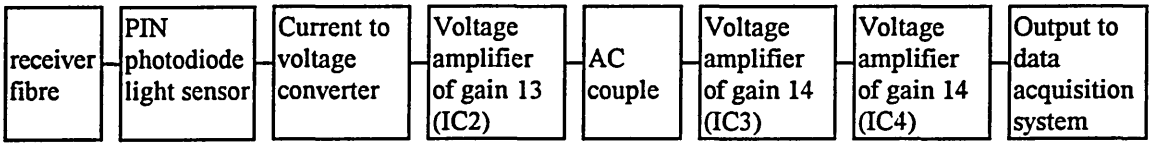

Figure 4.15 Signal conditioning circuit block diagram

4.4.1 Test on individual receiver optical fibres

Both ends of the receiver fibres were prepared by polishing on a flat surface (section 4.3.2). To test the equality of the receiver fibres the following test was carried out. The individual receiver fibres were mounted on an optical bench in-line with a transmitter fibre with a separation of 81 mm. The output end of each receiver fibre was connected to a PIN photodiode connected as shown in figure 4.15 and the output voltage monitored. The results of these tests are shown

in Appendix C. The mean output voltage for all the receiver fibres is 25 mV with a standard deviation of ±1.4 mV.

4.4.2 The receiver circuit

The light energy output of the receivers has to be converted to electrical energy by a PIN photodiode. A selection of different diodes were investigated to assess their effectiveness using the equivalent circuit is shown in figure 4.16 (Chaimowicz 1989), where I_s signal current; C_D depletion capacitance; C_p package capacitance; R_D dynamic diode resistance; R_S series resistance; R_L external load resistance. The chosen optical receiver was a PIN photodiode, BPX65.

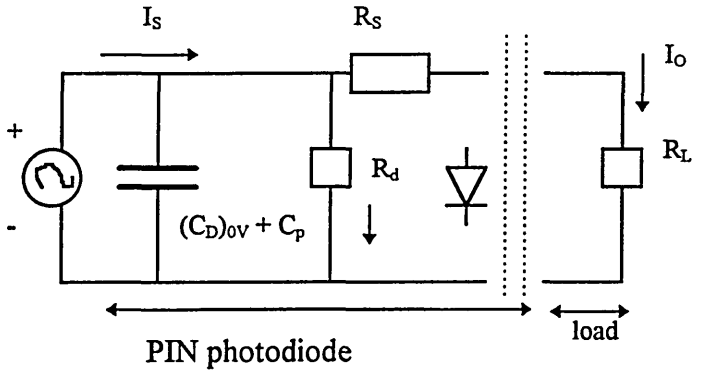

Figure 4.16 Equivalent circuit of PIN photodiode

The change in current from no light to full light is typically 0.011 μA (Full light = 0.0122 μA, zero light = 0.78 nA) under the lighting conditions discussed below. The current to voltage converter provides a voltage level proportional to the received current which with a 160 kΩ feedback resistor provides a full scale output voltage of 1.96 mV.

When the PIN photodiode receives full light the output voltage arriving at the ac coupling capacitor is approximately 26 mV. However drift in the working point

of the PIN photodiode due to temperature change and changes in the offset bias in the amplifier due to variations in temperature and power supply fluctuations can give rise to voltage variations of 2 mV at the coupling capacitor. The coupling capacitor is used to remove the effects of drift before further amplification of the wanted signal. The coupling capacitor has the further advantage of conditioning the signal so that no flow corresponds to zero volts and high flow rates to five volts dependent upon the gains chosen. The coupling capacitor is also advantageous when measuring small particles (micron size) which provide a very small reduction in the total amount of light being received by enabling larger amplifier gains to used than is possible where offsets are present.

The graph in figure 4.17 shows the d.c output of the amplifier preceding the coupling capacitor when the light intensity is varied. The sensitivity of voltage change due to a change in light level is low at lamp voltages below 2 V and above 13 V. Between these two voltages the sensitivity remains approximately constant. The system bulb supply is 12V, because it provides a level of illumination at the receiver consistent with high sensitivity (figure 4.17) and the greatest signal to noise ratio before the saturation value shown in figure 4.17 is reached.

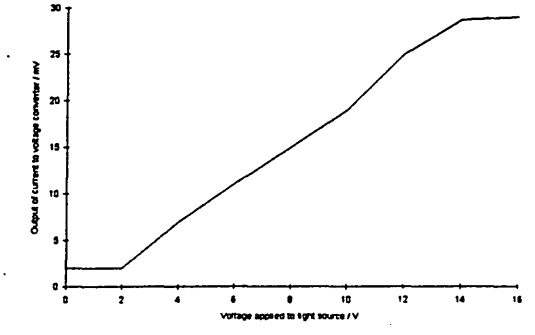

Figure 4.17 Variation in output level with bulb supply voltage

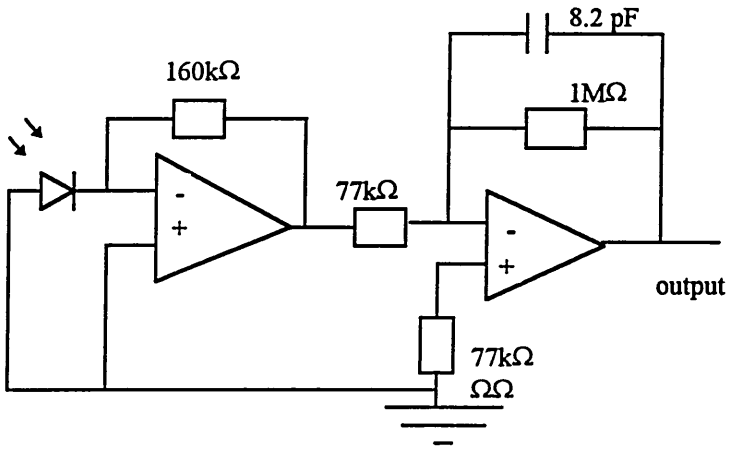

Figure 4.18 Two stage amplification

The second amplifier acts as buffer to remove any potential change in load due to the following circuit and provides a gain of -13. The bandwidth of the amplifier is set to 20 kHz. Previous work with a pneumatic conveyor (Shackleton 1981) measured the bandwidth associated with flowing solid particles as approximately 2 to 8 kHz. The sensors were electrodynamic and of length 5 mm. To enable this optical system to be used under similiar conditions (section 8.3) the bandwidth has been increased to 20 kHz because of the spatial filtering effect of the optical fibres (Green *et al* 1995). Hence,

$$\omega = 2\pi(20\text{kHz})$$
$$= 0.126 \times 10^{6}\ \text{rad/s}$$
$$\tau = \frac{1}{\omega}$$
$$= 8 \times 10^{-6}\ s$$

therefore,

$$C = \frac{\tau}{R}$$
$$= 8\ \text{pF (used 8.2 pF)}$$

The signal is amplified by the second stage to provide a maximum output level of 26 mV (figure 4.18). The change in level of this output when the sensor input is change from no light to full light is 24.38 mV; the dark current providing 1.62mV. This output is connected to the following amplifier via a capacitor. This makes the amplifier into a band pass system. The lower corner frequency is a compromise to ensure that all signals from the flowing particles are detected with a sensible value of coupling capacitor. The time constant has been set at one second and the corner frequency to 0.16 Hz (Shackleton, 1981), where comparable work in pneumatic conveying and gravity drop conveyor has been carried out by Shackleton. The coupling capacitor uses polycarbonate as the dielectric and is chosen for high stability and close tolerance.

$$\tau = RC$$
$$= (1x10^{6})(1x10^{-6})$$
$$= 1s$$
$$f_{co} = \frac{1}{2\pi\tau}$$
$$= 0.159Hz$$

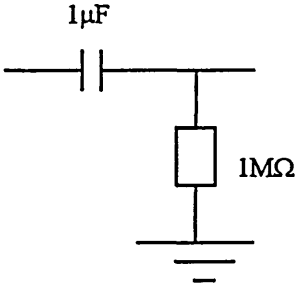

Figure 4.19 Ac coupling network

The ac voltage at the output of the coupling network (figure 4.19) varies between zero and 26 mV. To provide a signal of up to 5 Volts into the analogue to digital

converter this ac signal must be amplified by approximately 200. This amplification is provided by a two stage amplifier each with a gain fourteen. These relatively low gain values are used to maintain an adequate signal bandwidth for this investigation (section 7). Further discussions on bandwidth are discussed in section 8.3.

The circuits have a high d.c gain, so to minimise the DC offset both amplifiers are provided with offset compensation and adjustment as shown in the figure 4.20.

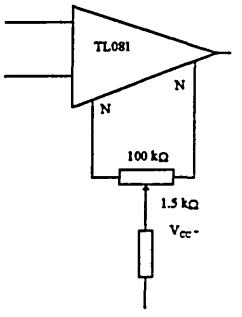

Figure 4.20 Circuit to minimise offset bias

This thesis is concerned with two main investigations. The first involves concentration measurement, the second relates to frequency components in the received signal. The circuit shown in figure 4.21 has been used in two forms :

1. For investigating the frequency components in the electrical signals arising arriving from the flowing particles (chapter 7). The system bandwidth is approximately 20 kHz.

2. For concentration measurements with a capacitor C_F (0.1μF), which is used to provide a low pass filter action (chapter 5 and 6).

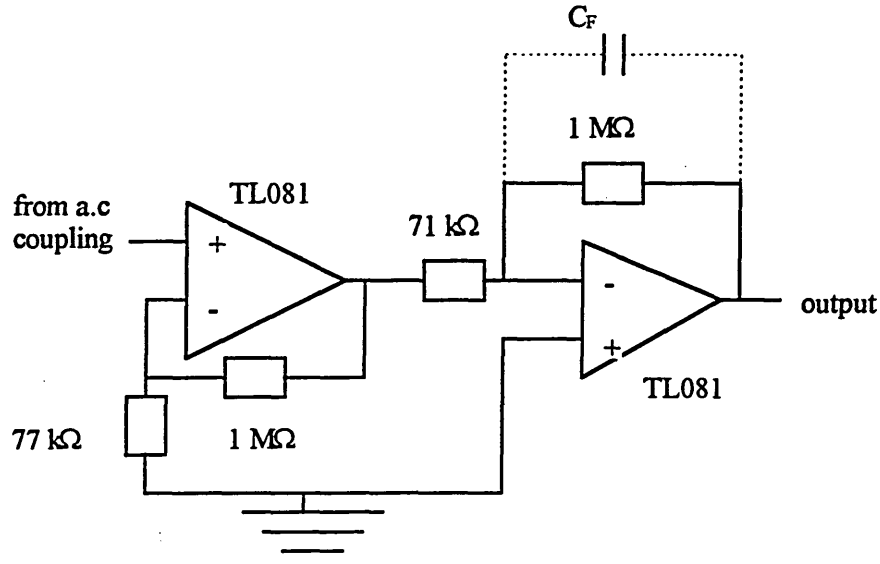

Figure 4.21 The conditioning circuit

The full circuit is shown in figure 4.22.

The electronic circuits are mounted in an earthed metal box to minimise electrical pick-up. Without shielding there is interference in the output as shown by the lower trace in figure 4.23. The top trace shows the interference is minimised when the electronics are placed in the shielded metal box.

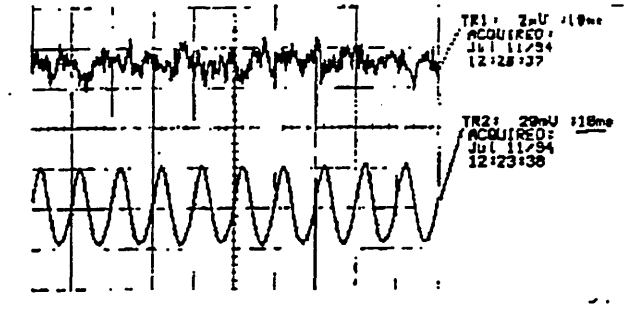

Figure 4.23 Shielding effect

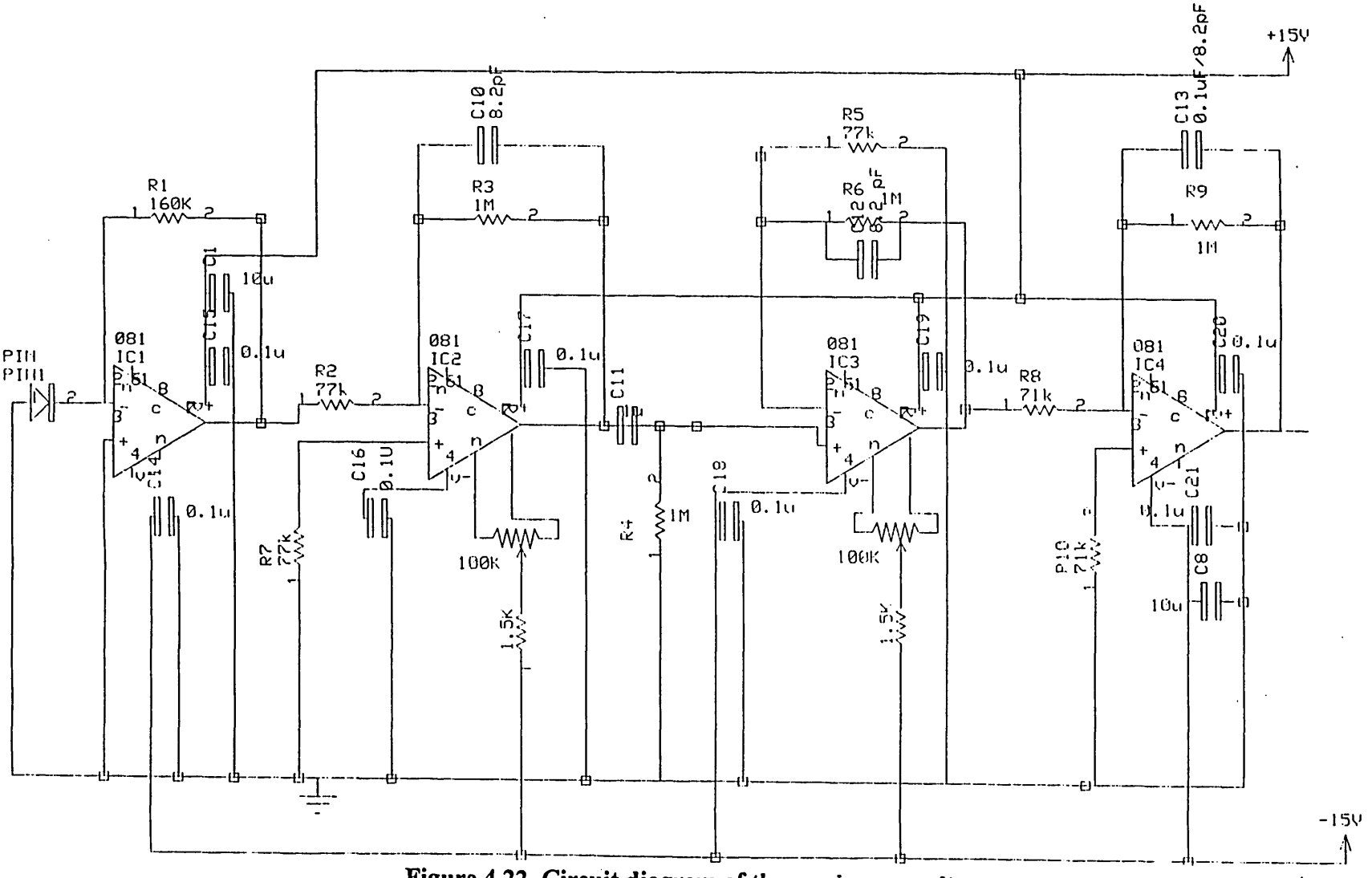

Figure 4.22 Circuit diagram of the receiver circuit

4.5 The data acquisition system (DAS)

The data acquisition system used in this project is the Keithely Instruments DAS-1801, which is a high performance data acquisition board for IBM PC. The features of this system are listed in Appendix A.

For concentration measurements (chapter 5 and 6) the band pass amplifier of the transducer system has a cut off frequency of 1.59 Hz. So a sampling frequency of 10 Hz per channel is chosen. This enables 312 data points to be collected for each of the 32 channels, which enables thirty-two seconds of flow data to be obtained.

For the frequency component investigation (chapter 7) the bandwidth of the measurement system is limited to 20 kHz. However, tests showed that meaningful measurement were restricted to a maximum frequency of 1.6 kHz. So a sampling frequency of 8 kHz was used for most of the tests.

CHAPTER 5

Concentration measurements

5.1 Concentration measurements: one transmitter/receiver pair

Measurements were made with a single optical fibre sensor using the gravity flow rig to investigate whether an optical sensor could be used to provide information about the solids concentrations and hence flow rate (section 3.3). The flow rig feeds silica sand (mean particle size 300 nm) vertically downwards through the measurement section at a controlled rate (section 5.1.1). The sensor at the centre of the sensing array (number 25 in figure 3.4, section 3.3) was used for the tests. The optical sensor output voltage was measured at several flow rates ranging from 40 to 520 gm/s.

5.1.1 The solids flow rig

The solids flow rig is a batch, gravity conveying system, which consists of three subsystems : a storage hopper, a screw feeder and a vertical pipe section. The sand used in the majority of the experiments has a mean size of 300 micron, with a particle size distribution as shown in figure 5.1 [Bidin, 1993].

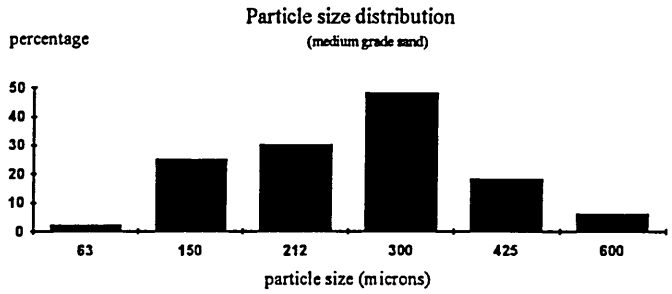

Figure 5.1 Particle size distribution of sand

The sand flowrate is controlled by a screw feeder whose speed of rotation is set by the control unit. A calibration of the actual mass flowrate and screw feeder setting is established by the collection of running sand over recorded time. The result of the calibration is shown in figure 5.2. Although these points could be fitted by a higher order polynomial, a first order polynomial has been fitted to the data.

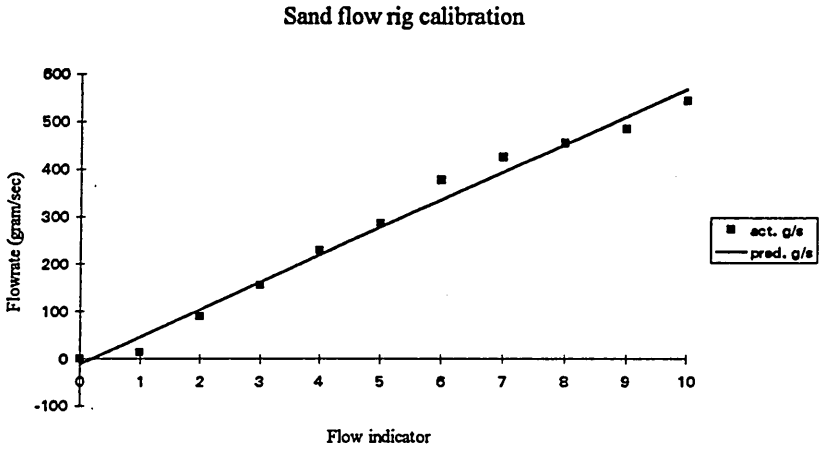

Figure 5.2 Sand flow rig calibration

This approach has been used for all screw feed calibrations. The equation of the regression line is,

$$\text{Flowrate (gm/s)} = 55.23\ (\text{flow indicator}) - 12.53 \qquad (5.1)$$

Figure 5.3 shows the result of the calibration when plastic beads of 2 mm nominal size is used instead of sand.

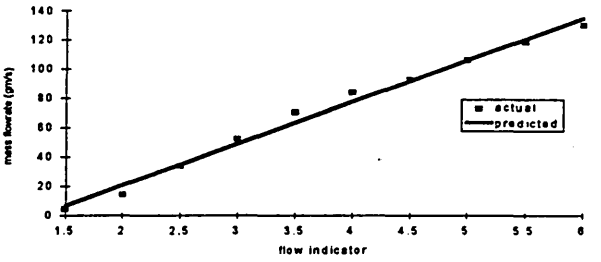

Figure 5.3 Flow rig calibration when plastic beads is used

Hence from figure 5.3, the equation of the linear regression line for plastic beads is,

$$\text{flowrate (gm/s)} = 28.512\ (\text{flow indicator}) - 36.316 \qquad (5.2)$$

A visualise inspection shows that screw feeder does not give a uniform distribution of the solid over the cross-section of the pipe. However, as the results of the experiments (section 5.2.1) show, the transducers are sensitive to this uneven distribution, which reinforces the concept of the measurement system being used to investigate concentration profiles.

5.1.2 Results of concentration measurements using sand

The sand flow was set to provide a flow rate of 40 gm/s. The output of the optical fibre sensor was monitored for several seconds and the mean voltage determined. The measurements were repeated for a range of feedrates up to 520 gm/s. The measurements presented in section 5.2 and chapter 6 were limited to maximum feedrates of 320 gm/s due to the data capture time of thirty two seconds and the amount of sand available in the hopper.

Results for the time averaged voltage are shown in figure 5.4 with a linear regression line fitted to the results. The negative reading at low flow rates is due to a DC offset voltage

in the amplifier. As mentioned in section 3.3, because a gravity drop conveyor is used, the velocity at a given length down the pipe is mainly the function of gravity and so is constant at a specific cross-section. Since the velocity is constant and

$$\dot{m} \propto \text{concentration x velocity} \qquad (5.3)$$

then for the conditions of the tests presented here concentration is directly proportional to $\dot{m}$.

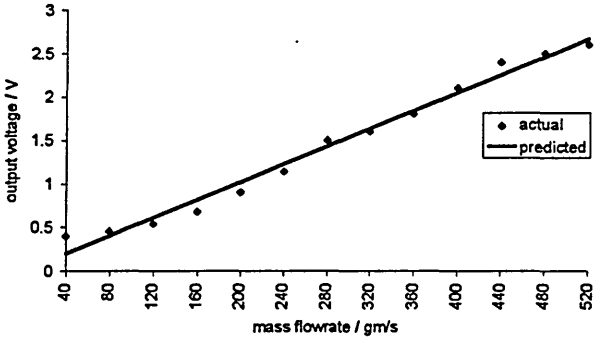

Figure 5.4 Relationship between mass flow rate and optical sensor output voltage for optical fibre receiver number twenty five

5.1.3 Analysis of results and discussion

The equation of the straight line graph shown in figure 5.4 is:

$$V_o = 0.005\dot{m} - 0.008 \qquad (5.4)$$

The average number of particles in the measurement volume should increase directly as a linear function of the solid flow rate (equation 3.4), so the linear relationship shown in figure 5.4 is expected. This linear relationship demonstrates the suitability of the optical sensor for concentration measurement for lightly loaded uniformly distributed flows (up

to approximately 2% solids by volume in the test) and providing the ends of the fibre can be kept free of dust during the measurement procedure.

5.1.4 Test on scattering effect

As described in section 4.3.2 the ends of the fibres receiver are cut and polished flat to minimise reception due to scattering effects arising from flowing particles. To test the interaction between adjacent receivers, a single transmitter fibre was energised and the outputs from all the receivers monitored for a range of sand feed rates. The results are shown in figure 5.5.

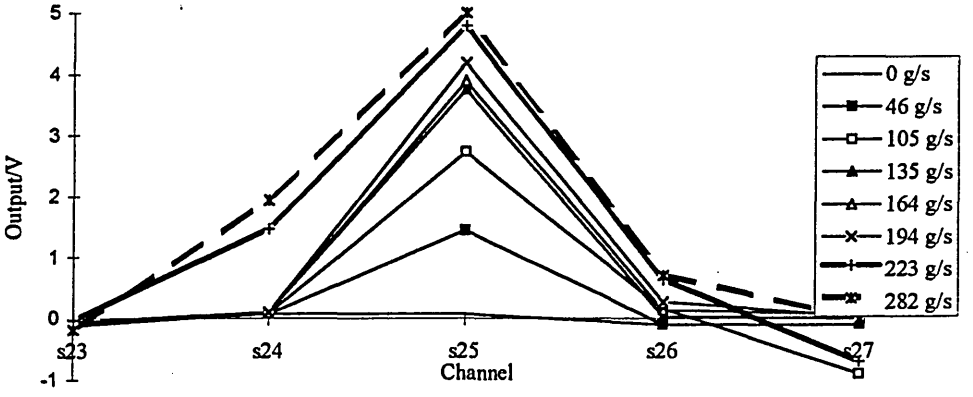

Figure 5.5 Scattering effect

At low feed rates (46 to 194 gm/s) no interaction was detected. At flow rates of 223 gm/s and above one adjacent receiver indicated approximately 1.5V (equivalent to 46 gm/s) and the other produced a small contribution towards the total concentration measurement.

5.2 Concentration measurement with thirty-two sensors

The aim of this section is to investigate the use of the optical array for concentration measurement across the pipe and also concentration profile determination (chapter 6). For all the measurements presented in chapter five and six the position of the sensors, relative to the screwfeeder and baffle, are as shown in figure 3.7b. Measurements were made by energising all 32 transmitters and monitoring the output at a solids flow rate of 40 gm/s using the data acquisition system to obtain 312 samples, with a sampling frequency of 10 Hz per channel for 32 seconds, for each flow measurement (section 4.5). The measurements were repeated for a range of solids mass flow rates from 40 to 320 gm/s using the dry sand and plastic beads. The tests were repeated for a range of artificially created flow regimes (section 3.4.1).

5.2.1 Results with sand flow

5.2.1.1 Full flow

No obstruction is used upstream of the sensor array so that, under ideal conditions, the solids would be uniformly distributed within the flow section. With a uniform distribution the number of particles passing through a given beam should be proportional to the path length of that beam inside the pipe, i.e. sensors numbered 7 and 8 should provide high readings relative to sensors numbered 0 and 15 (section 3.3).

Figure 5.6 shows the averaged output of each sensor at different feed rates for full flow. The predicted values (section 3.4.2.1) have been scaled to provide the same mean flow rate and are shown along side for comparison. In figure 5.6 the predicted values are only approximately achieved. The peak values for the measured readings are skewed with

respect to the predicted values. This is probably a characteristic of the screw feeder, because it enters the flow pipe from the side (figure 3.7b).

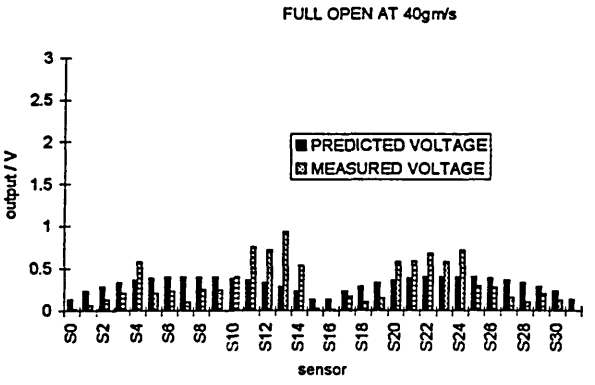

Figure 5.6a Full flow for sand at 40 gm/s

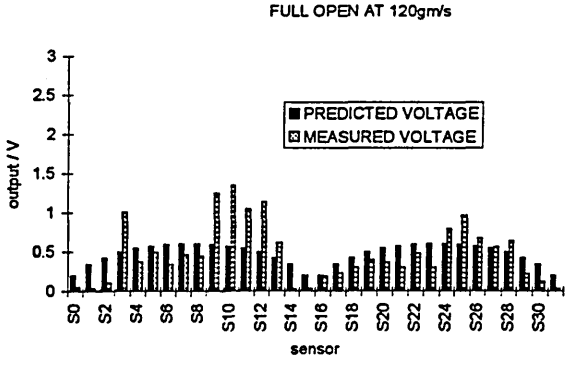

Figure 5.6b Full flow for sand at 120 gm/s

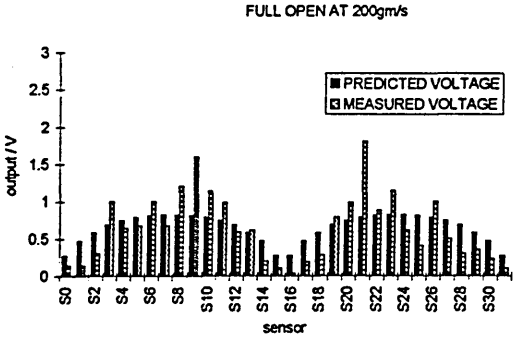

Figure 5.6c Full flow for sand at 200 gm/s

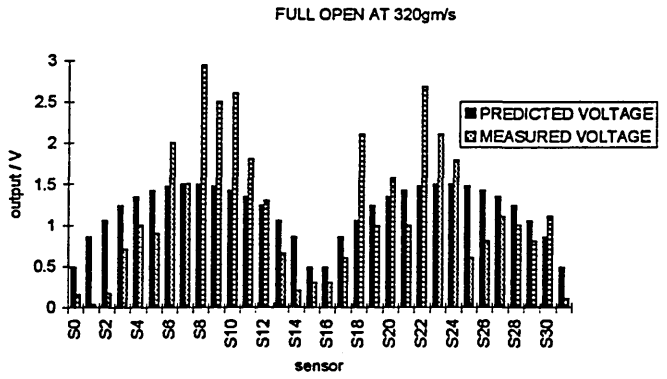

Figure 5.6d Full flow for sand at 320 gm/s

5.2.1.2 Three quarter flow

This is created by the baffle blocking a quarter the pipe diameter leaving three quarters clear for the sand flow (figure 3.6b). Results for different flow rates are shown in figure 5.7, which includes values predicted using the model in section 3.4.2.2.

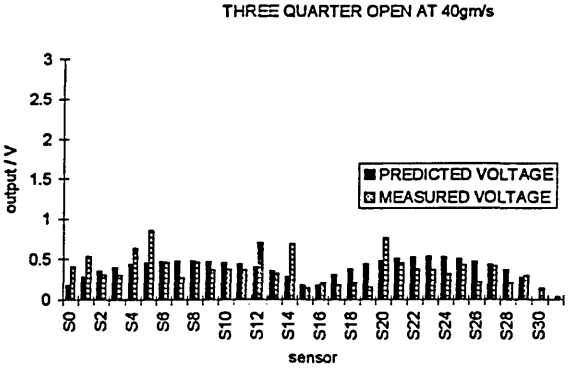

Figure 5.7a Three-quarter flow for sand at 40 gm/s

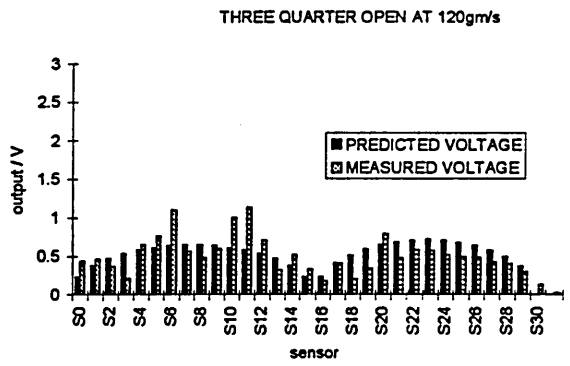

Figure 5.7b Three-quarter flow for sand at 120 gm/s

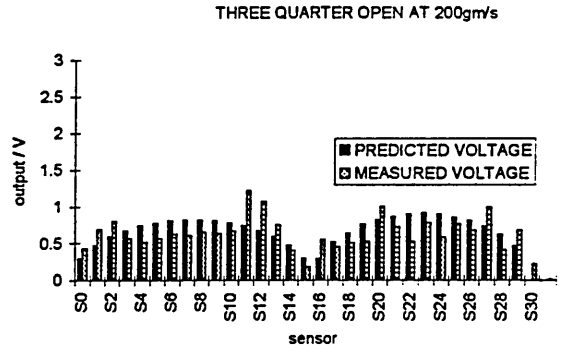

Figure 5.7c Three-quarter flow for sand at 200 gm/s

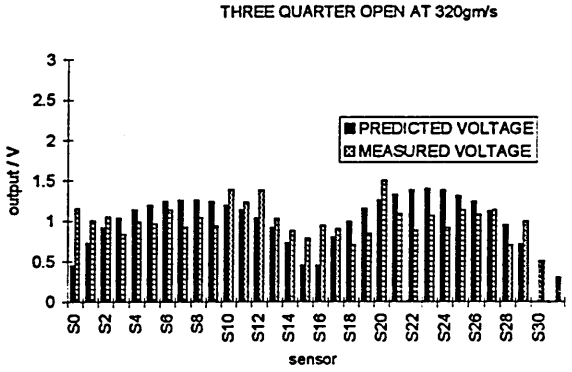

Figure 5.7d Three-quarter flow for sand at 320 gm/s

5.2.1.3 Half flow

This is created by the baffle blocking half the pipe diameter so that the other half will be clear for sand flow (figure 3.6c).

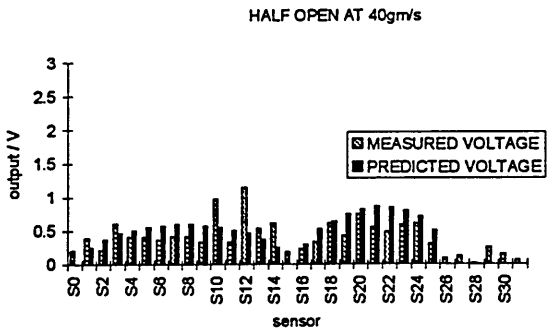

Figure 5.8a Half flow for sand at 40 gm/s

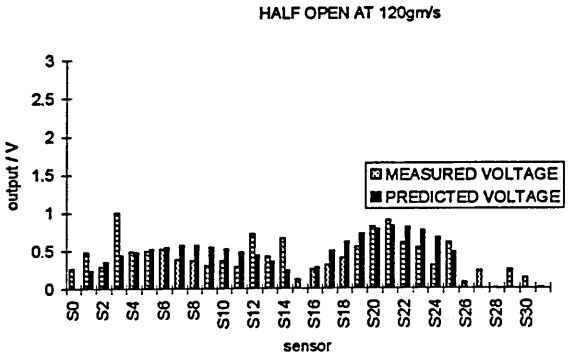

Figure 5.8b Half flow for sand at 120 gm/s

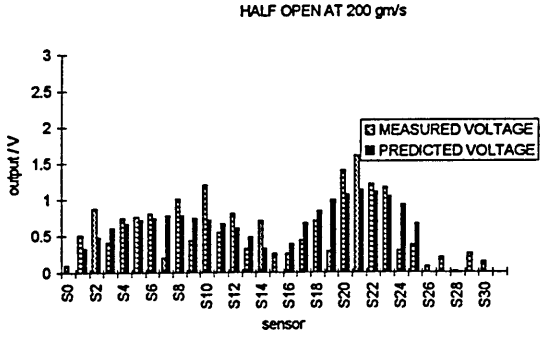

Figure 5.8c Half flow for sand at 200 gm/s

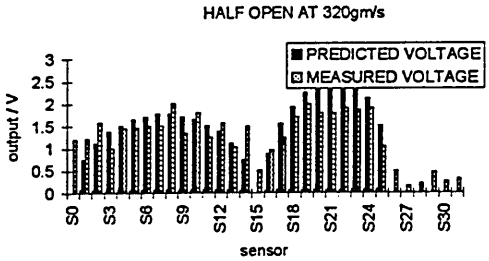

Figure 5.8d Half flow for sand at 320 gm/s

5.2.1.4 Quarter flow

This is created by the baffle blocking three quarters of the pipe diameter so that only a quarter is clear for sand flow (figure 3.6d).

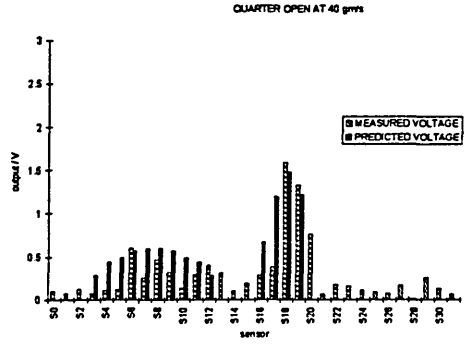

Figure 5.9a Quarter flow for sand at 40 gm/s

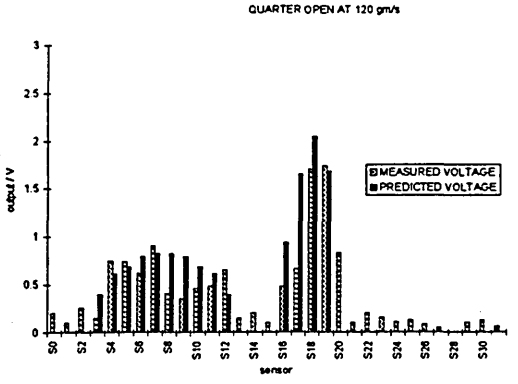

Figure 5.9b Quarter flow for sand at 120 gm/s

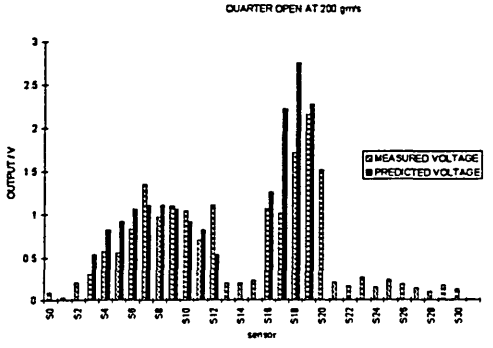

Figure 5.9c Quarter flow for sand at 200 gm/s

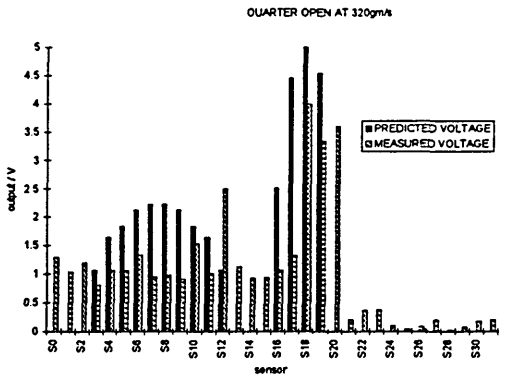

Figure 5.9d Quarter flow for sand at 320 gm/s

5.2.2 Results with plastic beads flow

5.2.2.1 Full flow

The experiment is repeated as in section 5.2.1.1 with plastic beads is used instead of sand. Figure 5.10 shows the average output of each sensor at different flow rates for full flow.

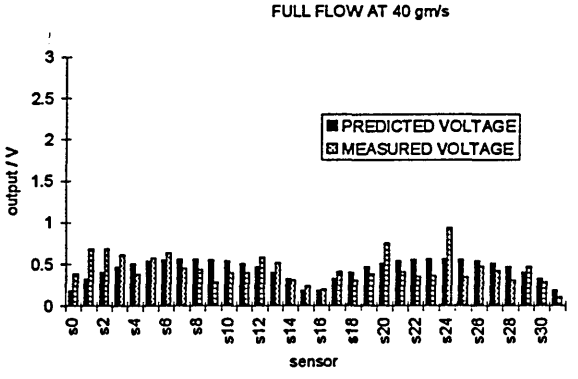

Figure 5.10a Full flow for plastic beads at 40 gm/s

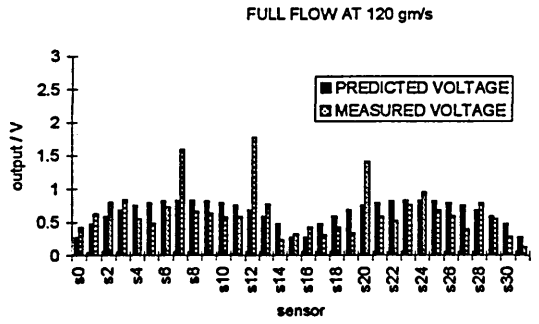

Figure 5.10b Full flow for plastic beads at 120 gm/s

5.2.2.2 Three quarter flow

The experiment is repeated as in section 5.2.1.2 with plastic beads is used instead of sand. Results for different flow rates are shown in figure 5.11c & d

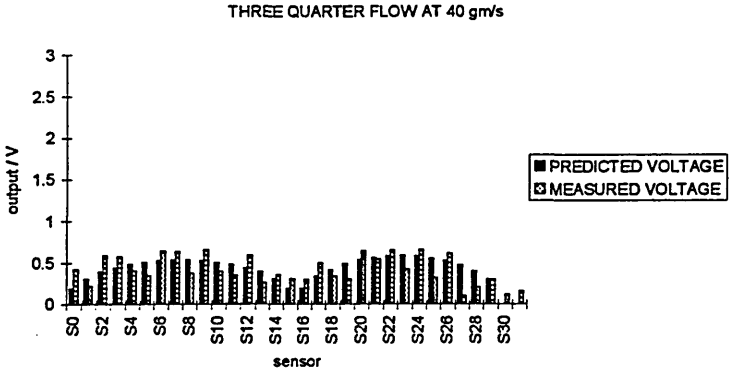

Figure 5.11c Three quarter flow for plastic beads at 40 gm/s

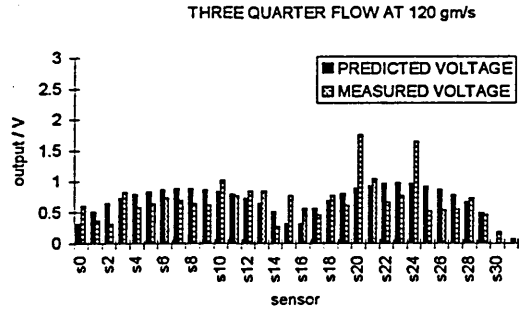

Figure 5.11d Three quarter flow for plastic beads at 120 gm/s

5.2.2.3 Half flow

This is created by the baffle blocking half the pipe diameter so that the other half will be clear for plastic beads flow (figure 3.6c).

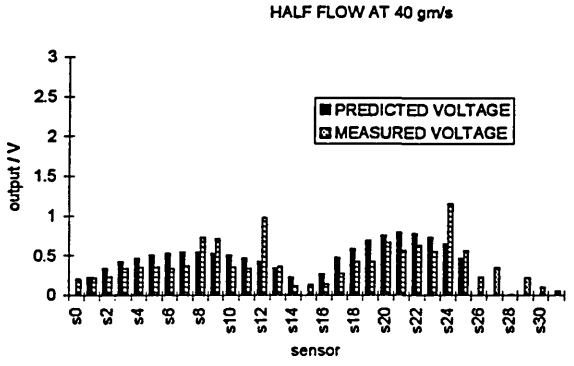

Figure 5.12a Half flow for plastic beads at 40 gm/s

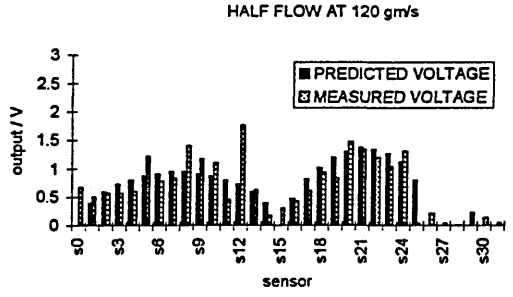

Figure 5.12b Half flow for plastic beads at 120 gm/s

5.2.2.4 Quarter flow

This is created by the baffle blocking three quarter of the pipe diameter so that only a quarter is clear for plastic beads to flow (figure 3.6d).

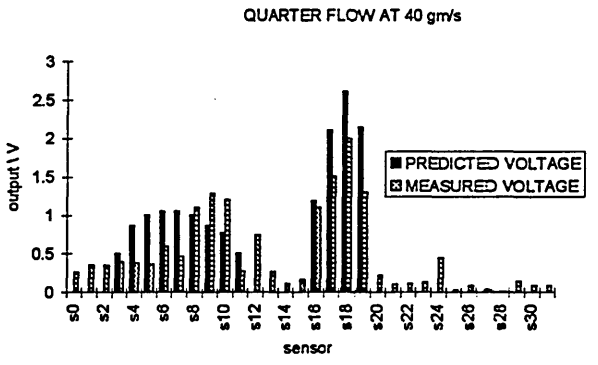

Figure 5.13a Quarter flow for plastic beads at 40 gm/s

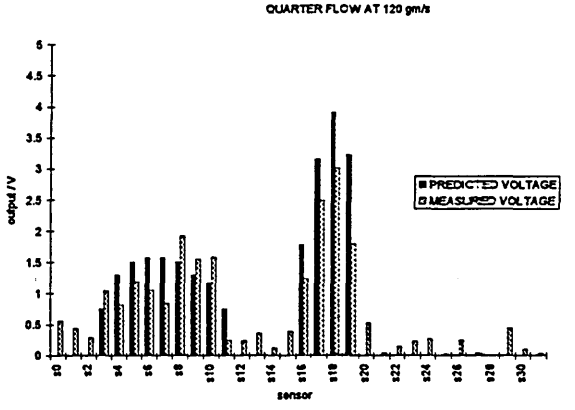

Figure 5.13b Quarter flow for plastic beads at 120 gm/s

5.2.3 Discussion on results from different types of flow

The results obtained by comparing the measured and predicted flow rates show some general agreement, however there are two noticeable discrepancies. Firstly, under half and quarter flows the predictions show several sensors with zero output. This is not achieved, though these sensors actually only show low levels of solids passing them. This result is probably due to inter particle collisions and particle wall collisions occurring while the solids travel between the baffle and the measurement section. Secondly, the voltage profile is different to the predicted profile. This is probably due to

a combination of two factors; the fact that the screw feeder fails to provide a uniform distribution across the pipe inlet (section 6.2) and the measured voltage profile only being a single sample of thirty-two seconds duration (a longer measurement period may improve the agreement between theory and practice (section 8.3)).

The total measured output for the thirty two sensors are summed for all the measurements. The values obtained for three quarter, half and quarter flow are compared with the total measured output for full flow at each mass flowrate to obtain an estimate the error of the system. Ideally the measurement should be independent of the flow regime, so that the system can be used to measured the mass flowrates.

Table 5.1 shows the error for each measurement for sand flow.

Profile	Mass flowrate (gm/s)	Total output voltage for 32 sensors (V)	Error (%)
Full flow	40	9.85	
	120	14.91	
	200	20.46	
	320	36.06	
Three quarter flow	40	10.79	9.54
	120	16.2	8.65
	200	20.39	0.33
	320	37.32	3.49
Half flow	40	10.23	3.86
	120	13.90	6.73
	200	19.10	6.65
	320	38.53	6.85
Quarter flow	40	9.35	5.08
	120	13.74	7.84
	200	18.83	7.97
	320	34.63	3.97

Table 5.1

The statistical parameters for the error have been calculated and show a mean of 6.76% and standard deviation of 3.94%. Figure 5.14 shows the comparison of the totallised

output voltage for different flow regimes at appropriate mass flowrates. The graph shows the system is reasonably independent of flow regime and so the optical fibre system is suitable as a concentration meter.

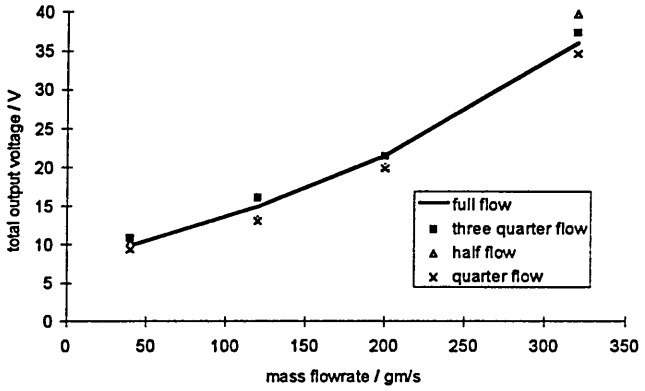

Figure 5.14 Comparison of the output for sand flow

Table 5.2 shows the error for each flow measurement for plastic bead flow.

Profile	Mass flowrate (gm/s)	Total output voltage for 32 sensors (V)	Error (%)
Full flow	40	13.91	
	120	20.63	
Three quarter flow	40	13.12	5.68
	120	21.60	4.70
Half flow	40	13.28	4.53
	120	21.57	4.56
Quarter flow	40	13.10	5.82
	120	21.72	5.28

Table 5.2

The statistical parameters for the error have been calculated and show a mean of 5.43% and standard deviation of 0.21%. Table 5.3 shows a comparison between the outputs of the sensors for sand and plastic beads.

Profile	Mass flowrate (gm/s)	Total output voltage for 32 sensors for plastic beads	Total output voltage for 32 sensors for sand
Full flow	40	13.91	9.85
	120	20.63	14.91
Three quarter flow	40	13.12	10.79
	120	21.60	16.20
Half flow	40	13.28	10.23
	120	21.57	13.90
Quarter flow	40	13.10	9.35
	120	21.72	13.74

Table 5.3

Table 5.3 shows that the output voltage for plastic beads is higher than sand at each flow rate. This may be due to the difference in particle sizes (chapter 7). Figure 7.4 suggests that at low frequency (frequencies below 160 Hz) the amplitude of the received signal is a function of particle size.

Table 5.4 shows the relation between sensitivity and beam length in terms of mass flowrate and output voltage. From equation 3.5

$$k = \frac{\sum_{0}^{31} V_i}{(\sum_{0}^{31} P_i)\,\dot{m}} \qquad (6.1)$$

Profile	Mass flowrate (gm/s)	Total output voltage for 32 sensors (V)	k
Full flow	40	9.85	1.21×10^{-4}
Three quarter flow		10.79	1.33×10^{-4}
Half flow		10.23	1.26×10^{-4}
Quarter flow		9.35	1.15×10^{-4}
Full flow	120	14.91	6.13×10^{-5}
Three quarter flow		16.20	6.65×10^{-5}
Half flow		13.90	5.71×10^{-5}
Quarter flow		13.74	5.65×10^{-5}
Full flow	200	20.46	5.04×10^{-5}
Three quarter flow		20.39	5.03×10^{-5}
Half flow		19.10	4.70×10^{-5}
Quarter flow		18.83	4.64×10^{-5}
Full flow	320	36.06	5.57×10^{-5}
Three quarter flow		37.32	5.75×10^{-5}
Half flow		38.53	5.94×10^{-5}
Quarter flow		34.63	5.34×10^{-5}

Table 5.4

The value of k is expected to be constant for each mass flowrate and independent of flow regime. Table 5.5 shows the average and standard deviation of k at each mass flowrate.

Mass flowrate (gm/s)	Average	Standard deviation
40	1.24×10^{-4}	4.24×10^{-6}
120	6.04×10^{-5}	3.39×10^{-6}
200	4.85×10^{-5}	2.83×10^{-6}
320	5.07×10^{-5}	1.41×10^{-7}

Table 5.5

The results obtained for k may be less reliable at low mass flowrates. Low flowrates of the order 40 gm/s are hard to control reliably and tend to pulse due to the operation of the screw feeder. This pulsing becomes less evident as the feed rate increases.

The statistical parameters for the error of the estimation of k over the flow range 120 gm/s to 320 gm/s have been calculated and show a mean of 5.84×10^{-5} and standard

deviation of 4.17×10^{-7}. The results of tables 5.4 and 5.5 are shown graphically in figure 5.15.

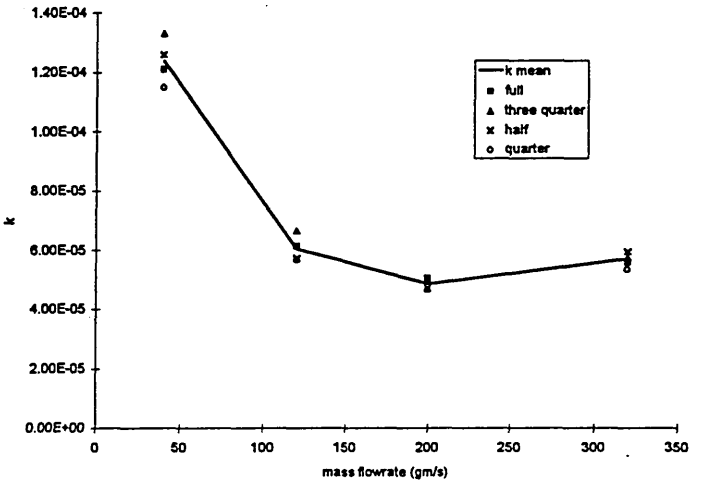

Figure 5.15 Value of *k* at each mass flowrate

Chapter 6

Concentration profiles

6.1 Concentration profiles

In this chapter, backprojection is used to generate an alternative representation of the data collected in chapter 5. This new representation provides a visual representation of optical density (concentration) information which is not obvious in the plots shown in chapter 5.

In chapter 5, sensor response was expressed as a one dimensional function of the arc length of a curve through the sensor set. After backprojection, density measurements are expressed with respect to a two-dimensional co-ordinate frame defining a plane through the sensor array. Each point in this co-ordinate system corresponds to a real-world location lying on a plane through the pipe. Density estimates are therefore registered with the pipe locations from which they arose.

The screw feeder is positioned on the right hand side with respect to the tomographic images (section 3.4.1). All the tomograms have the same sensor orientation with respect to the baffle, which is positioned relative to the left hand side of the image. As the flow profile is changed from full to quarter, the baffle is moved progressively to the right hand side of the pipe.

6.2 Concentration profiles for sand flow

6.2.1 Full flow

No baffle is used. Ideally the solids should be uniformly distributed across the measurement section.

Figure 6.1 shows the concentration profile at 40 gm/s.

Figure 6.1 Concentration profile for sand : full flow at 40 gm/s

This shows an uneven concentration profile, with most of the solids being imaged into the top part of the diagram.

Figure 6.2 shows the concentration profile at 120 gm/s.

Figure 6.2 Concentration profile for sand : full flow at 120 gm/s

The solids are distributed a little further over the cross-section than in figure 6.1.

Figure 6.3 shows the concentration profile at 200 gm/s.

313029 282726 2524 2322212019181716

Figure 6.3 Concentration profile for sand : full flow at 200 gm/s

The solids appear to be fairly uniformly distributed over the central part of the image.

Figure 6.4 shows the concentration profile at 320 gm/s.

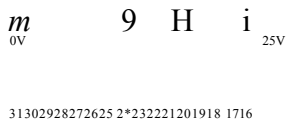

Figure 6.4 Concentration profile for sand : full flow at 320 gm/s

This diagram shows a slightly higher solids concentration at the centre of the pipe than at the edges. The profile does not appear completely uniform, but this may be due to the effects of the screw feeder and particles bouncing off the conveyor wall.

6.2.2 Three quarter flow

This is created by the baffle blocking a quarter of the pipe diameter so that three quarters is clear for sand flow (figure 3.6b)

Figure 6.5 shows the concentration profile at 40 gm/s.

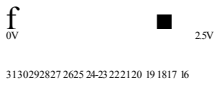

Figure 6.5 Concentration profile for sand : three quarter flow at 40 gm/s

Figure 6.6 shows the concentration profile at 120 gm/s.

Figure 6.6 Concentration profile for sand : three quarter flow at 120 gm/s

Figure 6.7 shows the concentration profile at 200 gm/s.

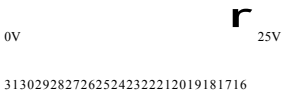

Figure 6.7 Concentration profile for sand : three quarter flow at 200 gm/s

Figure 6.8 shows the concentration profile at 320 gm/s.

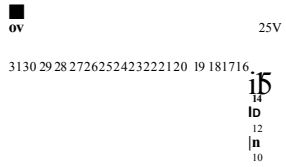

Figure 6.8 Concentration profile for sand : three quarter flow at 320 gm/s

The concentration profiles for three quarter flow are similar to these obtained with full flow (section (6.2.1).

6.2.3 Half flow

This is created by the baffle blocking half the pipe diameter so that the other half is clear for sand flow (figure 3.6c).

Figure 6.9 shows the concentration profile at 40 gm/s.

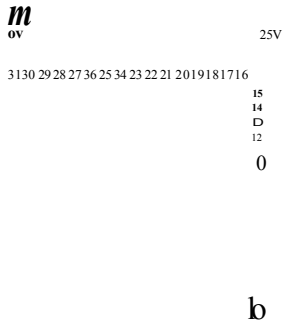

Figure 6.9 Concentration profile for sand : half flow at 40 gm/s

This shows the sand fairly evenly spread i.e. less variation in orange level than appears in figure 6.1 and 6.5 and mainly confined to the top right hand side of the image (the effect of the screw feeder).

Figure 6.10 shows the concentration profile at 120 gm/s.

Figure 6.10 Concentration profile for sand : half flow at 120 gm/s

Figure 6.11 shows the concentration profile at 200 gm/s.

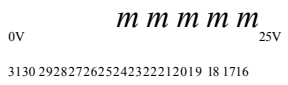

Figure 6.11 Concentration profile for sand : half flow at 200 gm/s

Figure 6.12 shows the concentration profile at 320 gm/s.

Figure 6.12 Concentration profile for sand : half flow at 320 gm/s

All four flow rates with half flow show most of the sand in the right hand side of the pipe, with much less flow beneath the obstruction.

6.2.4 Quarter flow

This is created by the baffle blocking three quarters of the pipe diameter so that the other quarter is clear for sand flow (figure 3.6d)

Figure 6.13 shows the concentration profile at 40 gm/s

Figure 6.13 Concentration profile for sand : quarter flow at 40 gm/s

Figure 6.14 shows the concentration profile at 120 gm/s.

Figure 6.14 Concentration profile for sand : quarter flow at 120 gm/s

Figure 6.15 shows the concentration profile at 200 gm/s

Figure 6.15 Concentration profile for sand : quarter flow at 200 gm/s

Figure 6.16 shows the concentration profile at 320 gm/s

31 30 29 28 27 26 25 21 23 22 21 20 19 18 17 16

Figure 6.16 Concentration profile for sand : quarter flow at 320 gm/s

The images for the four flow rates show the solids very close to the right hand side of the pipe. This agrees well with the position of the obstruction.

6.3 Concentration profiles for plastic beads

6.3.1 Full flow

No baffle is used. Ideally the solids should be uniformly distributed across the measurement section.

Figure 6.17 shows the concentration profile at 40 gm/s

Figure 6.17 Concentration profile for plastic beads : full flow at 40 gm/s

Figure 6.18 shows the concentration profile at 120 gm/s

Figure 6.18 Concentration profile for plastic beads : full flow at 120 gm/s

6.3.2 Three quarter flow

Figure 6.19 shows the concentration profile at 40 gm/s

Figure 6.19 Concentration profile for plastic beads : three quarter flow at 40 gm/s

Figure 6.20 shows the concentration profile at 120 gm/s.

Figure 6.20 Concentration profile for plastic beads : three quarter flow at 120 gm/s

The results shown in figure 6.17 to 6.20 show a reasonable uniform distribution.

6.3.3 Half flow

Figure 6.21 shows the concentration profile at 40 gm/s.

Figure 6.21 Concentration profile for plastic beads : half flow at 40 gm/s

Figure 6.22 shows the concentration profile at 120 gm/s.

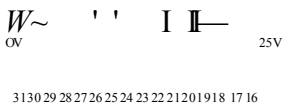

Figure 6.22 Concentration profile for plastic beads : half flow at 120 gm/s

The images shown in figure 6.21 and 6.22 show that the flow is virtually confined to the right hand side of the conveyor.

6.3.4 Quarter flow

Figure 6.23 shows the concentration profile at 40 gm/s.

Figure 6.23 Concentration profile for plastic beads : quarter flow at 40 gm/s

Figure 6.24 shows the concentration profile at 120 gm/s.

Figure 6.24 Concentration profile for plastic beads : quarter flow at 120 gm/s

Figure 6.23 shows most of the flow confined to the right hand side of the conveyor. Figure 6.24 is similar but more particles seem to have spread into the covered area of the conveyor probably due to particle/particle and particle/wall interactions at the higher feedrate.

6.4 Analysis of results and discussion

An alternative way of presenting the results shown in figure 6.1 to 6.24 is to represent the voltage in the third dimension. Figure 6.25 shows the isometric representation for sand flow at each flow regime at 200 gm/s. There is little effect from the baffle at three quarter flow (figure 6.25b) and the picture is similar to full flow (figure 6.25a). At half and quarter flow the baffle becomes more effective (figure 6.25c and 6.25d).

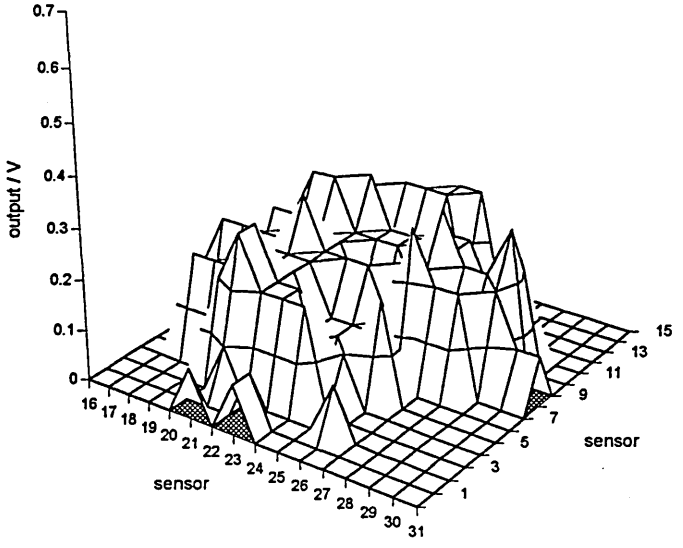

Figure 6.25a Full flow for sand at 200 gm/s

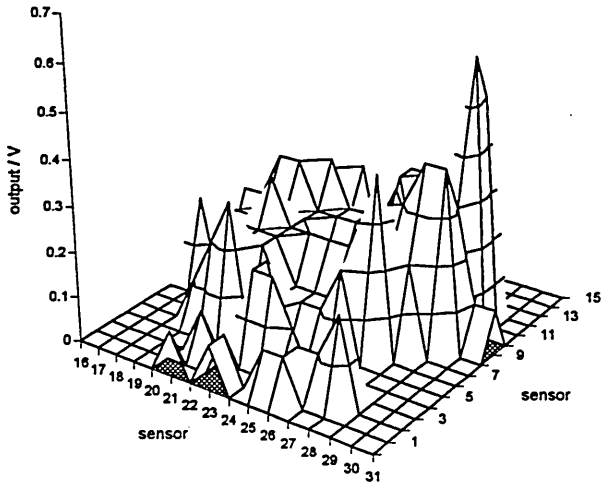

Figure 6.25b Three quarter flow for sand at 200 gm/s

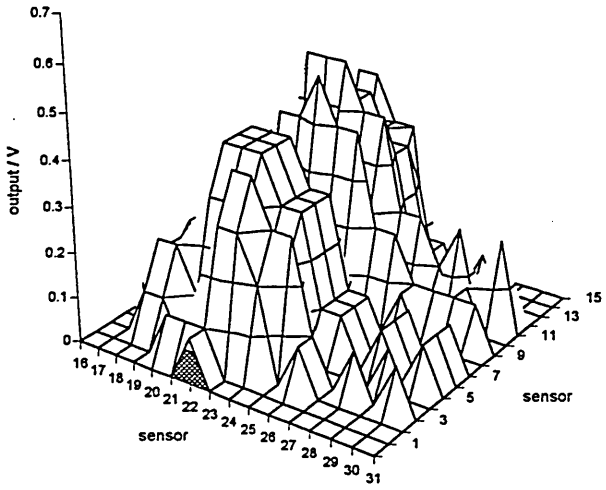

Figure 6.25c Half flow for sand at 200 gm/s

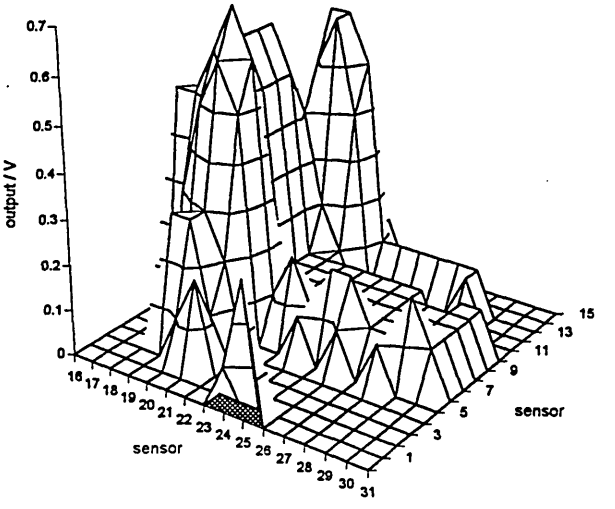

Figure 6.25d Quarter flow for sand at 200 gm/s

Figure 6.26 shows the three dimensional of picture for plastic beads with different flow regimes at a flow rate of 120 gm/. The baffle effects the flow profile at half and three quarter setting.

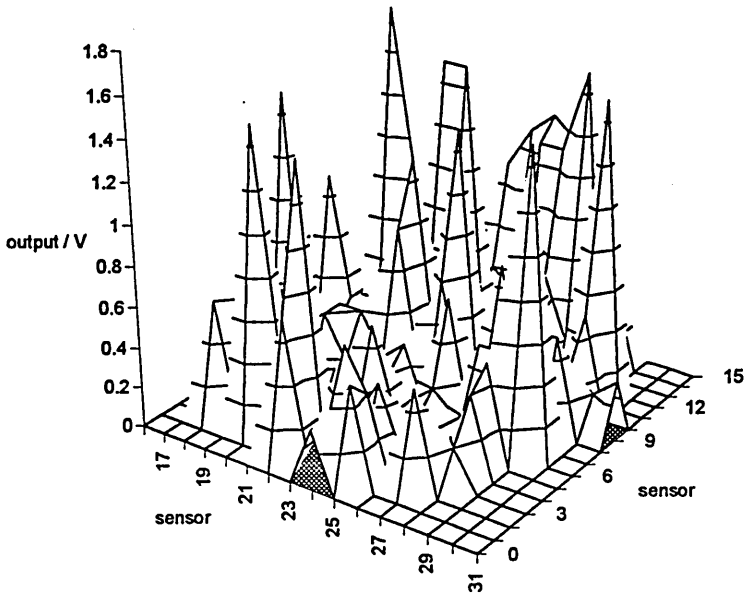

Figure 6.26a Full flow for plastic beads at 120 gm/s

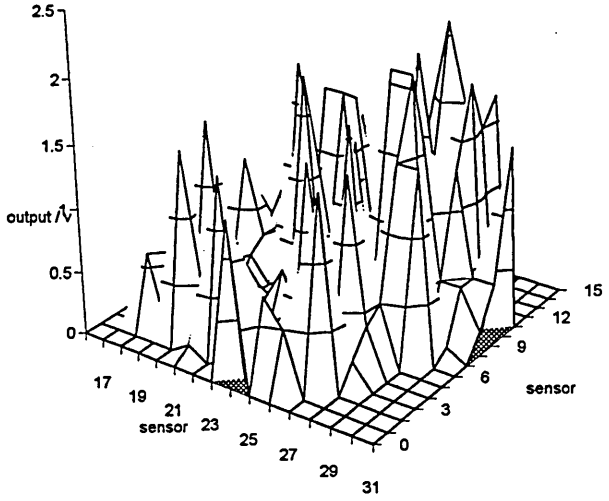

Figure 6.26b Three quarter flow for plastic beads at 120 gm/s

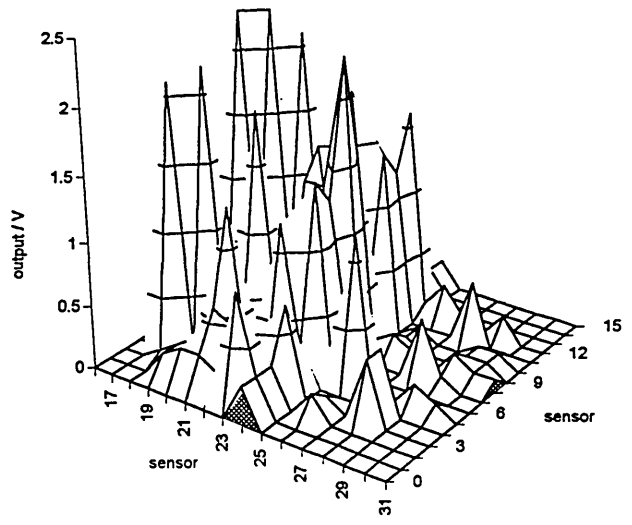

Figure 6.26c Half flow for plastic beads at 120 gm/s

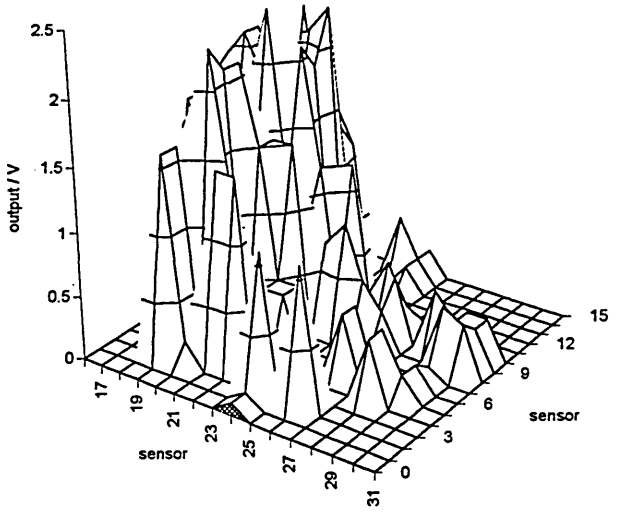

Figure 6.26d Quarter flow for plastic beads at 120 gm/s

Table 6.1 and 6.2 shows the error of the image reconstruction for sand and plastic beads. Solids concentration is obtained by summing each colour of pixel and multiplying by its weighting. The solids concentration value is then compared with the total output voltage

for the thirty two sensors at particular mass flowrates to get the error of the image reconstruction.

Profile	Mass flowrate (gm/s)	Total output voltage for 32 sensors (V)	Estimate solids concentration (V)	Error (%)
Full flow	40	9.85	9.35	5.08
	120	14.91	13.50	9.46
	200	20.46	18.62	9.00
	320	36.06	32.50	9.87
Three quarter flow	40	10.79	10.23	5.19
	120	16.2	15.10	6.79
	200	20.39	18.08	11.33
	320	37.32	33.26	10.88
Half flow	40	10.23	9.24	9.68
	120	13.23	11.54	12.77
	200	19.10	16.63	12.93
	320	39.74	35.16	11.52
Quarter flow	40	9.35	8.19	12.41
	120	13.02	11.35	12.83
	200	18.83	16.88	10.36
	320	34.63	30.54	11.88

Table 6.1 Error for sand flow

Profile	Mass flowrate (gm/s)	Total output voltage for 32 sensors (V)	Estimate solids concentration (V)	Error (%)
Full flow	40	13.91	12.70	8.70
	120	20.63	22.60	9.55
Three quarter flow	40	13.12	11.88	9.45
	120	21.60	19.89	7.92
Half flow	40	13.28	12.22	7.98
	120	21.57	19.20	10.99
Quarter flow	40	13.10	11.59	11.53
	120	21.72	18.73	13.77

Table 6.2 Error for plastic beads

Errors arise in using the data from the tomograms because of the quantisation level. Each colour step corresponds to a voltage change of 0.1 Volt. Thus zero to 0.09V is

quantised to 0.0V, 0.01V to 0.19V is quantised to 0.01V. The total colour graduations from 0 volt to 2.5 volt in 26 steps of interval 0.1V. Improvements in error could be obtained by using more colour levels e.g. 256 instead of the existing 26.

CHAPTER 7

Particle size range determination

7.1 Introduction

An aim of the project (section 1.3) was to investigate the signals produced by the receiver optical fibres for particle size information. As the particles passes the of optical fibre receiver the light intensity will vary depending upon the particle size; large particles may obscure all the light while smaller particles will only attenuate it. Further, the light intensity will initially decrease and then increase back to its original level as the particle passes by. Figure 7.1 shows a diagrammatic view of the phenomena.

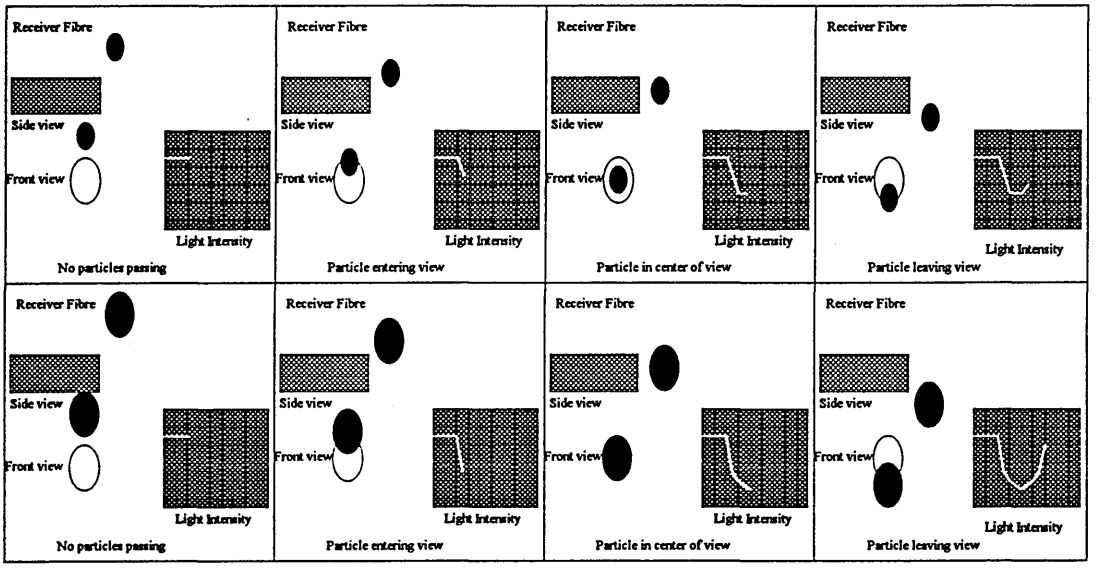

Figure 7.1 Particle size

The experiments to investigate the effect of particle size were carried out using approximately spherical particles with sizes between 44 μm and 5 mm diameter.

7.2 Power spectrum analysis

A belt feed system (figure 7.2) provided an approximately continuous, uniform flow rate of a predetermined size of solid particles into a vertical pipe containing a single transmitter/receiver pair. The bandwidth limited (section 4.4.2) continuous analogue signal from the receiver (section 4.4.2) was fed into a Hewlett-Packard spectrum analyser and the power spectrum obtained. The experiment was repeated with each size of particle and their characteristic power spectrums obtained (figure 7.3). The amplitudes of the power spectra were different for the different particle sizes (figure 7.4).

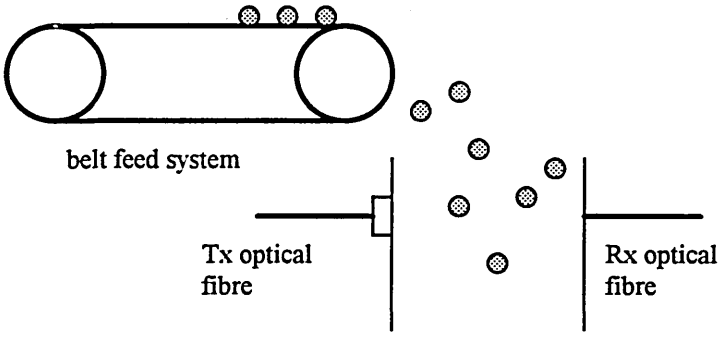

Figure 7.2 System for investigating relationship between particle size and power spectra

Figure 7.3 shows the power spectrum for particle sizes of 44 μm, 600 μm, 1 mm, 2 mm and 5 mm.

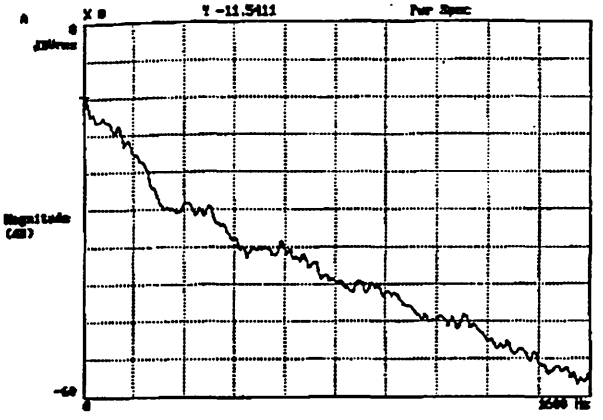

Figure 7.3 (a) Power spectrum for particle approximately 5 mm in diameter

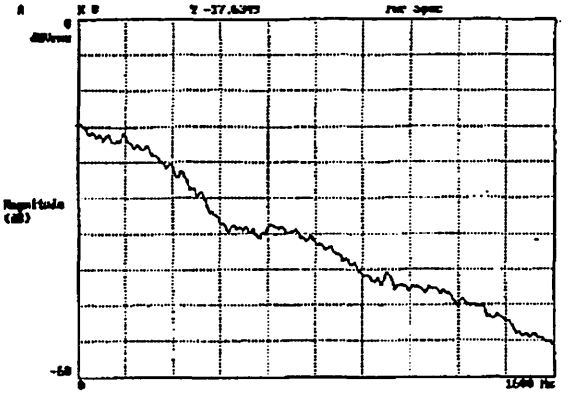

Figure 7.3 (b) Power spectrum for particle approximately 2 mm in diameter

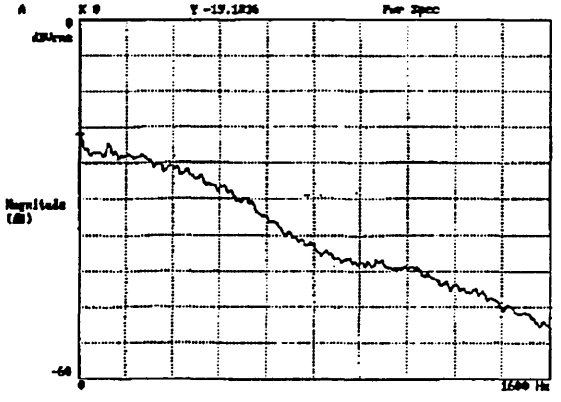

Figure 7.3 (c) Power spectrum for particle approximately 1 mm in diameter

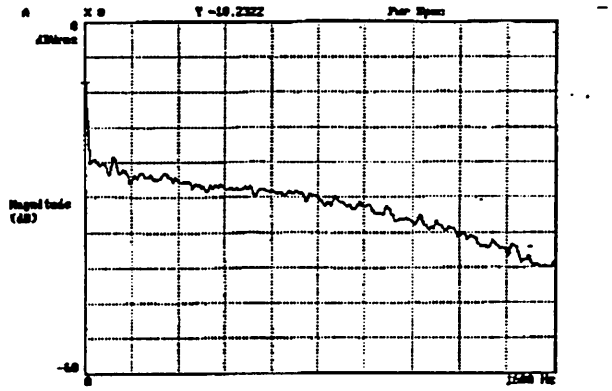

Figure 7.3 (d) Power spectrum for particle approximately 600 μm in diameter

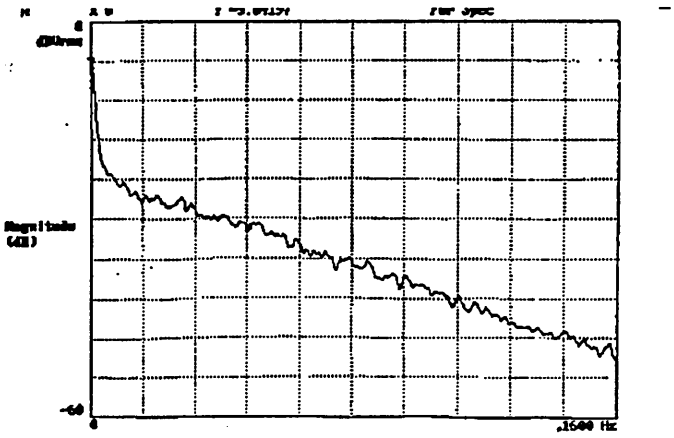

Figure 7.3 (e) Power spectrum for particle approximately 44 μm in diameter

The results shown in figure 7.3 represent 401 points over a range of 1.6 kHz. All the results from figure 7.3 are combined in figure 7.4. Each point on the graph represents an average of ten measurements at a given flow rate for a fixed particle size range.

o

Frequency/ Hz

Figure 7.4 The combined power spectra

To remove the effect of particle concentration from the measurements, all the spectra were normalised by dividing each spectrum by its magnitude in dBVrms (e.g. -25 dB) at a frequency of 160Hz (figure 7.5). This results in all the responses passing through (160,1) and all y values being positive (figure 7.5).

7.3 Discussion of results

A comparison of the results for different sizes of particle shows the magnitude of the power spectra are approximately the same at 160 Hz (figure 7.4). Normalising the power spectrum at 160 Hz, as shown in figure 7.5, demonstrates a significant and progressive change of gradient between 160 Hz and 480 Hz for the 600 pm to 2 mm diameter particles. The gradient for the 2 and 5 mm diameter particles are very similar to each other at frequencies above 160 Hz, however they are distintly different at frequencies below 160 Hz. The results for the 44 pm particles do not follow this trend and suggest that useful information on particle size is restricted to particles greater in

size than 44 pm. It is believed that information regarding particles size may be extracted from the flow signals, however, further work is required (section 8.3).

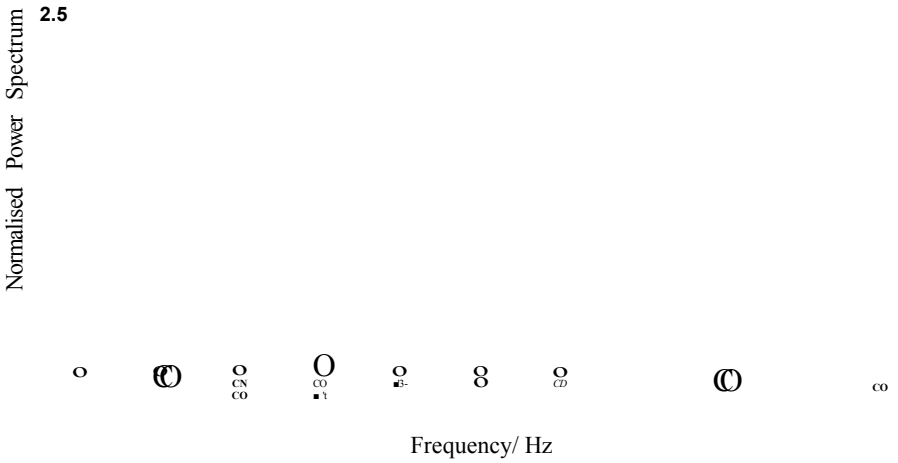

Figure 7.5 Normalised power spectra for different particles sizes

CHAPTER 8

Conclusion and suggestions for future work

8.1 Conclusion

The specific objectives of the thesis have been met as follows

- The review of sensor types presented in chapter two covers the first objectives.
- Chapter three presents a model representation of an optical fibre concentration measurement system (objective two) and introduces the back projection reconstruction algorithm which is tested in chapter six (objectives six).
- An optical sensor has been designed (objectives three). It has been used singly for concentration measurement (chapter five)(objective three) and to investigate particle size distribution (chapter seven)(objectives five).
- Arrays of optical fibre sensors have been used for concentration measurements (chapter five) to determine concentration profiles (chapter six, objectives four and five).
- Tomographic images of concentration are presented in chapter six (objectives six). All the concentration testing made use of the gravity drop conveyor (objectives seven).
- Seventeen suggestions for further work are presented in chapter eight (objectives eight).

8.2 Contribution to the field of process tomography

The 16 x 16 optical sensor array is capable of making concentration measurements using sand of size range of 300 μm and plastic beads of nominal diameter 2 mm and mass flowrates ranging from 40 gm/s to 320 gm/s on a gravity drop conveyor with an error of better than ±5% of reading. Tomograms of the concentration profile have been determined and the optical sensors are sensitive to particle size, though further work is needed on this aspect (section 8.3).

8.3 Suggestions for future work

- The present system should be evaluated on a pneumatic conveyor with a range of different solids. Throughout the tests, the accuracy should be noted. The effect of the solids particle size range should be noted and related to the accuracy obtained.

- The measurement system should be used with a wider range of concentrations than has been presented in this work. It may be possible to significantly increase the maximum concentrations determinable by reducing the gains of the final two stages. The error in the measurement is expected to increase with higher concentrations when several particles intercept the same beam simultaneously.

- This investigation has been restricted to vertical flow where the particles are subject to gravity. The system should be evaluated using pneumatic conveyor with the measurement system positioned in both horizontal and vertical sections of the conveyor.

- The averaging time constant of one second was chosen arbitrarily. The effect of different time constants should be investigated with different particle size distributions over a range of conveying velocities.

- The optical coupling needs to be examined to improve collimation and increase the intensity of the detectable radiation. Improved collimation may be obtained by producing spherical surfaces as the optical fibres taking light into the conveyor. This may be possible using mechanical methods and should be investigated.

- More information would be obtained by increasing the resolution, that is increasing the number of sensors in each projection to 32 x 32. With improved collimation fibres sensors could be placed 1 or 2 mm apart and provide very high resolution. Also using optical fibre emission it would be physically easier to increase the number of projections without a significant increase in the sensing volume. This would require a new reconstruction algorithm and the ability to handle larger amounts of data. In addition, increasing the number of projections would reduce the problems of aliasing, which have not been addressed in this thesis because with the lean flows used aliasing is unlikely to happen very frequently.

- Increasing the number of transducers above sixty-four would mean the present sequential data capture system could not be used. The fall in cost of data acquisition circuits means that projection or arrays of transducers could be read in parallel, enabling larger numbers of views to be read in within the present data capture period.

- The electronics for the existing transducer should be modified in several ways. Two outputs should be provided for each channels; one with 8 kHz bandwidth for

frequency information relating to particle size distribution., the other with a low pass filtered output for concentration measurement. All the amplifiers should be selected for adequate gain bandwidth product and low dc offset voltage and offset drift.

- To enable a wide range of flowrates to be investigated a programmable gain amplifier, with low offset, is required. This will improve the receiver in two ways; by reducing the dc offset voltage and by enabling the system gain to be varied to suite the application.

- A more detailed investigation of particle size distributions should be carried out. A wide range of samples with different mean diameters and particle size distributions should be used in a pressure type pneumatic conveyor.

- The possibility of combining tomograms of the cross section showing the concentration distribution with particle size distribution tomograms should be investigated. This would provide an investigative system for plant optimisation and design.

- Flow regime image reconstruction could use a continuous algorithm that produced a new image for every set of data captured in a similar way to direct Fourier reconstruction (Xie et. al 1991), as used in medical tomography. However, if processing is difficult to do in real time, due to the complexity of the reconstruction and large quantity of information, a more discrete algorithm could be employed.

- To reconstruct images of complex flow regimes more information will be required from the tomographic cross-section. This will necessitate a larger number of

transducers, a rise in the number of projections and an increase in the complexity of the image reconstruction algorithm used.

- The present work investigates component concentration within the sensing cross-section. In order to extend the system to determine volume flow rates of the solid components it is necessary to measure component velocities, etc. This possibility should be investigated using suitable instrumentation, cross-correlation and a flow-rig.

- Application of image segmentation algorithms to the reconstructed images may provide opportunities to extract specific features of the flow. This may have specific relevance to velocity measurement by enabling cross-correlation of features instead of pixels. This would speed up the correlation when the features consist of several pixels.

- The reconstruction algorithms should be improved and the data acquisition and CPU speeds determined with the aim of providing on-line measurements.

- The effect of scattering and diffraction of light due to the particles has been neglected. Further work to determined their importance in the flow measurement is required. The information, presently being neglected, may have relevance to particle size distribution.

References

Abdullah M.Z., Dyakowski T, Dickin FJ and Williams RA, Observation of hydrocyclone separator dynamics using resistive electrical impedance tomography, *ECAPT93 Conference, Germany 1993.*

Banholzer, W.F, Spiro, C.L, Kosky, P.G, and Maylotte, D.H. : Direct imaging of time-averaged flows pattern in a fluids reactor using X-ray computed tomography, *Ind. & Eng. Chem. Res.*, 1987, 26.

Barber, D.C and Brown, B.H, Applied potential tomography, *J Phys.E: Sci Instrum,* vol 17 p 723-733, 1984.

Beck, C.M, Instrumentation and control for minimum energy consumption in pneumatic conveying, *Ph.D thesis,* University of Bradford, 1986(Dec).

Bemrose, C.R., Fowles, P., Hawkesworth, M.R., and O'Dwyer, M.A.. : *Application of positron emission tomography to particulate flow measurement in chemical engineering process. Nucl. Instrum. & Methods Phys. Res.*, 1988, A273.

Bidin A.R Electrodynamics sensors and neural networks for electrical charge tomography, *Thesis*, 1993, School of EIT Sheffield Hallam University.

Cady, E. B., 1990. Clinical magnetic resonance spectroscopy. *Plenum Press, New York.*

Chaimowicz J.C.A., Lightwave technology, *Butterworths* England, 1989.

Chen Q, Hoyle BS and Strangeways HJ, Electric field interaction and enhanced reconstruction algorithm in capacitance process tomography, *ECAPT 1992,* page 170-177

Dickin, F.J., Zhao, X.J., Abdullah, M.Z. and Waterfall, R.C. : Tomographic imaging of industrial process equipment using electrical impedance sensors. *Proc. V Conf. Sensors and their applications,* Edinburgh, Scotland, September 1991a, pp. 215-220

Dickin FJ, Hoyle BS, Hunt SM, Illyas O, Lenn C, Waterfall RC, Williams RA, Xie CG and Beck MS, Tomographic Imaging of industrial equipment - reviews of needs and methods in Grattan, KTV (ed); *Sensors - Technology, Systems and applications*, 1991b.

Dickin, F. J., 1992b. Tomography for improving the design and control of particulate processing systems. *KONA - Powder and Particle,* 10, pp 4-14.

Dugdale P, Green RG, Hartley AJ . Jackson RJ, Landauro J, Tomographic imaging in industrial process equipment using optical sensor arrays, *Sensor technology systems and application 5th conference* paper edited by K. T. V. Grattan, 1993.

Dugdale P, Green RG, Hartley AJ . Jackson RJ, Landauro J, Optical sensors for process tomography, *ECAPT 1992, Process Tomography: A Strategy for Industrial Exploitation, European Concerted Action on Process Tomography* 26 - 29 March 1992, Manchester, United Kingdom.

Dugdale P, Green RG, Hartley AJ, Jackson A, Laundro, Using optical sensor arrays in Grattan, KTV (ed); *Sensors - Technology, Systems and Applications,* 1991.

ECAPT92, first meeting of the European Concerted Action on Process Tomography, Manchester 1992.

Gabor H., Image reconstruction from projections : the fundamental of computerized tomography, *Academic press* 1980.

Ghassemlooy Z, Fibre optic a revolution in communication, Page 2, *EIT Publication for ESCE IV,* 1992.

Green R.G., Holberry N. M., Abdul Rahim R., Dickin F. J., Naylor B.D, Pridmore T. P., Optical fibre sensors for process tomography, *Journal Measurement Science And Technology,* to be published

Helicon encyclopaedia, Helicon publishers 1991

Henry RM and Beck MS, *I*ncipient fault detection in pipeline transporting solid material, On-line surveillance and monitoring of process plant, *Society of chemical industry* 1977.

Horowitz P., The art of electronics, *Cambridge university press,* 1993

Hoyle B.S and Xu L.A Ultrasonic sensors, *Process Tomography: Principles, techniques and applications,* edited by R.A williams and M.S Beck , chapter 8 page 118 published by Butterworth-Heinemann Ltd Oxford 1995.

Huang SM, Stott AL, Green RG and beck MS, Electronic transducers for industrial measurement of low value capacitance, *J Phys E: Sci Instrum* vol 21 1988.

Huang SM, Xie CG, Thorn R, Snowden D, Beck MS, Tomographic Imaging of industrial process equipment - design of capacitance sensing electronics for oil and gas based processes, in Gratan, KTV (ed); *Sensors - Technology, Systems and applications,* 1991.

Ilyas O and Williams R, Will tomography make cfd models redundant ?, *ECAPT93* Karlshure, 1993.

Isaksen O and Nordtvedt JE, Capacitance tomography: Reconstruction based on optimisation theory, *ECAPT 1992*, page 178-189.

Jaffe, C., 1984. Vascular and Doppler ultrasound, *Churchill Livingstone.*

Jenkins T.E., Optical sensing techniques and signal processing, Prentice Hall, 1987.

Kremkau, F. W., 1990. Doppler ultrasound: principles and instruments, *Saunders.*

Li W and Hoyle BS, Sensor optimisation for ultrasonic process tomography, *ECAPT 93* Conference, Germany 1993.

Li W and Hoyle BS, Multiple active sensors in ultrasonic process tomography systems, *Frontiers on process tomography* conference in California 1995, pp 289.

Longhurst R. S., *Geometrical and physical optics*, Published by Longman 1957

Mckee S. L., Applications of nuclear magnetic resonance tomography, *Process Tomography: Principles, techniques and applications,* edited by R.A williams and M.S Beck , chapter 24 page 539 published by Butterworth-Heinemann Ltd Oxford 1995.

Nordin, M. J., An image reconstruction algorithm for a dual nodality tomographic system, *Thesis* 1995, Sheffield Hallam University.

Omotosho O.J., Frith B., Plaskowski A. and Beak M. 1989 A sensing system for non destructive imaging using externally compton-scattered gamma photons *Sensors and Actuator,* 18 1-15.

Parker, D. J 1992. Process engineering studies using positron-based imaging techniques, *Proceeding ECAPT 92, Process Tomography: A Strategy for industrial exploitation, European Concerted Action on Process Tomography*, March 92, Manchester.

Plaskowski A, Bukalski P, Habdas T, Skolimaski, Tomographic imaging of process equipment - application to pneumatic transport of solid material, Grattan, KTV (ed); *Sensors - Technology, Systems and Applications*, 1991.

Plaskowski A, Beck MS, Thorn R, Dyakowski T, Imaging industrial flows: Application of electrical process tomography, *Institute of Physics Publishing Bristol and Philadelphia*, 1995.

Rhodes M. J., Pneumatic conveying, chapter 7 in *Principles of powder technology,* ed M Rjodes, John Wiley & Sons 1990.

Saeed N,. Browne MA, Green RG and Martin P, Two component flow regime identification and imaging with optical sensors, *IMEKO XI Houston,* Texas, 16 - 21 October 1988.

Shackleton M.E., Electro dynamic transducer for gas/solids flow measurement, Mphil thesis, 1981, University of Bradford..

Simon, G., 1975. X-ray diagnosis for clinical students. *Butterworths*, England.

Snyder R and Hesselink L, Three-dimensional optical tomographic measurements of mixing fluids, *Proceedings of the SPIE : The International Society for Optical Engineering,* Vol 1083, page 281-9, date 1989.

Wells, P. N. T., 1977. Biomedical Ultrasonics, *Academic Press*, London.

Xie C.G., Electrical Capacitance Tomography, *ECAPT 1993*, page 225-228.

Xie C.G., Huang SM, Hoyle BS, Beck MS, Tomographic Imaging of industrial process equipment - development of system model & image reconstruction algorithm for

capacitive tomography, in Grattan, KTV (ed); *Sensors - Technology, Systems and applications,* 1991.

Xie C.G., Plaskowski A, Beck MS, 8 electrode capacitance for two component flow 3

identification, *IEE proc* vol 136 ptA no 4 July 1989.

Xu, L. A., Green, R. G., Plaskowski, A. and Beck, M. S., 1988. The pulsed ultrasonic cross-correlation flowmeter for two-phase flow measurement, *Journal of Physics, E: Sci. Instrum*, Vol. 21, pp 406-414.

Yan. Y, Woodhead. S, Byrne. B, Coulthard. J, 1992, Measurement of pneumatically conveyed pulverised fuel using non-restrictive techniques, *International Conference On Electronic Measurement & Instrumentation (ICEMI) 1992,* China, pp 153-156.

PUBLICATIONS RELATING TO THE THESIS

Journal

1. *Further development of a tomographic imaging using optical fibres for pneumatic conveyors,* Journal Measurement , Science and to be published R. Abdul Rahim, R G Green, N. M. Horbury, F. J. Dickin, B. D. Naylor, T. P. Pridmore

2. *Optical fibre sensors for process tomography,* Journal Measurement , Science and Technology to be published. R G Green, N. M. Horbury,. R. Abdul Rahim ,F. J. Dickin, B. D. Naylor, T. P. Pridmore.

3. *Optical fibre sensors for process tomography : Concentration measurements and scattering effect* Journal of Industrial Technology SIRIM (awaiting referees reports) R. Abdul Rahim, R G Green, N. M. Horbury, F. J. Dickin, B. D. Naylor, T. P. Pridmore

4. *Tomographic imaging using optical sensor arrays* Journal Computing & Control Engineering (awaiting referees reports) R. Abdul Rahim, MJ Nordin, N. Horbury, Dr. F. J. Dickin, Prof. R. G. Green , B.D. Naylor

(Note : Paper 1, 2 and 3 are presented in Appendix D)

International conference

1. *Initial work on tomographic imaging using optical fibres for pneumatic conveyors,* ECAPT95 conference Norway, page 127-133, 1995 R. Abdul Rahim, R G Green, N. M. Horbury, F. J. Dickin, B. D. Naylor, T. P. Pridmore

2. *An investigation into the use of optical fibres to produce on-line particle size information and tomographic images for hydraulic processes,* ECAPT95 conference Norway, page 134-138, 1995 R. Abdul Rahim, R G Green, N. M. Horbury, F.J. Dickin, B. D. Naylor, T. P. Pridmore

3. *A prototype tomographic imaging system using optical fibres for pneumatic conveyors,* ICAST95 conference at UKM Malaysia, page 197-204, vol. 3 Electronics and information technology), 1995 R. Abdul Rahim, M.J. Nordin, R G Green, N. M. Horbury,. F.J. Dickin, B. D. Naylor, T. P. Pridmore

4. *A preliminary result on tomographic imaging system using optical fibres for pneumatic conveyors,* Sensor and Application VI Conference at Dublin, 10 - 13 September 1995, organised by Institute of Physics (IOP). page 290. R. Abdul Rahim, MJ Nordin, R G Green, N. M. Horbury,. F.J. Dickin, B. D. Naylor, T. P. Pridmore

5. T*omographic imaging system using optical fibres for pneumatic conveyors* Frontiers on Process Tomography Conference at California November 1995 R. Abdul Rahim, R G Green, N. M. Horbury, F. J. Dickin, B. D. Naylor, T. P. Pridmore

6. *Tomographic imaging of transparent slurries with particle sizing using optical fibres,* Frontiers on Process Tomography Conference at California November 1995 R. Abdul Rahim, R G Green, N. M. Horbury, F. J. Dickin, B. D. Naylor, T. P. Pridmore

7. *Optical fibre sensor for process tomography use on pneumatic conveyors* IEE colloquium on progress in fibre-optic sensors and their applications November 1995 at Savoy Place, UK. R. Abdul Rahim, R G Green, N. M. Horbury, F. J. Dickin, B. D. Naylor, T. P. Pridmore

8. *Particle size measurement and scattering effect on tomographic imaging system using optical fibres for pneumatic conveyors*, Particle science and technology in the 21st century conference at Tata Research Development & Design Centre, Pune, India on 8-21 December 1995 , ,R. Abdul Rahim, N. M. Horbury, G Green, N. M. Horbury, F. J. Dickin, B. D. Naylor, T. P. Pridmore

9. *Initial investigation into the use of optical fibres to produce on line particle size information and tomographic images for hydraulic processes* Particle science and technology in the 21st century conference at Tata Research Development & Design Centre, Pune, India on 18-21 December 1995 , .R. Abdul Rahim, N. M. Horbury, R G Green, N. M. Horbury, F. J. Dickin, B. D. Naylor, T. P. Pridmore

10. *Tomographic Imaging System Using Optical Fibres* Research Seminar at School Of Engineering Information Technology, Sheffield Hallam University on 10th January 1996. R. Abdul Rahim, N. Horbury,. R G Green, F. J. Dickin, B. D. Naylor, T. P. Pridmore

11. *Optical fibre sensor for process tomography : Application to pneumatically conveyed solids* Engineering foundation conference on Pneumatic and Hydraulic Conveying Systems, on 21-26 April 1996 at Florida USA. R. Abdul Rahim, N. Horbury,. R G Green, F. J. Dickin, B. D. Naylor, T. P. Pridmore

Presented papers

1. European Concerted Action On Process Tomography (ECAPT95) conference in Bergen, Norway, April 1995.

2. International Conference On Advances In Strategic Technologies (ICAST95) at University Kebangsaan Malaysia (UKM), June 1995.

3. Sensor and Application VI Conference at Dublin, 10 - 13 September 1995,

4. Research Seminar at School Of Engineering Information Technology, Sheffield Hallam University on 10th January 1996

APPENDICES

Appendix A Data acquisition system data sheet

Appendix B Transmitter fibre output powers

Appendix C Tests on the receiver optical fibre

Appendix D Selection of papers relating to work presented in this thesis

1. Further development of a tomographic imaging system using optical fibres for pneumatic conveyors.

2. Optical fibre sensors for process tomography : Concentration measurements and scattering effect.

3. Optical fibre sensors for process tomography.

Tables A-1 to A-4 list specifications for the DAS-1800HC Series boards.

Table A-1. Analog Input Specifications

Attribute	DAS-1801HC Boards	DAS-1802HC Boards
Number of channels	Software-selectable as 32 differential or 64 single-ended	
Input mode	Software-selectable as unipolar or bipolar	
Resolution	12-bit (1 part in 4096)	
Data format	16-bit twos complement, right-justified	
FIFO size	1024 word	
Channel-gain QRAM size	64 locations	
Gain (range)	1 (0.0 to +5.0 V for unipolar) 1 (±5.0 V for bipolar)	1 (0.0 to +10 V for unipolar) 1 (±10 V for bipolar)
	5 (0.0 to +1.0 V for unipolar) 5 (±1.0 V for bipolar)	2 (0.0 to +5.0 V for unipolar) 2 (±5.0 V for bipolar)
	50 (0 to 100 mV for unipolar) 50 (±100 mV for bipolar)	4 (0.0 to +2.5 V for unipolar) 4 (±2.5 V for bipolar)
	250 (0 to +20 mV for unipolar) 250 (±20 mV for bipolar)	8 (0.0 to 1.25 V for unipolar) 8 (±1.25 V for bipolar)
Absolute accuracy	Typical: 0.01% of reading ±1 LSB for all ranges	
	Maximum error: • 0.02% of reading ±1 LSB max @ 25° C for gain < 250 • 0.03% of reading ±1 LSB max @ 25° C for gain = 250	

Table A-1. Analog Input Specifications (cont.)

Attribute	DAS-1801HC Boards	DAS-1802HC Boards
Temperature coefficient of accuracy (includes ADC)	Offset: • Bipolar: ±20 µV/ °C ±(12 µV/° C ÷ gain) max • Unipolar: ±20 µV/ °C ±(14 µV/° C ÷ gain) max	
	Gain: • ±20 ppm/ °C for gain of < 50 • 30 ppm/° C for gain = 50 • 35 ppm/° C for gain = 250	
Linearity[1]	Integral: ±½ LSB typical, ±1 LSB max.	
	Differential: ±1 LSB	
Throughput	Refer to "Maximum Achievable Throughput Rates" on page 2-4	
Dynamic parameters	Acquisition time: 0.3 µs	
	Aperture delay: 13.0 ns	
	Aperture uncertainty: 150 ps rms	
	Conversion time: 3.0 µs max. (includes acquisition time)	
Input bias current	±40 nA max. @ 25° C	
	±60 nA max. over operating range	
Common mode rejection ratio	74 dB for gain = 1	74 dB for gain = 1
	80 dB for gain = 5	80 dB for gain = 2
	100 dB for gain = 50	80 dB for gain = 4
	100 dB for gain = 250	86 dB for gain = 8
Input overvoltage	±15 V continuous powered	
	±15 V continuous unpowered	

Table A-1.. Analog Input Specifications (cont.)

Attribute	DAS-1801HC Boards	DAS-1802HC Boards
Noise:[2]	Bipolar electrical noise (in counts) • Gain = 1: p-p = 1; rms = 0.1 • Gain = 5: p-p = 1; rms = 0.1 • Gain = 50: p-p = 4; rms = 0.5 • Gain = 250: p-p = 8; rms = 1.0	Bipolar electrical noise (in counts) • Gain = 1: p-p = 1; rms = 0.1 • Gain = 2: p-p = 1; rms = 0.1 • Gain = 4: p-p = 1; rms = 0.1 • Gain = 8: p-p = 1; rms = 0.1
	Unipolar electrical noise (in counts): • Gain = 1: p-p = 1; rms = 0.1 • Gain = 5: p-p = 1; rms = 0.1 • Gain = 50: p-p = 6; rms = 0.9 • Gain = 250: p-p = 9; rms = 1.4	Unipolar electrical noise (in counts): • Gain = 1: p-p = 1; rms = 0.1 • Gain = 2: p-p = 1; rms = 0.1 • Gain = 4: p-p = 1; rms = 0.1 • Gain = 8: p-p = 1; rms = 0.1
DMA levels	5, 6, and 7	
Interrupt levels	3, 5, 7, 10, 11, and 15	
Minimum external pacer clock pulse width	10 ns	
Maximum external pacer clock rate	333 kHz	
Minimum hardware trigger pulse width	10 ns	

Notes

[1] Monotonicity is guaranteed over the operating range.

[2] The figures in the table show the electrical noise introduced by the analog front end *but do not include the uncertainty inherent in the quantization process.* The inherent quantization noise introduced by any ADC is due to uncertainty at code boundaries and adds a peak-to-peak value of 1 LSB to the electrical noise; it also makes the rms level 0.5 LSBs.

Table A-2. Analog Output Specifications

Attribute	DAS-1801HC Specifications	DAS-1802HC Specifications
Resolution	12-bit (one part in 4096 or 224 ppm)	
Data format	Right justified, offset binary	
Range	±10.00 V	
Linearity[1]	Integral: ±¼ LSB typical; ±½ LSB max.	
	Differential: ±1 LSB	
Output current drive	±5 mA max.	
Capacitive load drive	100 µF	
Gain accuracy	Adjustable to 0	
Offset accuracy	Adjustable to 0	
Glitch energy	300 nV * seconds	
Power up	DACs power up to 0.0 V at reset	

Notes

[1] Monotonicity is guaranteed over the operating range.

Table A-3. Digital I/O Specifications

Attributes	DAS-1801HC Specifications	DAS-1802HC Specifications
Digital output (including SSHO, DOSTB, and TGOUT)	V_{OH} (min.) = 2.7 V @ I_{OH} = –400 µA	
	V_{OL} (max.) = 0.5 V @ I_{OL} = 8 mA	
Digital input	V_{IH} (min.) = 2.0 V; I_{IH} (max.) = 20 µA	
	V_{IL} (max.) = 0.8 V; I_{IL} (max.) = –0.2 mA	
Digital output strobe pulse width	300 ns typical; data is latched on the rising edge of DOSTB	

Table A-4. Power Supply Requirements

Attribute	DAS-1801HC and DAS-1802HC Specifications
+5 VDC input	430 mA typical; 870 mA maximum
+12 VDC input	400 mA typical; 550 mA maximum
Maximum current available at the ±15 V outputs	30 mA
Maximum current available at the +5 V output	1.0 A

APPENDIX B

Transmitter fibre output powers

Transmitter	Output/μW
0	5.2
1	4.9
2	5.2
3	5.0
4	4.9
5	5.1
6	5.1
7	5.0
8	4.9
9	5.1
10	5.1
11	5.1
12	5.0
13	5.0
14	5.1
15	4.9
16	5.0
17	5.0
18	5.1
19	5.1
20	5.1
21	4.9
22	4.9
23	5.2
24	5.1
25	4.8

26	5.1
27	5.0
28	4.9
29	5.0
30	5.1
31	5.1

APPENDIX C

Tests on the receiver optical fibre.

Receiver	Output/mV
0	26
1	26
2	25
3	27
4	28
5	24
6	26
7	26
8	25
9	26
10	24
11	25
12	27
13	26
14	28
15	28
16	24
17	26
18	26
19	26
20	25
21	26
22	28
23	24
24	26
25	24

26	25
27	26
28	24
29	24
30	24
31	25

Further development of a tomographic imaging system using optical fibres for pneumatic conveyors

R. Abdul Rahim[1 3], Professor R.G.Green[1], N. Horbury[1], Dr. F.J.Dickin[2], B.D. Naylor[1], Dr. T.P.Pridmore[1]

1 School of Engineering Information Technology, Sheffield Hallam University, Pond Street, Sheffield S1 1WB. FAX 0742 533306
2 Process Tomography Unit, UMIST
3 Control Dept., Faculty of Electrical Engineering, Universiti Teknologi Malaysia

ABSTRACT: This paper describes the further development of optical sensor hardware for a process tomography system in which emitters and detectors are used to exploit the optical characteristics of multiphase flow regimes. The optical arrangement is described and importance of fibre beam position discussed. The proportion of the measurement volume interrogated by the beams is derived. The response of a single fibre is shown followed by a reconstructed concentration profile.

1. Introduction

Process tomography provides real-time methods of viewing the cross-section of a process to provide information relating to the material distribution. This involves taking numerous measurements from sensors placed around the section of the process being investigated and processing the data to reconstruct an image.

An optical transmitter projects a pencil of light through the process to a receiver, the received light level is then compared with the level achieved with no obstruction in the light path to determine if the light has been attenuated. A transmitter-receiver pair forms a view and by using several such views in parallel to form a projection, and two or more projections, images may be formed which provide information about the behaviour of the process in that cross-section [2, 3, 4]. The resolution of such a system is limited by the physical size of the component used as light transmitter (often some form of LED) and receiver (photodiode or similar). The use of optical fibres allows more sensors to be placed around the process and thus a higher resolution can be achieved.

The proposed system uses two orthogonal projections, each consisting of 16 views with optical fibres coupling light to the process and from the process to the receiver. The analogue signals from each transducer vary in amplitude due to the received light caused by particle passing through the beam [7]. By using collimated beam of light, reconstruction can be carried using algorithms developed for x-ray tomography [1, 2] to provide an image of the spatial variations in concentration across the cross-section. By cross-correlating pixels of two suitably spaced images, it may be possible to gain information about the velocity profile of the flowing material [2, 5].

2. Optical imaging system

The image reconstruction work carried out in this project is based upon techniques developed for transmission tomography systems which use radiation sources such as X-rays and γ-rays. These rays pass through an object without refraction, but with their radiation intensity attenuated [2, 6]. In this optical system the light is attenuated by particles passing through the beam.

The system uses an array of optical fibres illuminated at one end from a common halogen white light source (DC) with the other end mounted in the pipe. Opposite each transmitter fibre and on the same optical axis, a receiving fibre is mounted, the other end of which is coupled to a photodiode, enabling the received light level to be measured [1,2]. As an object passes through the light beam, the level of light energy falling on the receiving fibre is reduced and a reduction in the output of the diode is observed.

The beam of light must diverge as little as possible to avoid overlap of the received signals and consequent loss of the beam intensity. The use of laser diodes or lenses in producing a high resolution system cause problems due to their physical size. They also result in a much more expensive system, with a variety of technical constructional problems. An alternative is used which reduces the amount by which the beam diverges.

This alternative method sets the light source in a metal block with a small hole in the middle to act as a light stop. The fibre optic is a push fit in the block as shown in figure 1. This has the effect, in conjunction with the stop, of reducing the angle of divergence. However a compromise is required between aperture diameter and beam intensity.

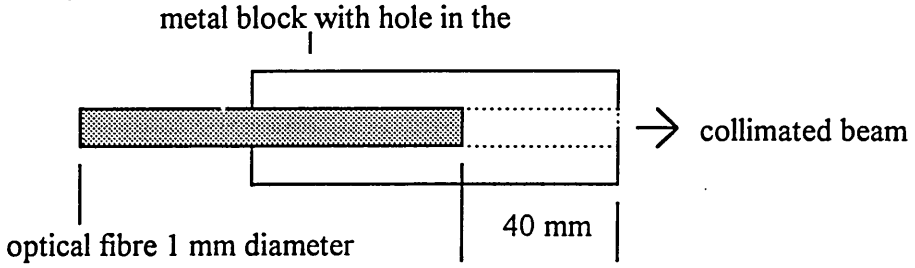

Figure 1. Cross section through optical stop.

The diameter of the beam at the receiver side of the 81 mm diameter pipe is 4 mm with a corresponding light intensity of 1.4 mW, as shown in figure 2. The intensity of the beam is strong enough to be detected by the photodiode light sensor.

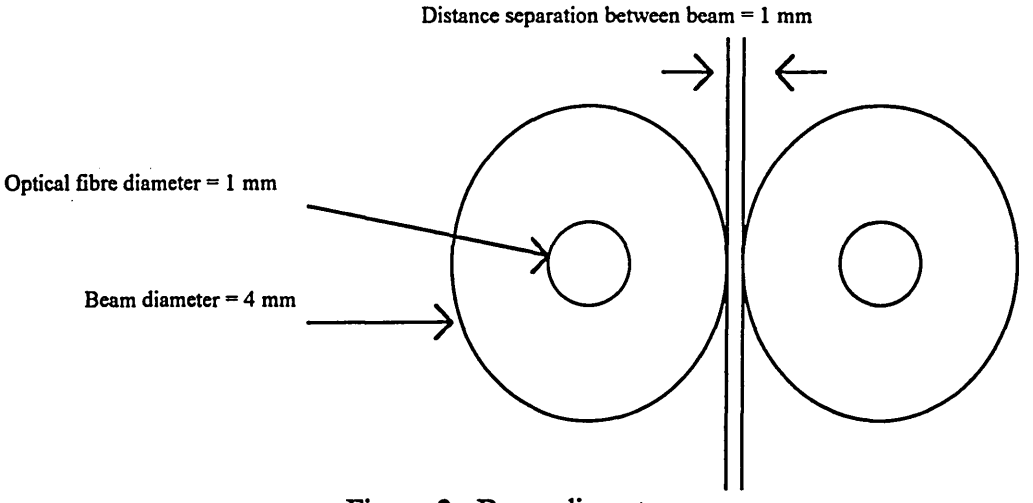

Figure 2. Beam diameter

3. Arrangements of transducers

Having developed suitable electronics for the receiver, initial work was carried out using an arrangement consisting of two arrays of sixteen transducers. The arrays are mounted orthogonally. The arrangement was built to monitor a cross section of an 81 mm diameter metal pipe as shown in figures 3 and 4.

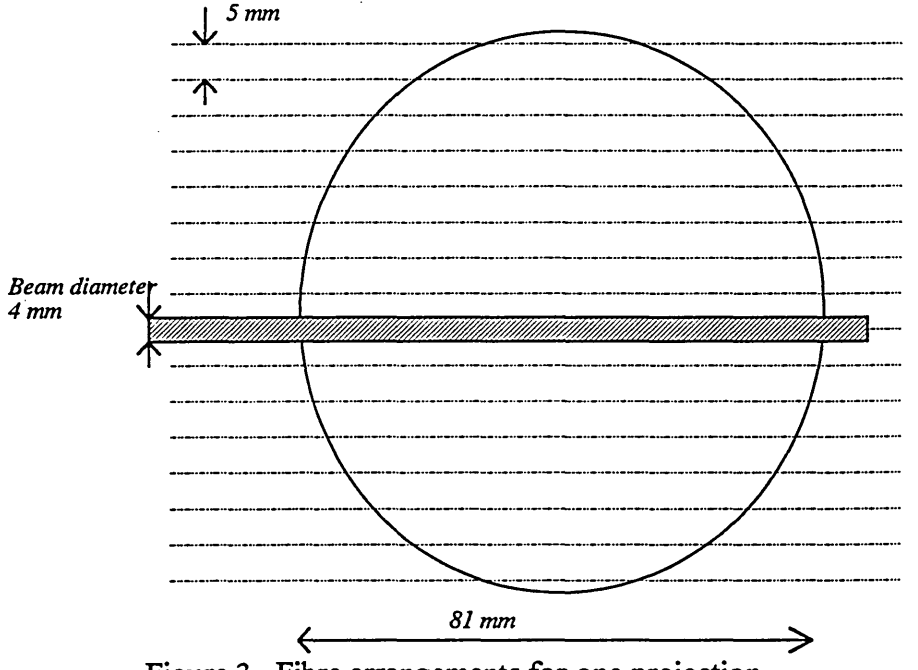

Figure 3. Fibre arrangements for one projection

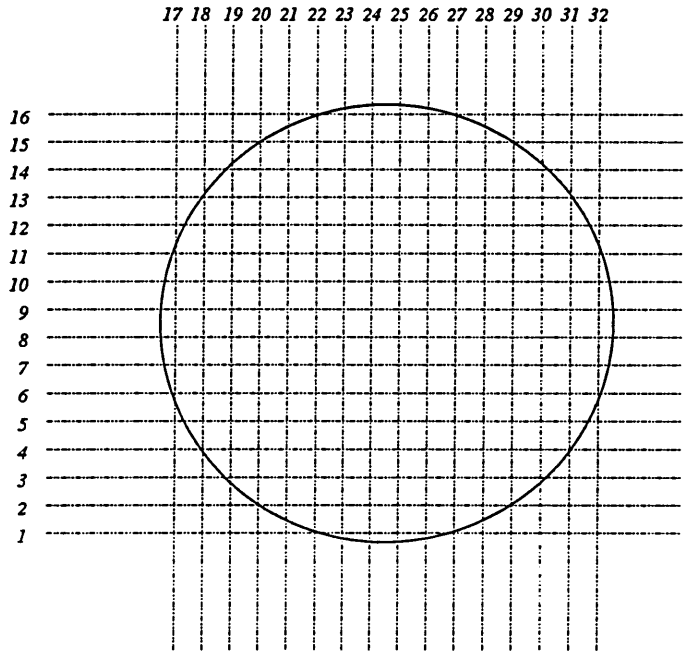

Figure 4. Arrangement for two projections.

Although the transmitted beam diameter expands to a maximum of 4 mm, the width of detectable beam is only 1 mm, the diameter of the optical fibre. The total volume in the sensing area is

$$\pi \frac{d^2 l}{4}$$
$$= 5.15x10^3 mm^3$$

where d=81 mm, l=1 mm is the width of the fibre. The volume being monitored by each projection is

$$16\pi \frac{l^2}{4}$$
$$= 12.6mm^3$$

This means that each projection provides a statistical sample consisting of 0.25% of the flow in the sensing volume. With two projections approximately 0.5% of the volume is sampled. To increase this resolution the sensors could be spaced at 2.5 mm without the expanded beams over-lapping the detectors. This would enable a 32 x 32 arrangement to be attained, and the volume sampled to be 1%.

4. Results and discussion

4.1 Concentration measurements

Measurements were made with the optical fibre sensor system using a laboratory scale gravity flow rig. This feeds silica sand (mean particle size 600μm) vertically downwards through the measurement section at a controlled rate. The optical sensor output voltage

was measured at several representative flow rates between 25000 $mm^3 s^{-1}$ and 325000 $mm^3 s^{-1}$. At the higher flow rate the transducers start to show saturation. The measured density of this sand is 1.6 gm cm^3 . This density figure has been used to convert the measured rig flow rates into volume flow rates, because the optical system is designed to determine volume flow rates. The results and a linear regression line are shown in figure 5. The units for volume flow rate are $mm^3 s^{-1}$.

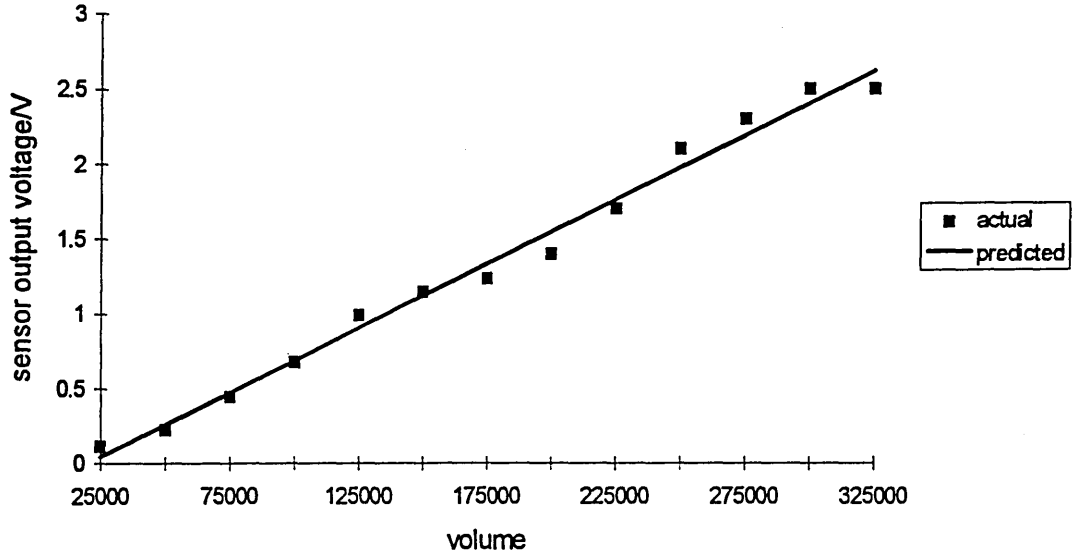

Figure 5. Relationship between mass flow rate and optical sensor output voltage for a typical optical fibre transducer.

The linear relationship is expected, because doubling the volume flow rate doubles the number of sand particles. The result demonstrates the suitability of the optical sensor for concentration measurement for lightly loaded flows (up to approximately 2% solids volume by volume) providing the ends of the fibre can be kept free of dust. In a practical system this could be achieved by placing an air purge upstream of the optical fibre.

4.2 Concentration profile

With the 16 x 16 array thirty-two individual readings are obtained in a data set The maximum value in the set is determined and scaled to sixteen. The same scaling factor is applied to the remaining members of the set and the resulting values rounded to the nearest whole number. The reconstruction then follows the method described in detail in [8]. After the reconstruction is finished the resulting values are rescaled by the scaling factor initially used on the data set resulting in quantified values. A typical result is shown in figure 6.

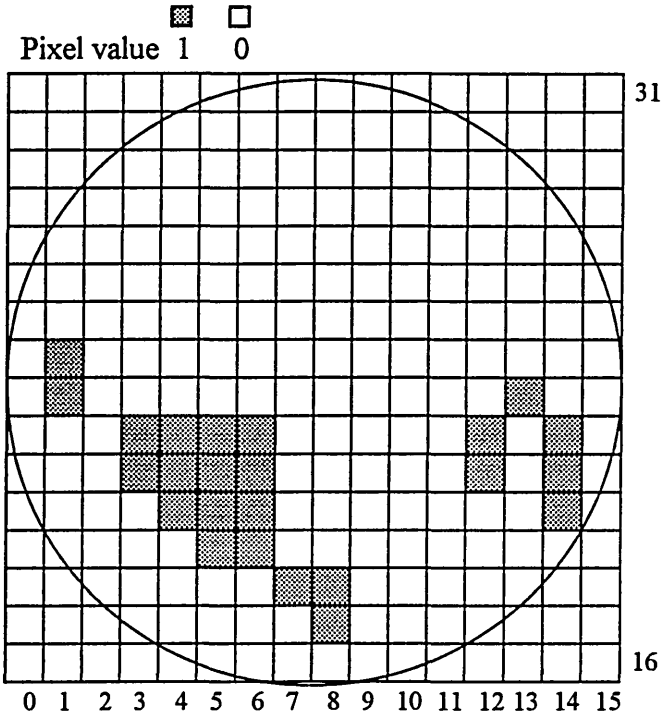

Figure 6. The concentration profile for a volume flowrate 125000 mm^3 s^{-1}

REFERENCES

1. R. Abdul Rahim ,Professor R.G.Green, N. Horbury, Dr. F.J.Dickin, B.D.Naylor, Dr. T.P.Pridmore. *Initial work on tomographic imaging system using optical fibres for pneumatic conveyors* ECAPT '95 proceeding, page 127-133.
2. N.M. Holbury, R.Abdul Rahim , Professor R.G.Green, .Dr. F.J.Dickin, B.D.Naylor, Dr. T.P.Pridmore *An investigation into the use of optical fibres to produce on-line particle size information and tomographic images for hydraulic processes* ECAPT '95 proceeding, page 134-138.
3. P.Dugdale, R. G. Green, A. J. Hartley, R. J. Jackson, J. Landauro, *Tomographic imaging in industrial process equipment using optical sensor arrays,* Sensor technology systems and application 5th conference paper edited by K. T. V. Grattan.
4. F. J. Dickin, B. S. Hoyle, A. Hunt, S. M. Huang, O. Illyas, C. Lenn, R. C. Waterfall, R. A. Williams, C. G. Xie, M. S.. Beck. *Tomographic imaging of industrial process equipment - review of needs and methods.* pp191-196 Sensor: Technology, Systems & Applications. ed. K. T. V. Grattan, pub, Adam Hilger.
5. M.S. Beck & A. Plakowski: *Cross Correlation Flowmeters - their design and Application,* Pub Adam Hilger 1987.
6. Xie *Review of process tomography image reconstruction methods* SensorTechnology, Systems & Applications VI ed. K. T. V. Grattan and A.T. Augousti, pub, Adam Hilger
7. R G Green, N. M. Horbury, R. Abdul Rahim, F. J. Dickin, B. D. Naylor, T. P. Pridmore. *Optical fibre sensor forprocess tomography,* Journal Measurement, Science and Technology to be published.
8. A B Plaskowski, M S Beck, R Thorn and T Dyakowski, *Imaging industrial flows: applications of electrical process tomography.* p126-131. IOP Publishing, 1995.

Optical fibre sensors for process tomography : Concentration measurements and scattering effect.

R. Abdul Rahim[1,3], R G Green[1], N. M. Horbury[1], F. J. Dickin[2], B. D. Naylor[1], T. P. Pridmore[1].

1. School of Engineering IT, Sheffield Hallam University, Pond Street, Sheffield, S1 1WB.
2. Process Tomography Unit, Dept. of Electrical Engineering, UMIST, PO Box 88, Manchester, M60 1QD.
3. Control Dept., Faculty of Electrical Engineering, Universiti Teknologi Malaysia.

Abstract

This paper describes an investigation into the use of an optical fibre sensor to measure the flow of pneumatically conveyed solid particles. Typical results for the mass flow rate of dry sand versus transducer output voltage are presented for a 1 mm diameter sensor fibre.

1. Introduction

Process tomography involves the use of instruments which provide cross-sectional profile of the distribution of materials in a process vessel or pipeline. By analysing two suitably space images it is also feasible to measure the vector velocity profile [1,2,]. Hence from this knowledge of material distributions and movement, internal models of the process can be derived and used as an aid to optimising the design of the process. This promises a substantial advance on present empirical methods of process design, often based on input/output measurements, with only a limited amount of information about the detailed internal behaviour of the process [3]

Process tomography [13] is a measurement technique that is being developed for measurement in two and multicomponent flows. These measurement systems use distributed groups of identical sensors, termed arrays, to investigate the physical properties of the material and its distribution within a container, e.g. a pneumatic

conveyor, in real time [14]. Most of the tomography systems being investigated aim to provide concentration distributions of moving components of interest within the measurement section in the form of a visual image, much like an x-ray picture of hand for example, which is updated at a refresh rate dependent upon the process being investigated [15]. However, the long term aim is to provide flow information such as mass flow rate, which will be calculated by combining both concentration and velocity profiles.

Many approaches to tomography are being investigated based on a range of physical principles, e.g. capacitance tomography for two/three component mixtures of oil, gas and water for oil company applications [4], electrical impedance tomography to investigate design parameters relating to hydrocyclone and dense medium separators [5], electromagnetic tomography to obtain information relating to permeability and conductivity distributions within the sensing volume [6], combinations of two kinds of sensor, for example capacitance and gamma ray for three component measurement in oil, gas and water mixtures [7]. However, for many two component flow systems, where the concentration of the conveyed component is low, e.g. pulverised coal dust being fed to coal fired electrical power station boiler [8], existing systems do not have the required sensitivity to detect the small variations in solids flow concentration. For mixtures of transparent fluids and small volume fractions, typically 5%, of opaque solids low-cost optical sensors merit investigation.

To investigate the cross-section of a conveyor with relatively high resolution, 2 mm per cm^2 for example, a large number of peripherally mounted sensors are required. Optical fibres are employed due to their small dimensions (order of 1 mm diameter) which will enable them to be spaced at 1.5 to 2.0 mm intervals around the vessel. For process tomography, the sensor must be capable of providing information relating to the concentration of conveyed material within the sensing volume being interrogated. For determining the velocity of the moving particles using cross-correlation techniques [9]

the dynamic performance of the sensor is important otherwise measurement 'blurring' artefacts will be produced leading to erroneous analysis. This paper investigates the use of a single optical fibre transducer (which is part of a sixteen by sixteen tomographic sensor array) to measure cross-sectional variations in bulk concentration due to flowing solids.

2. Optical fibre sensors

Optical fibres provide an opportunity to design sensors with a very wide bandwidth [10], enabling measurements of high speed flowing particles. To generate high resolution tomographic images, a large number of optical fibres are needed [11] and this infers that high speed signal processing must be used.

The system uses multiple arrays of optical fibres as both light transmitters and receivers. Ideally, light is supplied in collimated beams. Collimation increases beam intensity and ensures that a particular sensor only detects light from its corresponding emitter. It also enables the use of reconstruction algorithms developed for medical x-ray tomography [12]. Collimation also results in the detected optical intensity being dependent on the length of attenuating component traversed by the beam, and being almost independent of the length of attenuating component from the source [11].

The sensor system investigated here uses the fibre arrangement shown in figure 2.1. The transmitter fibre, along with the other thirty-one fibres, is part of an optical fibre bundle which is illuminated with white light from a 50 W, dichroic halogen bulb with integral reflector, with a beam angle of 12°, excited from a stabilised DC. voltage (necessary to prevent fluctuations in supply voltage modulating the light intensity).

Figure 2.1 The transducer system

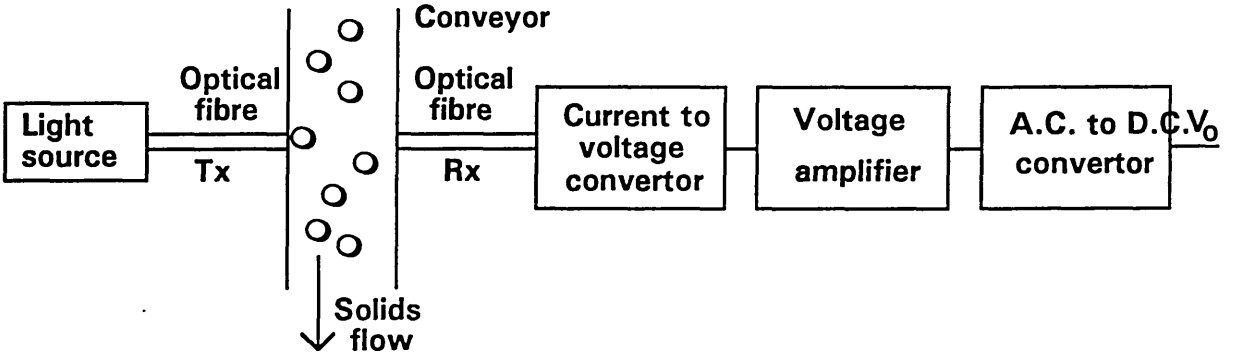

The light passes through the fibre and then into the volume being interrogated. A receiving fibre detects the transmitted beam and relays it to a photo-diode and associated electronics, which converts it to an electrical voltage. This voltage is conditioned so that no flow (full light on the receiver) indicates zero voltage and with high flow rates of solids, the system is fully driven, providing a maximum output of five volts. The ends of the fibres in contact with the vessel, are cut and polished flat to minimise scattering effects. The fibres are mounted into holes machined into the measurement section in an invasive but non-intrusive (i.e. the flow pattern is not affected by their presence) manner. The effects of diffraction are ignored, because the primary effect is attenuation of optical energy by particles intercepting the beam.

The pipe in which the sensors are mounted has a nominal bore of 80 mm and the sensor spacing is 5 mm. This spacing means that approximately one fifth of the cross-section is directly interrogated, the remaining four fifths not being in a direct path between a source and its receiver, though there may be some output due to the beam spreading out from

the transmitter fibre due to its optical aperture and light scattering by the particles. Thus each fibre is taking only a sample measurement of the particles flowing in the pipe. However, it is assumed that each fibre produces readings which represent a realistic sample of the solids passing through the space at each side of the fibre. The light source transmits continuously and any particle passing through the volume interrogated by a fibre sensor is detected as a variation in the level of illumination of the sensor. The resulting voltage is available in two forms: as a time averaged signal and as a rapidly varying or dynamic voltage. The time averaged voltage produces a signal which is shown to vary linearly with solids flow rate (figure 4.1).

3. Concentration measurements

Measurements were made with a single optical fibre sensor using a laboratory scale gravity flow rig. This feeds silica sand (mean particle size 600 nm) vertically downwards through the measurement section at a controlled rate. The optical sensor output voltage was measured at several representative flow rates ranging from 40 to 575 gm/s.. The time averaged voltage produces a signal which is shown to vary linearly with solids flow rate (figure 3.1). The results are shown in figure 4.1 in which linear regression line has been fitted to the results. The negative reading at low flow rates is due to a DC offset voltage in the amplifier. At higher flow rates the transducer saturates with a maximum reading of 3 volts. Figure 3.2 shows a typical recording from one transducer at an approximate flowrate of 40 gm/s.

Figure 3.1 Relationship between mass flow rate and optical sensor output voltage for a single optical fibre receiver.

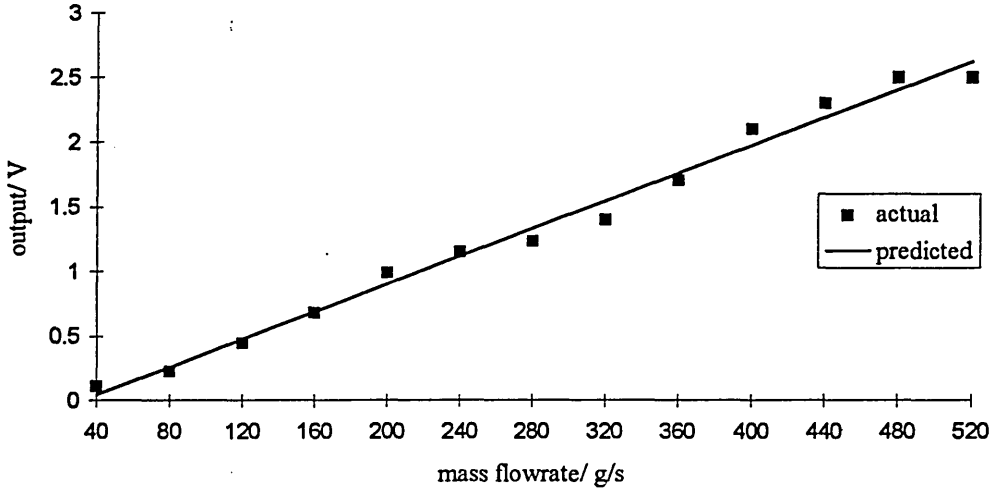

Figure 3.2 Graph shows the output from one transducer at mass flow rate of 40gm/s

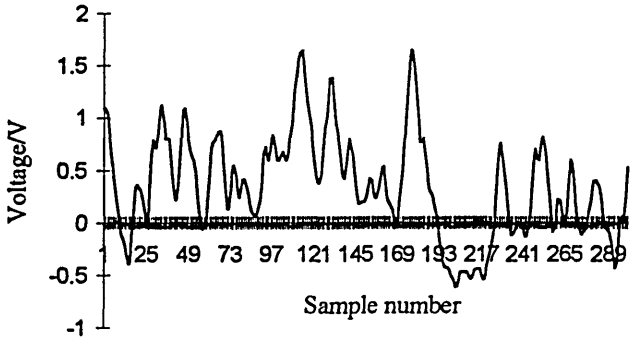

The average number of particles in the measurement volume should increase directly as a linear function of the solid flow rate, so linear relationship shown in figure 3 is expected, and this demonstrates the suitability of the optical sensor for concentration measurement for lightly loaded flows (up to approximately 5% solids by volume in the test) and providing the ends of the fibre can kept free of dust during the measurement procedure.

4. Scattering effect

As mention before end of fibres are cut and polished flat to minimise scattering effects. To test the interaction between adjacent receivers, a single transmitter was energised and the outputs from all the receivers monitored for a range of sand feed rates. Graph in figure 4.1 shows the result.

Figure 4.1 Scattering effect

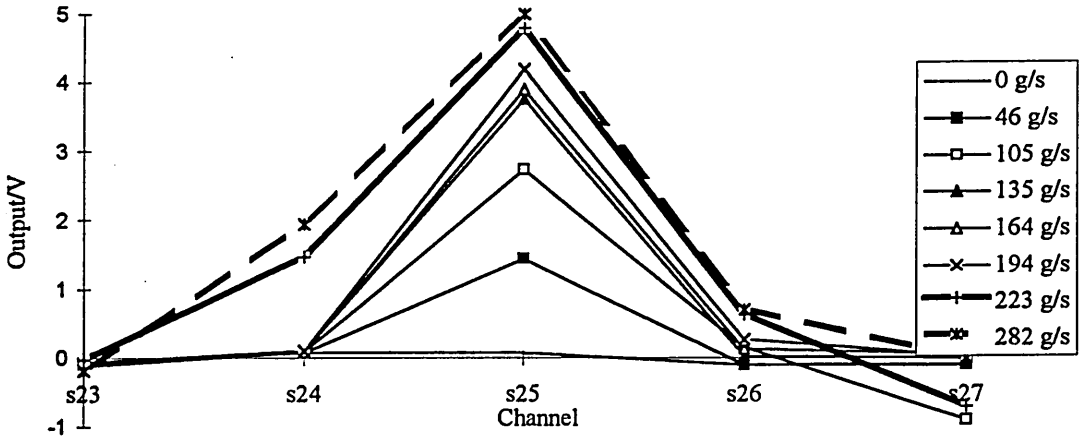

At low feed rates (46 to 194 gm/s) no interaction was detected and at a flow rate of 223 gm/s and above one adjacent receiver indicated approximately 1.5V (equivalent to 46 gm/s) and the other produced no detectable effect.

5. Conclusions

Optical fibres exhibit good linearity when used to measure solids flow rate. These results demonstrate the suitability of low-cost optical fibre sensors for monitoring flowing materials. In particular, their frequency bandwidth, when used to measure passing objects is very high, typically tens of kilohertz. This high bandwidth makes them suitable for velocity measurement using cross-correlation techniques [9].

8. Reference

1. Hayes D.G., Gregory I.A,and Beck M.S. Velocity profile measurement in two-phase flows, *Proc. European Concerted Action on Process Tomography*, Manchester, 26-29 March 1992.
2. Thorn R., Huang S.M, Xie C.G., Salkeid J.A, Hunt A. and Beck M.S, Flow imaging for multicomponent flow measurement, *Flow Meas. Instrum*, 1 (1990), 259-268).
3. Dickin F.J., Hoyle B.S., Hunt A., Huang S.M., Ilyas O., Lenn C., Waterfall R.C., Williams R.A., Xie C.G., Beck M.S., Tomography imaging of industrial process equipment : techniques and applications. *IEE Proc.*-G, 139 (1992), 72-82
4. Huang S.M., Plaskowski A.B., Xie C.G. and Beck M.S. (1989) Tomographic imaging of two-component flow using capacitance sensors. *J Phys E*, **22**, 173-177.
5. Williams, R.A.,Ilyas, O.M., and Dyakowski, T. (1995) Air core imaging in cyclonic coal separators using electrical impedance tomography. *Coal Preparation*, **15**, 3-4.

6. Scaife, J.M., Tozer, R.C. and Freeston, I.L. (1994) Conductivity and permittivity images from an induced current electrical impedance tomography system. *IEE Proc. A*, ,(5), 356-362, Sept. 1994.

7. Dykesteen, E. and Frantzen, K.H. (1990) The CMI multiphase fraction meter. *Proc. Int. Conf. on Basic Principles and Industrial Applications of Multiphase Flow*. (24-25 April) (London: BHRA).

8. Green, R.G., Foo, S.H. and Phillips, J.G. (1981) Flow measurement for optimising the feedrate of pulverised fuel to coal fired boilers. *Symposium on Fossil Energy Processes, (San Francisco).*

9. Y Yan, B Byrne, S Woodhead, J Coulthard, (1995), "Velocity measurement of pneumatically conveyed solids using electrodynamic sensors." *Meas. Sci. Technol.* **6,** 515-537.

10. Dr. Z. Ghassemlooy, Fibre optic a revolution in communication, *Page 2, EIT Publication for ESCE IV, 1992.*

11. Ray Snyder and Lambertus Hesselink, Three-dimensional optical tomographic measurements of mixing fluids, *Proceedings of the SPIE : The International Society for Optical Engineering,* Vol. 1083, page 281-9, date 1989.

12. P.Dugdale, R. G. Green, A. J. Hartley, R. J. Jackson, J. Landauro, Tomographic imaging in industrial process equipment using optical sensor arrays, *Sensor technology systems and application 5th conference paper* edited by K. T. V. Grattan.

13. C G Xie, (1993) "Review of image reconstruction methods for process tomography." *Process Tomography - A Strategy for Industrial Exploitation,* Ed M S Beck et al., Pub by UMIST.

14. Process Tomography: Principles, Techniques and Applications, Ed R.A.Williams and M.S.Beck, Butterworth-Heinemann, 1995, 101-118.

15. Wiegand, F. and Hoyle, B.S. (1991) Development and implementation of real-time ultrasound process tomography using a transputer network. *Parallel Computing*, **17**, 791-807.

Meas. Sci. Technol. 6 (1995) 1699–1704. Printed in the UK

Optical fibre sensors for process tomography

R G Green†, N M Horbury†, R Abdul Rahim†‡, F J Dickin§, B D Naylor† and T P Pridmore†

† School of Engineering IT, Sheffield Hallam University, Pond Street, Sheffield S1 1WB, UK
‡ Control Department, Faculty of Electrical Engineering, Universiti Teknologi, Johor Bahru, Malaysia
§ Process Tomography Unit, Department of Electrical Engineering, UMIST, PO Box 88, Manchester M60 1QD, UK

Received 30 May 1995, in final form 14 August 1995, accepted for publication 5 September 1995

Abstract. This paper describes an investigation into the use of an optical fibre sensor to measure the flow of pneumatically conveyed solid particles. Typical results for the mass flow rate of dry sand versus transducer output voltage are presented for a 1 mm diameter sensor fibre. The frequency bandwidth of the sensor is determined for a range of fibre diameters and compared with the calculated response obtained using spatial filtering considerations.

1. Introduction

Process tomography [1] is a measurement technique that is being developed for measurement in two-component and multicomponent flows. These measurement systems use distributed groups of identical sensors, termed arrays, to investigate the physical properties of the material and its distribution within a container, for example a pneumatic conveyor, in real time [2]. Most of the tomography systems that are being investigated are intended to provide concentration distributions of moving components of interest within the measurement section in the form of a visual image, much like an x-ray picture of a hand for example, which is updated at a refreshment rate dependent upon the process being investigated [3]. However, the long-term aim is to provide flow information such as the mass flow rate, which will be calculated by combining concentration and velocity profiles.

Many approaches to tomography are being investigated based on a range of physical principles, such as capacitance tomography for two- or three-component mixtures of oil, gas and water for oil company applications [4], electrical impedance tomography to investigate design parameters relating to hydrocyclone and dense medium separators [5], electromagnetic tomography to obtain information relating to permeability and conductivity distributions within the sensing volume [6] and combinations of two kinds of sensor, for example capacitance and gamma ray for three-component measurement in oil, gas and water mixtures [7]. However, for many two-component flow systems, in which the concentration of the conveyed component is low, such as pulverized coal dust being fed into a coal-fired electrical power station's boiler [8], existing systems do not have the required sensitivity to detect the small variations in solids flow concentration. For mixtures of transparent fluids and small volume fractions, typically 5%, of opaque solids, low-cost optical sensors merit investigation.

To investigate the cross section of a conveyor with relatively high resolution, 2 mm per square centimetre for example, a large number of peripherally mounted sensors are required. Optical fibres are employed due to their small dimensions (order of 1 mm diameter) which will enable them to be spaced at 1.5–2.0 mm intervals around the vessel. For process tomography, the sensor must be capable of providing information relating to the concentration of conveyed material within the sensing volume being interrogated. For determining the velocity of the moving particles using cross correlation techniques [9] the dynamic performance of the sensor is important. otherwise measurement 'blurring' artefacts will be produced, leading to erroneous analysis. This paper investigates the use of a single optical fibre transducer (which is part of a 16 × 16 tomographic sensor array) to measure cross sectional variations in bulk concentration due to flowing solids and one aspect of the dynamic response of the sensor by determining the spatial filtering effect [10] of a range of multimode plastic fibres.

2. Optical fibre sensors

The sensor system investigated here uses the fibre arrangement shown in figure 1. The transmitter fibre, together with the other 31 fibres, is part of an optical fibre bundle which is illuminated with white light from a 50 W, dichroic halogen bulb with integral reflector, with a

0957-0233/95/121699+06S19.50

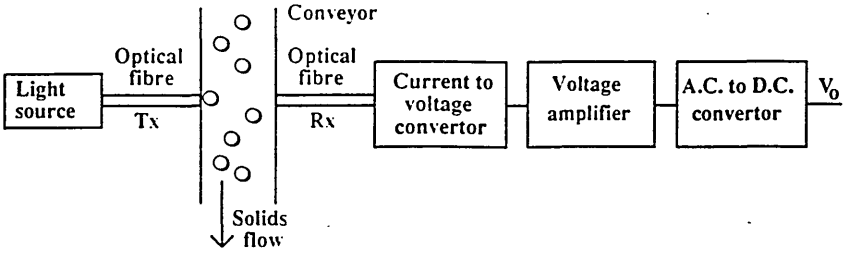

Figure 1. The transducer system.

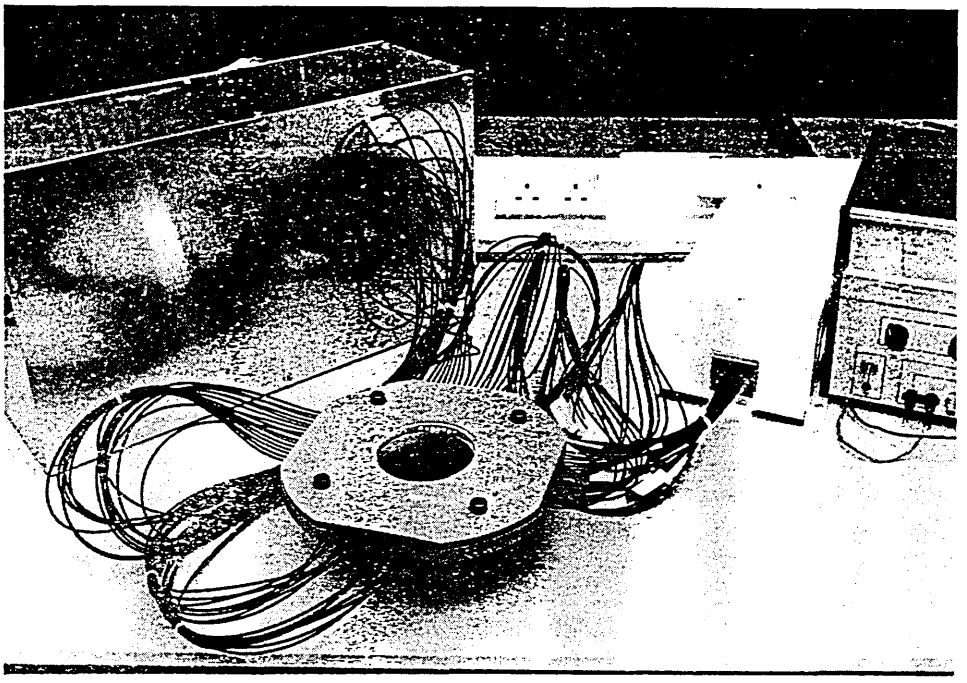

Figure 2. The measuring section for the pneumatic conveyor showing the 16 × 16 array of optical fibres.

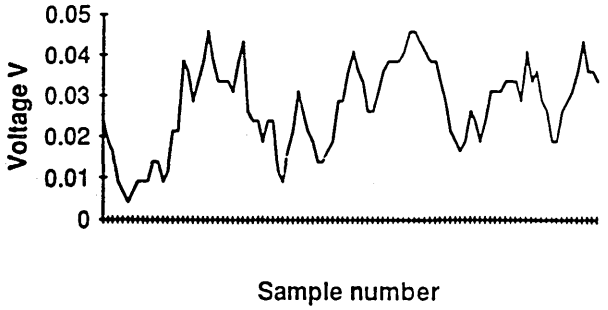

igure 3. A recording from a single sensor at a flow rate of pproximately 40 g s^{-1}. The average number of particles in e measurement volume should increase directly as a near function of the solids flow rate, so the linear elationship shown in figure 4 is expected, and this emonstrates the suitability of the optical sensor for oncentration measurement for lightly loaded flows (up to pproximately 5% solids by volume in our tests), provided at ends of the fibre can be kept free of dust during the easurement procedure.

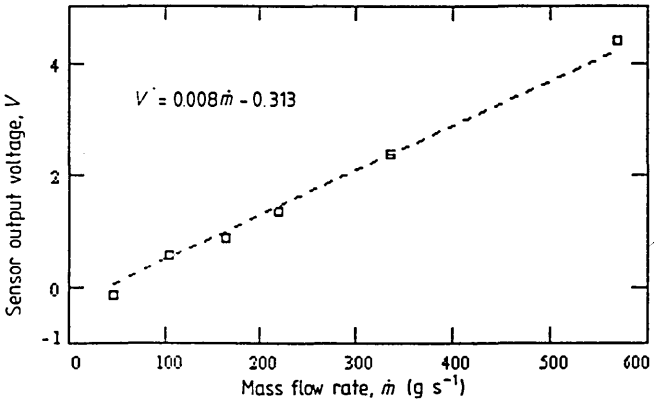

Figure 4. The relationship between mass flow rate and optical sensor output voltage for a single optical fibre receiver.

eam angle of 12°, excited from a stabilized DC voltage this is necessary in order to prevent fluctuations in supply oltage modulating the light intensity). A simple bi-convex lens is used to provide an approximately collimated light beam to the fibre bundle. The light passes through the fibre and then into the volume being interrogated. A receiving fibre detects the transmitted beam and relays it to a reverse-biased photo-diode and associated electronics, which convert it into an electrical voltage. This voltage

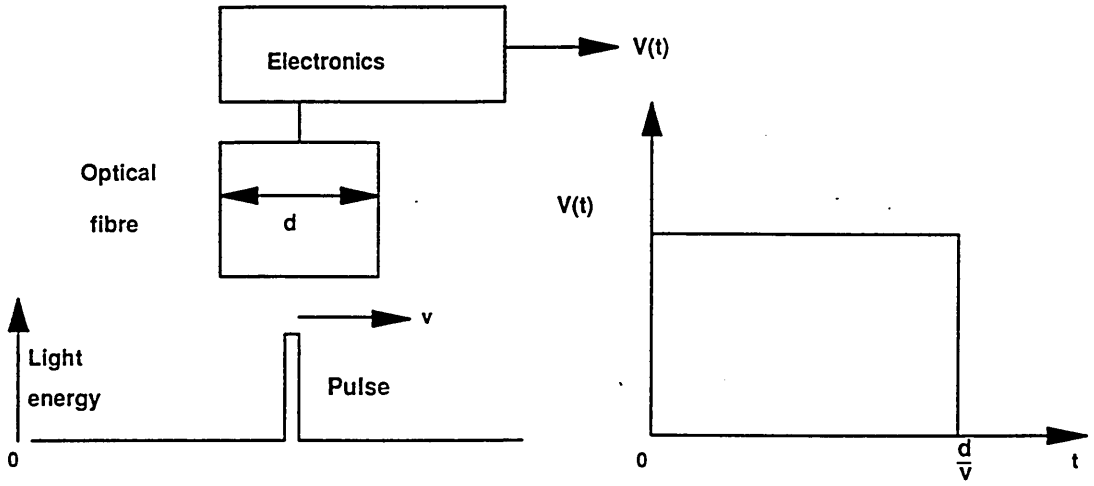

Figure 5. The light pulse input to the optical fibre.

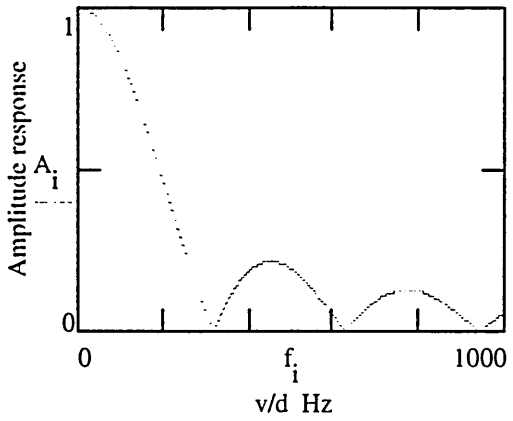

Figure 6. The calculated spatial filtering response. Results of practical measurements are presented in the next section.

is conditioned so that no flow (full light on the receiver) indicates zero voltage and so that, with high flow rates of solids, the system is fully driven, providing a maximum output of 5 V. The ends of the fibres in contact with the vessel are cut and polished flat to minimize scattering effects. The fibres are mounted into holes machined into the measurement section in an invasive but non-intrusive (the flow pattern is not affected by their presence) manner. The effects of diffraction are ignored, because the primary effect is attenuation of optical energy by particles intercepting the beam.

In the present arrangement, as a compromise between accuracy and cost, 16 fibres are used for each projection, as shown in figure 2. The pipe in which the sensors are mounted has a nominal bore of 80 mm and the sensor spacing is 5 mm. This spacing means that approximately a fifth of the cross section is directly interrogated, the remaining four fifths not being in a direct path between a source and its receiver, though there may be some output due to the beam spreading out from the transmitter fibre due to its optical aperture and light scattering by the particles. Thus each fibre is taking only a sample measurement of the particles flowing in the pipe. However, it is assumed that each fibre produces readings which represent a realistic sample of the solids passing through the space at each side of the fibre. The light source transmits continuously and any particle passing through the volume interrogated by a fibre sensor is detected as a variation in the level of illumination of the sensor. The resulting voltage is available in two forms: as a time averaged signal and as a rapidly varying or dynamic voltage. The time averaged voltage produces a signal which is shown to vary linearly with solids flow rate (figure 3). The dynamic voltage output is used for the spatial frequency measurements (section 5).

3. Concentration measurements

Measurements were made with a single optical fibre sensor using a laboratory scale gravity flow rig. This feeds silica sand (mean particle size 600 μm) vertically downwards through the measurement section at a controlled rate. The optical sensor output voltage was measured at several representative flow rates in the range 50–575 g s^{-1}. The results are shown in figure 4, in which a linear regression line has been fitted to the results. The negative reading at low flow rates is due to a DC offset voltage in the amplifier. At higher flow rates the transducer saturates with a maximum reading of 5 V. Figure 3 shows a typical recording from one transducer at an approximate flow rate of 40 g s^{-1}. To test the interaction between adjacent receivers, a single transmitter was energized and the outputs from all the receivers monitored for a range of sand feed rates. At low feed rates (40–100 g s^{-1}) no interaction was detected and at a flow rate of 350 g s^{-1} one adjacent receiver indicated approximately 45 g s^{-1} and the other produced no detectable effect.

4. Frequency domain measurements

The spatial filtering effect, which exists for most sensors used to measure moving material, was applied to capacitance electrodes by Hammer and Green [10]. They

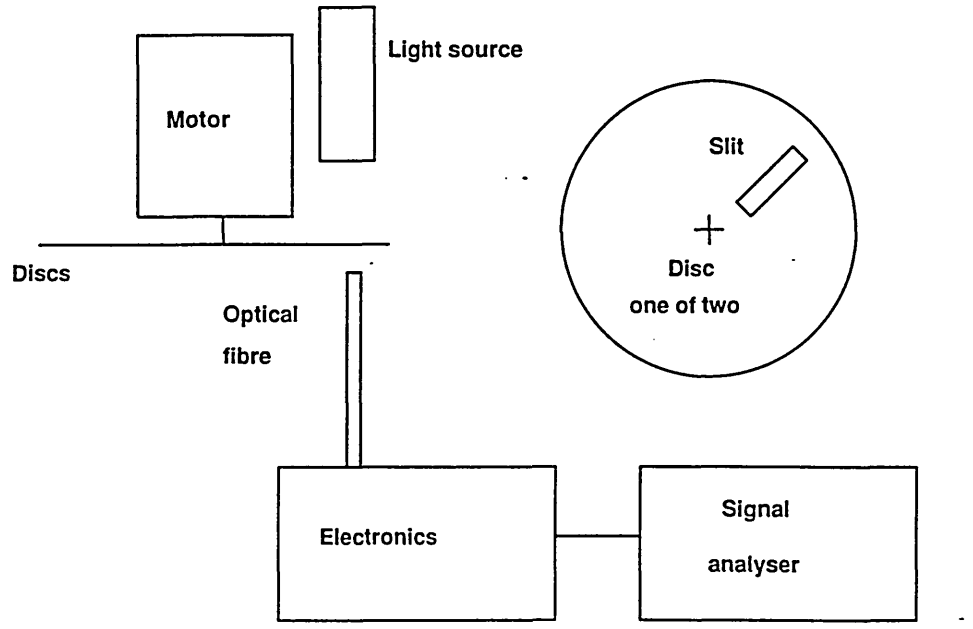

Figure 7. The spatial filtering test arrangement.

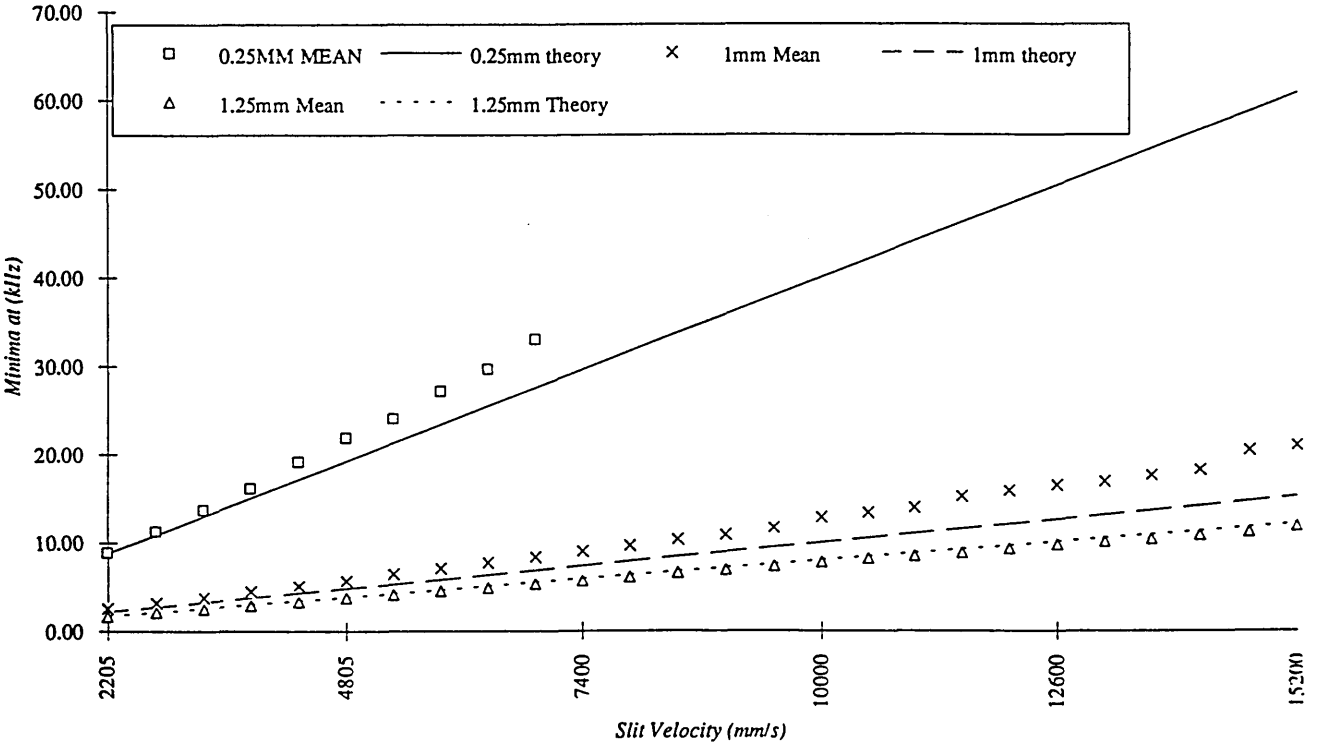

Figure 8. Comparison of measured and calculated first minima.

elated the velocity of flowing, discontinuous material to e frequency bandwidth of the sensed signal. A similar pproach, described below, extends the concept to optical bre sensors. Assume that a small, narrow beam of light oving past the optical fibre sensor, of diameter d, with velocity v, can be considered as a pulse of light $\delta I(t)$. is pulse of light results in a change in voltage being roduced by the transducer. This change in voltage may be escribed by a rectangular pulse of duration d/v (figure 5). e amplitude of the change in voltage produced by the transducer is given by

$$\delta I_i(t) = k\frac{v}{d}\int_0^\infty V(t)\,\mathrm{d}t \qquad (1)$$

where $V(t)$ represents the change in voltage pulse provided by the moving beam and k is a constant of proportionality with appropriate dimensions. If the pulse duration is short compared with d/v it can be shown [10] that the response is a 'sinc' function with the effect of d and v on the modulus that is shown graphically in figure 6. Results of practical measurements are presented in the next section.

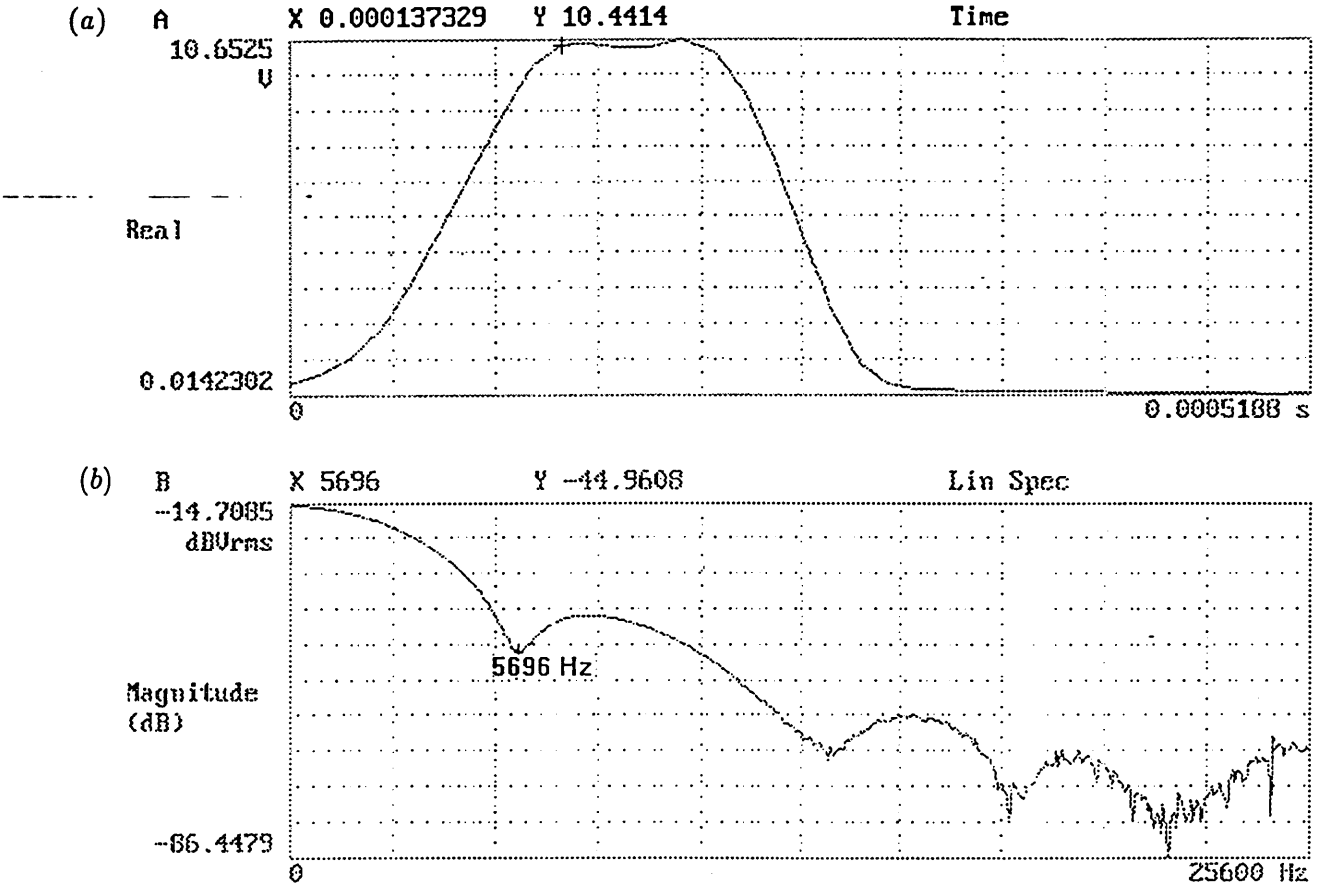

Figure 9. The frequency spectrum obtained for the 1 mm fibre with $v = 4.8$ m s^{-1}. (*a*) Measured voltage from ransducer and (*b*) frequency response.

5. Measurements on spatial filtering

Three different fibre diameters (0.25, 1.0 and 1.25 mm) were used in these tests. The experimental arrangement is shown in figure 7. The illumination system is modified from that shown in figure 1 by using direct illumination of the narrow slit (approximately 40 μm), which acts as the object for the receiving fibre. The slit is provided by two identical, co-axial discs which have slots in them. By rotating one slot relative to the other a narrow slit can be produced. The discs are locked together and rotated by the motor. When the source of light, the slit and the fibre are in alignment a pulse of light energy flows from the light source into the optical fibre. Ideally this should be a Dirac pulse; however, in practice it seems to be more like the flat-topped pulse with linear sides that would be expected to result from the convolution of a rectangular slit illuminated with the fibre acceptance region. The velocity at which the light pulse crosses the end of the fibre is determined by measuring the pulse repetition frequency, f, of the output voltage and the radial position, r, of the fibre relative to the axis of the disc. Then $v = 2\pi fr$ m s^{-1}.

A test is performed by rotating the aperture at a fixed speed and determining the frequency spectrum (figure 9). The frequency at which the first minimum occurs is determined. The test is repeated for a range of speeds with each diameter of fibre. Results are discussed in section 6. Tests were repeated several times to obtain a measurement of the standard deviation of each set of measurements.

6. Discussion on the spatial filtering effect

Figure 8 shows the relationship between the calculated values and measured values for the three different sizes of optical fibre tested. The results for the 0.25 and 1.00 mm fibres show that the measured points lie systematically above the values predicted by the rectangular pulse model, which may be due to the approximation used to describe the input pulse by a rectangular 'top hat' function. The gradient for the measured results of the 0.25 mm fibre is 1.11 times the gradient of the predicted value. The corresponding values for the 1.00 and 1.25 mm fibres are 1.25 and 0.97 respectively.

The frequency spectrum shown in figure 9 is an approximation to the 'sinc' function predicted by the analysis. This approximation is probably due to the voltage input not being represented by the ideal Dirac function. The position of the first minimum occurs at 5696 Hz, which is a factor of 1.19 greater than the predicted value of 4800 Hz for a 1 mm diameter fibre passed at a velocity of 4.8 m s^{-1}.

7. Conclusions

Optical fibres exhibit high linearity when used to measure solids flow rates. They also show agreement between predicted and measured values for the spatial filtering effect. These results demonstrate the suitability of low-cost optical fibre sensors for monitoring flowing materials.

n particular, their frequency bandwidth, when used to easure passing objects is very high, typically tens of lohertz. This high bandwidth makes them suitable for elocity measurement using cross correlation techniques [9].

eferences

[1] Xie C G 1993 Review of image reconstruction methods for process tomography *Process Tomography—A Strategy for Industrial Exploitation* ed M S Beck *et al* (Manchester: UMIST)

[2] Williams R A and Beck M S (eds) 1995 *Process Tomography: Principles, Techniques and Applications* (London: Butterworth-Heinemann) pp 101–18

[3] Wiegand F and Hoyle B S 1991 Development and implementation of real-time ultrasound process tomography using a transputer network *Parallel Comput.* **17** 791–807

[4] Huang S M, Plaskowski A B, Xie C G and Beck M S 1989 Tomographic imaging of two-component flow using capacitance sensors *J. Phys. E: Sci. Instrum.* **22** 173–7

[5] Williams R A, Ilyas O M and Dyakowski T 1995 Air core imaging in cyclonic coal separators using electrical impedance tomography *Coal Preparation* **15** 3–4

[6] Scaife J M, Tozer R C and Freeston I L 1994 Conductivity and permittivity images from an induced current electrical impedance tomography system *IEE Proc.* A **141** 356–62

[7] Dykesteen E and Frantzen K H 1990 The CMI multiphase fraction meter *Proc. Int. Conf. on Basic Principles and Industrial Applications of Multiphase Flow* (London: BHRA)

[8] Green R G, Foo S H and Phillips J G 1981 Flow measurement for optimising the feedrate of pulverised fuel to coal fired boilers *Symp. on Fossil Energy Processes, San Francisco*

[9] Yan Y, Byrne B, Woodhead S and Coulthard J 1995 Velocity measurement of pneumatically conveyed solids using electrodynamic sensors *Meas. Sci. Technol.* **6** 515–37

[10] Hammer E A and Green R G 1982 The spatial filtering effect of capacitance transducer electrodes *J. Phys. E: Sci. Instrum.* **16** 438–43

A TOMOGRAPHIC IMAGING SYSTEM FOR PNEUMATIC CONVEYORS USING OPTICAL FIBRES

by

R. ABDUL RAHIM (AMIEE)
BEng(Hons)(UK)

A thesis submitted to
Sheffield Hallam University
for the degree of Doctor of Philosophy
in the School of Engineering Information Technology

FEBRUARY 1996

Dedication

This work is dedicated to my family and my wife Hafidzah for being very patient, understanding and for organising everything in an excellent manner for the whole family especially looking after our beloved children, Khairulhafiy Muhammad and Raudhatusyahirah during those difficult years.

Acknowledgements

I would like to record my sincere thanks to my main supervisor, Professor Bob Green, for his intelligent supervision, helpful suggestions and constructive criticisms of my work. I am extremely grateful for his outstanding support and encouragement throughout the course of this research.

I would like also to express my sincere thanks to my co-supervisors, Dr. Tony Pridmore and Dr. Fraser Dickin for their help and advice. Also thanks to Stuart Birchall for helping me to use EE Design, Brett Naylor for the power supply design and all the technicians, especially Don Rimmer, Ken Duty, Adrian and Imad for their part in helping me during my research.

For my colleagues in Room 2302 School of Engineering Information Technology, Jan, Fuad, Neil, Marshall, Joe, Roy and Paul thank you for your valuable discussions and suggestions.

The financial assistance from the Malaysian Government and Universiti Teknologi Malaysia is highly appreciated and without which this research could not have been possible.